INFORMATION TO USERS

This was produced from a copy of a document sent to us for microfilming. While the most advanced technological means to photograph and reproduce this document have been used, the quality is heavily dependent upon the quality of the material submitted.

The following explanation of techniques is provided to help you understand markings or notations which may appear on this reproduction.

1. The sign or "target" for pages apparently lacking from the document photographed is "Missing Page(s)". If it was possible to obtain the missing page(s) or section, they are spliced into the film along with adjacent pages. This may have necessitated cutting through an image and duplicating adjacent pages to assure you of complete continuity.

2. When an image on the film is obliterated with a round black mark it is an indication that the film inspector noticed either blurred copy because of movement during exposure, or duplicate copy. Unless we meant to delete copyrighted materials that should not have been filmed, you will find a good image of the page in the adjacent frame. If copyrighted materials were deleted you will find a target note listing the pages in the adjacent frame.

3. When a map, drawing or chart, etc., is part of the material being photographed the photographer has followed a definite method in "sectioning" the material. It is customary to begin filming at the upper left hand corner of a large sheet and to continue from left to right in equal sections with small overlaps. If necessary, sectioning is continued again—beginning below the first row and continuing on until complete.

4. For any illustrations that cannot be reproduced satisfactorily by xerography, photographic prints can be purchased at additional cost and tipped into your xerographic copy. Requests can be made to our Dissertations Customer Services Department.

5. Some pages in any document may have indistinct print. In all cases we have filmed the best available copy.

University
Microfilms
International

300 N. ZEEB RD., ANN ARBOR, MI 48106

Downloaded from SHAREOK. Persistent Handle URL: https://hdl.handle.net/11244/4945

8209443

Teeters, Dale Carl

COMPARATIVE TEMPERATURE-DEPENDENT POLARIZED RAMAN STUDY OF LITHIUM POTASSIUM SULFATE, SODIUM POTASSIUM SULFATE, AND THE FAST ION CONDUCTOR LITHIUM SODIUM SULFATE

The University of Oklahoma PH.D. 1981

University
Microfilms
International 300 N. Zeeb Road, Ann Arbor, MI 48106

Copyright 1981

by

Teeters, Dale Carl

All RIghts Reserved

PLEASE NOTE:

In all cases this material has been filmed in the best possible way from the available copy. Problems encountered with this document have been identified here with a check mark __✓__.

1. Glossy photographs or pages _____
2. Colored illustrations, paper or print _____
3. Photographs with dark background _____
4. Illustrations are poor copy _____
5. Pages with black marks, not original copy _____
6. Print shows through as there is text on both sides of page _____
7. Indistinct, broken or small print on several pages __✓__
8. Print exceeds margin requirements _____
9. Tightly bound copy with print lost in spine _____
10. Computer printout pages with indistinct print _____
11. Page(s) _____ lacking when material received, and not available from school or author.
12. Page(s) _____ seem to be missing in numbering only as text follows.
13. Two pages numbered _____. Text follows.
14. Curling and wrinkled pages _____
15. Other _____

University
Microfilms
International

THE UNIVERSITY OF OKLAHOMA

GRADUATE COLLEGE

COMPARATIVE TEMPERATURE-DEPENDENT POLARIZED RAMAN STUDY OF LITHIUM POTASSIUM SULFATE, SODIUM POTASSIUM SULFATE, AND THE FAST ION CONDUCTOR LITHIUM SODIUM SULFATE

A DISSERTATION

SUBMITTED TO THE GRADUATE FACULTY

in partial fulfillment of the requirements for the degree of

DOCTOR OF PHILOSOPHY

BY

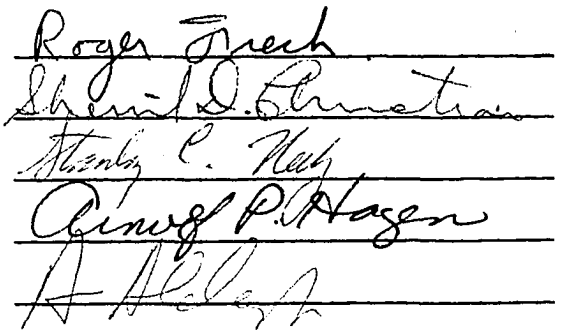
DALE CARL TEETERS

Norman, Oklahoma

1981

COMPARATIVE TEMPERATURE-DEPENDENT POLARIZED RAMAN STUDY OF LITHIUM POTASSIUM SULFATE, SODIUM POTASSIUM SULFATE, AND THE FAST ION CONDUCTOR LITHIUM SODIUM SULFATE

APPROVED BY



DISSERTATION COMMITTEE

© 1981

DALE CARL TEETERS

ALL RIGHTS RESERVED

Dedication

To mother and father

ACKNOWLEDGEMENTS

During my graduate work at the University of Oklahoma, I have been fortunate enough to have had interactions with many people who have been of inmeasurable help to me both personally and in my scientific work. I would like to acknowledge some of those people.

I would like to express my gratitude to Dr. Roger Frech for his guidance and support. Graduate study can be a very fruitful experience if one has a person of knowledge and integrity to learn from. I have been fortunate enough to have been associated with such an individual. I will always respect Dr. Frech as a scientist, leader, and as a caring individual.

I would like to thank Dr. Roger Frech and the National Science Foundation for financial assistance in the form of a research assistantship and the Chemistry Department of the University of Oklahoma for teaching assistantships. Fee waivers awarded to me by the Graduate College were also appreciated.

A preliminary low temperature Raman experiment was done at Oklahoma State University with the help of Dr. J. Paul Devlin. The far infrared reflection work presented in Chapter II was done at The Oak Ridge National Laboratory under the direction of Dr. John Bates. Appreciation is extended to both

these individuals and The Oak Ridge National Laboratory.

My first experiences in this research laboratory were made much more rewarding by Dr. Henry Nichols. As the senior graduate student at the time of my first endeavors in spectroscopy, he proved to be both an excellent teacher and friend. I extend my thanks to him.

My fellow graduate students have been extremely helpful by stimulating scientific thinking and by providing an enjoyable working atmosphere. I would particularly like to thank Mr. Charles Myers, Mrs. Echung Chiang Wang, and Mr. Mike Madden for their friendship and help.

I have had many helpful discussions with the faculty and post-doctoral fellows during my graduate career. I appreciate their time and suggestions.

Mr. Fred Dillon and Mr. Ron Stermer have been extremely helpful in repairing and maintaining research equipment. Mr. Denny Kolb, Miss Susan Wilburn, and Miss Dru Legate have all helped in proofreading, drawing various diagrams, typing, and by extending me friendship. To all these individuals I extend my gratitude.

The greatest source of encouragement and support that I have received has been from my mother and father. Their never ending love and faith in my ability have served as my inspiration for this work. I will never adequately be able to express my appreciation for all they have done for me, but in an effort to show my gratitude I dedicate this work to them with all my love.

TABLE OF CONTENTS

Page

LIST OF TABLES viii

LIST OF FIGURES x

Chapter

I. GENERAL INTRODUCTION 1

II. ROOM TEMPERATURE VIBRATIONAL SPECTROSCOPIC MEASUREMENTS AND MODE ASSIGNMENTS 17

III. TEMPERATURE-DEPENDENT RAMAN STUDY OF THE LITHIUM ION MODES IN LITHIUM POTASSIUM SULFATE AND LITHIUM SODIUM SULFATE 63

IV. EXTERNAL MODE TEMPERATURE DEPENDENCE OF LITHIUM SODIUM SULFATE, LITHIUM POTASSIUM SULFATE, AND SODIUM POTASSIUM SULFATE 93

V. INTERNAL MODE TEMPERATURE DEPENDENCE OF LITHIUM SODIUM SULFATE, LITHIUM POTASSIUM SULFATE, AND SODIUM POTASSIUM SULFATE 125

VI. SUMMARY OF CONCLUSIONS AND FUTURE STUDIES 159

ADDENDUM 166

LIST OF TABLES

TABLE		Page
2.1.	Crystallographic Data for $LiNaSO_4$	24
2.2.	Frequencies of Internal Optic Modes in $LiNaSO_4$	32
2.3.	Frequencies of External Optic Modes in $LiNaSO_4$	36
2.4.	Lithium Mode Frequencies in Isotopically Substituted $LiNaSO_4$ with Calculated Frequency Ratios	43
2.5.	Crystallographic Data for $LiKSO_4$	45
2.6.	Summary of Internal Mode Frequencies	47
2.7.	External Mode Frequencies in Isotopically Substituted $LiKSO_4$ with Calculated Frequency Ratios	50
2.8.	Crystallographic Data for $NaK_3(SO_4)_2$	55
2.9.	Internal Mode Frequencies in $NaK_3(SO_4)_2$	56
2.10.	External Mode Frequencies for $NaK_3(SO_4)_2$	57
3.1.	Calculated Activation Energies for Lithium Modes in $LiKSO_4$.	80

TABLE Page

3.2. Calculated Activation Energies for Lithium Modes in $LiNaSO_4$ 87

5.1. Frequencies of the ν_1 Modes for Various Lithium, Potassium, and Sodium Sulfate Crystals . . 156

6.1. Phase Transition and Melt Data for Li_2SO_4, $LiNaSO_4$, $LiKSO_4$, and $NaK_3(SO_4)_2$ 161

LIST OF FIGURES

FIGURE		Page
2.1.	The Geometry of the Raman Scattering Experiments . .	23
2.2.	Infrared Reflectivity Spectra of the ν_1 and ν_3 Spectral Region in $LiNaSO_4$.	25
2.3.	Raman Scattering from the ν_1 and ν_3 internal mode Region in $LiNaSO_4$	26
2.4.	Raman Scattering Spectra and Infrared Relfectivity Spectra of Internal Optic Modes in the ν_4 reqion in $LiNaSO_4$.	29
2.5.	Raman Scattering From the ν_2 Reqion and the Lithium Mode Region in $LiNaSO_4$	31
2.6.	Correlation Diagram for the External Modes in $LiNaSO_4$	33
2.7.	Raman Scattering from the External Mode Region in $LiNaSO_4$	35
2.8.	Raman Spectra of $^6LiNaSO_4$ and $^7LiNaSO_4$, A_1 Lithium Modes	38
2.9.	Infrared Relfectivity Spectra of $^6LiNaSO_4$ and $^7LiNaSO_4$, A_1Lithium Modes	39

FIGURE Page

2.10. Raman Spectra of $^{6}LiNaSO_4$ and $^{7}LiNaSO_4$, E Lithium Modes 40

2.11. Infrared Reflectivity Spectra of $^{6}LiNaSO_4$ and $^{7}LiNaSO_4$, E Lithium Modes 41

2.12. Raman Scattering From the External Mode Region of $LiKSO_4$ 48

2.13. Raman Spectra of Lithium Modes in $LiKSO_4$ 49

2.14. Raman Spectra of $^{6}LiKSO_4$ and $^{7}LiKSO_4$, E_2 Lithium Modes 52

2.15. Raman Spectra of $^{6}LiKSO_4$ and $^{7}LiKSO_4$, E_1 Lithium Modes 53

2.16. Correlation Diagram for the External Modes of $NaK_3(SO_4)_2$ 58

2.17. Raman Scattering from the External Mode Region in $NaK_3(SO_4)_2$ 59

3.1. High-temperature Raman Cell 66

3.2. Temperature-dependent Raman Scattering from the A and E_2 Lithium Modes in $LiKSO_4$ 68

3.3. Graph Showing a Typical Fit for Curve Resolving . . 70

3.4. Graph Showing Temperature-dependent Linewidth Data for the E_2 Lithium Mode in $LiKSO_4$ 71

3.5. Linewidth Versus Temperature Data for the A Lithium Mode of $LiKSO_4$ 72

FIGURE Page

3.6. Temperature-dependent Frequency Data for the E_2 and A Lithium Modes in $LiKSO_4$ 73

3.7. Temperature-dependent Linewidth Data for the E_2 Lithium Mode in Three Different Crystals 75

3.8. Curve Fitting Proceedure for the Lithium E_2 Mode Linewidth Data in $LiKSO_4$ 78

3.9. Curve Fitting Proceedure for the Lithium A Mode Linewidth Data in $LiKSO_4$ 79

3.10. Temperature-dependent Raman Scattering form the A_1 Lithium Modes in $LiNaSO_4$ 83

3.11. Temperature-dependent Raman Scattering from the E Lithium Modes in $LiNaSO_4$ 84

3.12. Normal Mode Linewidths of the Lithium Modes in $LiNaSO_4$ as a function of Temperature 85

3.13. Normal Mode Frequencies of the A_2 and E Lithium Modes in $LiNaSO_4$ as a Function of Temperature 86

4.1. Temperature-dependent Frequency Data for the External Modes in $LiNaSO_4$ 95

4.2. Temperature-dependent Raman Scattering from the A_1 Normal Mode Centered at 63 cm^{-1} in $LiKSO_4$ . . . 97

FIGURE Page

4.3. Raman Scattering at Temperatures just above and below the Phase Transition in $LiNaSO_4$ 98

4.4. Reduced Raman Spectra of the Resolved 63 cm^{-1} A_1 Mode in $LiNaSO_4$ at Various Temperatures 103

4.5. Temperature Dependence of the Low Frequency A_1 Mode Band Maximum in $LiNaSO_4$ 104

4.6. Raman Spectra of the Low Frequency A_1 Mode in $LiNaSO_4$ Corrected for Thermal Population Effects . 106

4.7. Orientational Contribution to the Bandwidth of the Low Frequency A_1 Mode in $LiNaSO_4$ 108

4.8. Temperature Dependence of the External Mode Frequencies in $LiKSO_4$ 109

4.9. Raman Spectra at Temperatures just above and below the Phase Transition in $LiKSO_4$ 111

4.10. Raman Spectra of the A Mode at 202 cm^{-1} in $LiKSO_4$ at varrious Temperatures 112

4.11. Temperature-dependent Frequency Data for the A 202 cm^{-1} Mode in $LiKSO_4$ 114

4.12. Temperature-dependent Linewidth Data for the A Mode at 202 cm^{-1} in $LiKSO_4$ 116

4.13. Temperature-dependent Frequency Data for the External Modes in $NaK_3(SO_4)_2$ 117

FIGURE Page

4.14. Temperature-dependent Raman Spectra of the External Modes in $NaK_3(SO_4)_2$ 119

4.15. Raman Spectra at Temperatures just above and below the Phase Transition in $NaK_3(SO_4)_2$ 120

5.1. Temperature-dependent Spectra of the ν_1 region in $LiNaSO_4$. 128

5.2. Temperature-Dependent Frequency Data for the A_1 Modes in the ν_1 Region in $LiNaSO_4$ 129

5.3. Temperature-dependent Frequency Data for the ν_2 Region E Mode in $LiNaSO_4$ 131

5.4. Temperature-dependent Raman Spectra of the A_1 Modes in the ν_3 Region in $LiNaSO_4$ 132

5.5. Temperature-dependent Raman Spectra of the E Modes in the ν_3 Region in $LiNaSO_4$ 133

5.6. Temperature-dependent Frequency Data for the Internal Modes in the ν_3 Region in $LiNaSO_4$ 134

5.7. Temperature-dependent Frequency Data for the Internal Modes in the ν_4 Region in $LiNaSO_4$ 136

5.8. Raman Spectra at various Temperatures for the A mode in the ν_1 Region in $LiKSO_4$ 137

5.9. Temperature-dependent Frequency Data for the A mode in the ν_1 Region in $LiKSO_4$ 139

5.10. Temperature-dependent Frequency Data for the E_1 Mode in the ν_2 region in $LiKSO_4$ 140

FIGURE Page

5.11. Temperature-dependent Raman Spectra of the E_1 Mode in the ν_3 Region in $LiKSO_4$ 141

5.12. Temperature-dependent Frequency Data for the ν_2 Region in $LiKSO_4$ 142

5.13. Temperature-dependent Frequency Data for the Modes in the ν_4 Region in $LiKSO_4$ 144

5.14. Raman Spectra at various Temperatures of the A_{1g} Mode in the ν_1 region in $NaK_3(SO_4)_2$ 146

5.15. Temperature-dependent Frequency Data for the A_{1g} Mode in the ν_1 Region in $NaK_3(SO_4)_2$ 147

5.16. Temperature-dependent Frequency Data for the E_g Mode in the ν_2 Region in $NaK_3(SO_4)_2$ 148

5.17. Raman Spectra at various Temperatures of the E_g Modes in the ν_3 Region in $NaK_3(SO_4)_2$ 150

5.18. Raman Spectra at various Temperatures of the A_{1g} Mode in the ν_3 Region in $NaK_3(SO_4)_2$ 151

5.19. Temperature-dependent Frequency Data for the Modes in the ν_3 Region in $NaK_3(SO_4)_2$ 152

5.20. Temperature-dependent Frequency Data for the Modes in the ν_4 Region in $NaK_3(SO_4)_2$ 153

COMPARATIVE TEMPERATURE-DEPENDENT POLARIZED RAMAN STUDY OF LITHIUM POTASSIUM SULFATE, SODIUM POTASSIUM SULFATE, AND THE FAST ION CONDUCTOR LITHIUM SODIUM SULFATE

CHAPTER I

GENERAL INTRODUCTION

Introduction

The development of new energy sources along with more efficient utilization of energy has been of prime importance in the 1970s and in the first few years of the 1980s. The importance of energy research and development to the United States can be appreciated if one looks at the funding for these areas. In 1976 federal funding for energy research and development totaled $2,231.6 million and was increased by 30 percent to $2,905.4 million dollars in 1977.[1]

One category of energy research that has received funding from such federal agencies as the Department of Energy and the National Science Foundation is the investigation of the fast ion conducting phenomenon in solids. Solids that have fast ion conducting properties are of

great commercial interest as solid electrolytes in high energy density batteries and in other technological applications such as fuel cells, electrochromic display elements, thermoelectric devices, memory elements, and measurement and control of liquid and gas compositions.[2-4] The use of fast ion conducting solids as solid electrolytes in batteries has received the most attention, however.

Prototype batteries using solid electrolytes already exist. These prototype solid electrolyte batteries can store four times the energy that a lead-acid battery of equal weight can, and can undergo three times as many charge-discharge cycles.[5] Companies such as General Motors, Ford Motor Company, TRW, and Toshiba Electric Company of Japan have established major research and development programs in this field of battery science.[6] Recently General Electric and Chloride Silent Power Ltd. of the United Kingdom merged their battery research programs to further develop batteries with solid electrolytes.[5]

Even with the numerous applications and potential applications of fast ion conducting solids, there is still a lack of basic understanding of the phenomenon. Much work needs to be done in the thermodynamic, kinetic, and structural aspects of the problem. At a microscopic level one would like to understand the dynamical behavior of the mobile ion species and how this mobile ion is affected by and interacts with the potential environment of the solid. The study

presented here is concerned with a vibrational spectroscopic investigation of a fast ion conducting sulfate system and two related non-conducting sulfates in an attempt to investigate the potential energy environment of the mobile species and the other dynamical processes in the crystal lattice.

Fast Ion Conduction in Solids

The fast ion transport phenomenon has been the subject of several reviews and books.[3,7-9] A material can be described as a solid electrolyte if an ionic conductivity of .1 ohm^{-1} $cm.^{-1}$ or more is observed. These solids usually have an activation energy for diffusion of approximately 0.1 eV. The concept of a liquid sublattice interpenetrating a rigid crystal lattice is usually associated with a fast ion conducting solid. Macroscopic evidence for this view usually involves some measure of increased disorder within the crystal.[10,11] O'Keeffe[11] has found that diffusion coefficients of the mobile ions (usually cations) in good solid electrolytes come close to those in molten salts. Other evidence for a liquid like sublattice is a high entropy increase at the phase transition which brings the material into the fast ion conducting phase. In many cases the entropy value for this transition is comparable to the value of the melting of salts which do not have solid-solid transitions. The use of transition entropies

has been proposed by van Gool for the screening of new fast ion conducting compounds.[12]

Structurally speaking, in order to have this liquid-like sublattice there must be available to the mobile ions more than the equivalent number of empty sites. Geller[13] has suggested that the ratio of available lattice sites to the number of charge carrying ions should not be less than 3. Also there must exist within the structure 2- or 3-dimensional branched pathways.[14] The concept of "pathways" has been studied in such compounds as $RbAg_4I_5$.[15]

Many materials have been discovered that meet the criteria listed above. Some compounds such as β-alumina have appreciable specific conductance at relatively low temperatures, while other compounds must go through a high temperature phase transition before they become fast ion conducting. McGeehin and Hooper's review[8] gives one of the most comprehensive lists of such compounds. Some of the most recently discovered fast ion conducting compounds can be found in papers presented at the 1981 International Conference on Fast Ion Transport in Solids.[4] Examples of fast ion conducting compounds are silver iodide and compounds based on silver iodide, β- and β"-alumina type compounds, and various sulfate salts. Many others are known.

The techniques used to study fast ion conducting compounds are also quite numerous. NMR and EPR,[16] x-ray crystallography,[13,17] and electrical conductivity and

diffusion measurements [18-20] are but a few of the methods employed. Many other techniques have been used, and reviews on these techniques are available.[3,7] Infrared and Raman spectroscopic techniques have also been applied to many fast ion conducting compounds and are discussed in the following section.

Infrared and Raman Studies of Fast Ion Conducting Compounds

An important aspect in understanding the fast ion conducting phenomenon is the examination of the dynamical behavior of the mobile ion species and how this is affected by the potential environment of the crystals. Both static and dynamical interactions of the mobile cations with the rest of the crystal lattice may be involved. Temperature-dependent vibrational spectroscopic measurements provide a means of investigating these areas.

One can view the mobile ionic species as being fixed in the crystal lattice at low temperatures, vibrating at a frequency indicative of the potential energy environment surrounding it. As the temperature of the system is raised the vibrational amplitude and the anharmonicity increase until the mobile ion species is able to "hop" to adjacent empty sites or interstitial regions. Viewing the phenomenon in this manner, one can see that vibrational spectroscopy

(infrared and Raman) can be very valuable in investigating the potential energy environment of the mobile species and in investigating other dynamical processes coupled with the motion of the conducting ion.

It has only been in the past ten years that both infrared and Raman spectroscopy have been used in the study of fast ion conducting compounds. Most of this work has been done on silver iodide, compounds related to silver iodide, or β or β"-alumina ($M_2O \cdot 11Al_2O_3$ and $M_2O \cdot XAl_2O_3$ respectively where M is usually an ion from Group IA or IB, but can be from group IIA[21] and X equals approximately 5 to 7).

Many studies have been done on AgI since it is considered the classical fast ion conductor.[8] Burns, Dacol, and Shafer[22] were the first to do temperature-dependent polarized Raman measurements at temperatures below and above the transition temperature (147°C) for the fast ion conducting phase. Early infrared studies of AgI from very low temperatures to 250°C did not produce a great deal of information on this first order phase transition.[23-25]. However, Burns et al. observed the Raman intensity below 80 cm^{-1} to greatly increase at temperatures above the transition. They attributed this to disorder in the system which breaks down the Raman selection rules. Fontana and Mariotto and their co-workers[26-31] have recently performed many temperature-dependent Raman studies on AgI. Temperature-dependent bandwidth data, intensity data, depolarization

ratios, and frequency values have led them to believe that a partial disordering of the silver ions (mobile ions) occurs below the phase transition followed by more disorder at the transition into the fast ion conducting phase. Their Raman studies indicate another disordering of the silver ions at approximately 430°C. This disordering of an ionic species is consistent with the description of the fast ion conducting phenomenon given previously.

Various compounds based on silver iodide have also been the subject of infrared and Raman spectroscopic studies. Shriver, Joy and Greig[32] did one of the first temperature-dependent Raman spectroscopic comparisons between two fast ion conducting compounds, $Ag_2[HgI_4]$ and $Cu_2[HgI_4]$, and the non-fast ion conducting $Tl_2[HgI_4]$. They found that the fast ion conducting compounds have vibrational bands that broadened considerably with temperature. A drastic broadening of corresponding bands in $Tl_2[HgI_4]$ was not found. Shriver et al. attributed this broadening to disorder in the system. The compounds $RbAg_4I_5$ and KAg_4I_5 were found to have a much different type of Raman temperature dependence than AgI in a study done by Burns, Dacol and Shafer.[33] They found no abrupt changes in the Raman spectra for $RbAg_4I_5$ and $KAgI_5$ except for the disappearance in both compounds of a small mode at approximately 23 cm^{-1} when the transition into the high temperature phase occurred. Delaney and Ushioda[34] also made a comparison between temperature-dependent Raman

data for AgI and $RbAg_4I$ and found that some modes in the two compounds have bandwidths which have a similar temperature dependence. Modes in $Ag_{26}I_{18}W_4O_{16}$ below 100 cm^{-1} were found to have strong temperature dependence in a study done by Habbal, Zvirgzda and Scott,[35] while modes at higher frequencies were not temperature dependent. Habbal et al. feel that these low energy vibrations are associated with heavy, loosely bound silver ions. Similar low frequency modes have been observed in other fast ion conducting compounds containing silver.[23,34]

Of all fast ion conducting compounds β and β"-alumina type compounds have been the object of the greatest number of spectroscopic investigations. No doubt this is because of their great commercial importance.[5] Early studies on these compounds utilized infrared spectroscopy to observe the vibrations due to the mobile ion species.[36,37] Using these vibrational frequencies, Allen and Remika[36] calculated attempt frequencies for ionic motion and compared these values to diffusion coefficients for the system. The data indicated that a single ion hopping motion was responsible for ionic conductance. Chase et al.[38,39] investigated these same modes by Raman scattering and discussed the possible existence of two superlattices in β-alumina.[39]

Other studies include those done by Bates and Frech[40] who found that the intensities of low frequency modes in sodium and silver β-alumina decreased drastically with

temperature and postulated that a second-order phase transition involving a redistribution of mobile cations over available lattice sites could be occurring. They were also the first to work out the infrared and Raman selection rules for β- and β"-alumina type structures.[41] Bates and his coworkers have also looked at the translational modes of ammonium ions doped into β-alumina in hopes of investigating the potential energy environment of the conduction plane.[42] They have substituted $^{6}Li^{+}$ ions into the lattice for $^{7}Li^{+}$ in order to study lithium-oxygen interactions[43] and also looked at low frequency modes in β"-alumina which they feel are attempt modes for ionic conduction.[44] Colomban and Lucazeau[45] noticed unusual band broadening for modes associated with various cations in their temperature-dependent Raman studies. They felt that their results indicated a transition from an ordered state at low temperatures to a state where the conducting cations are dynamically disordered at higher temperatures.

The presence of water in β-alumina has been found to have effects on fast ion conduction in these compounds. Infrared[46] and Raman studies[47] have been performed on β-aluminas containing water molecules in order to understand the effects that water molecules have on fast ion conduction in this system. It is certain that the β- and β"-alumina compounds will be the object of many more studies in the future.

One group of fast ion conducting compounds has not been the subject of temperature-dependent vibrational spectroscopy, however. Sulfate compounds such as Li_2SO_4,[48] $LiAgSO_4$,[49] $LiZnSO_4$,[50] and $LiNaSO_4$[51] all have reported fast ion conducting phases, yet no Raman studies have been done on these compounds. Raman studies on these sulfate systems could provide basic insight into the fast ion conducting phenomenon for several reasons. First, they are simple stoichimetric compounds. The complexity and the non-stoichiometry of β- and β"-alumina type compounds make Raman studies difficult. The sulfate systems should be much easier to characterize. Second, comparisons between the fast ion conducting $LiNaSO_4$ with $LiKSO_4$ and $NaK_3(SO_4)_2$, which are structurally similar at room temperature but do not have a fast ion conducting phase, could be very interesting. Third, Nilsson, Thomas and Tofield[52] have suggested that a new type of diffusion mechanism exists where ionic motion can be enhanced by rotational motion of the translationally static sulfate ions. Temperature-dependent Raman spectroscopy would seem to be an ideal way to study this dynamically enhanced ionic diffusion mechanism.

Outline of the Study

The goal of this study was to perform a temperature-dependent Raman study of $LiNaSO_4$, $LiKSO_4$, and $NaK_3(SO_4)_2$. Before temperature-dependent work could be done a thorough vibrational study of the compounds at room temperature was necessary, however. Raman spectroscopy was used to make vibrational band assignments for the external modes of $LiKSO_4$ and $NaK_3(SO_4)_2$. Both infrared reflection studies and Raman scattering were used to assign both the internal and external modes of $LiNaSO_4$. The results from this work are discussed in Chapter II.

Chapter III reports temperature-dependent Raman work on modes consisting predominantly of lithium ion motion in $LiKSO_4$ and $LiNaSO_4$. This is particularly important in understanding the dynamics of the cation species and the interaction of the species with the ordered crystal lattice for the fast ion conductor $LiNaSO_4$ and the non-fast ion conductor $LiKSO_4$. Measurements of temperature-dependent frequencies and bandwidths were made and used in calculations of activation energies.

The temperature dependence of the external modes not of lithium ion origin in $LiNaSO_4$, $LiKSO_4$, and $NaK_3(SO_4)_2$ is dealt with in Chapter IV. Assignments of certain modes as sulfate librational modes and as modes containing translational contribution are suggested. Contributions to the

bandwidth of a sulfate librational mode directly related to the phase transition in $LiNaSO_4$ is also investigated.

Chapter V looks at the Raman temperature dependence of the internal modes in the three sulfate systems. This data provides information concerning the sulfate sublattice as it undergoes the phase transition in the three sulfate salts.

Finally, Chapter VI summarizes the work presented here and comments on possible areas for future studies.

REFERENCES

1. A National Plan for Energy Research, Development and Demonstration: Creating Energy Choices for the Future (Energy Research and Development Administration, 1976), Vol. 1, p. 10.

2. R. A. Huggins, Electrochem. Acta 22, 773 (1977).

3. K. P. Jagannathan, S. K. Tiku, H. S. Ray, A. Ghosh, and E. C. Subbarao, in Solid Electrolytes and Their Applications, edited by E. C. Subbarao (Plenum Press, New York, 1980).

4. Proceedings of the 1981 International Conference on Fast Ion Transport in Solids, in Solid State Ionics (to be published).

5. Chem. Eng. News 59 (21), 5 (1981).

6. M. L. Kyle, E. J. Cairus, and D. S. Webster, in Energy and Man: Technical and Social Aspects of Energy, edited by M. G. Morgan (IEEE Press, 1975), p. 312.

7. Solid Electrolytes, edited by P. Hagenmuller and W. Van Gool (Academic Press, New York, 1978).

8. P. McGeehin and A. Hooper, J. Mater. Sci. 12, 1 (1977).

9. Superionic Conductors, edited by G. D. Mahan and W. L. Roth (Plenum Press, New York, 1976).

10. M. O'Keeffe, in Fast Ion Transport in Solids, edited by W. Van Gool (North-Holland Publ., Amsterdam, 1973), p. 233.

11. M. O'Keeffe, in Superionic Conductors, edited by G. D. Mahan and W. L. Roth (Plenum Press, New York, 1976), p. 101.

12. W. Van Gool, in Phase Transitions, edited by H. K. Henisch, R. Roy, and L. E. Cross (Pergamon, Oxford, 1974), p. 373.

13. S. Geller, Acc. Chem. Res. 11, 87 (1978).

14. W. Van Gool, in Solid Electrolytes, edited by H. K. Hagenmuller and W. Van Gool (Academic Press, New York, 1978), p. 9.

15. S. Geller, Sci. 157, 310 (1967).

16. J. L. Bjorkstam and M. Villa, Magn. Reson. Rev. 6, 1 (1980).

17. A. Kahn, P. Columban, and J. P. Biolot, J. Solid State Chem. 33, 149 (1980).

18. H. Rickert, in Fast Ion Transport in Solids, edited by W. Van Gool (North-Holland Publ., Amsterdam, 1973), p. 3.

19. Y. Haven, in Fast Ion Transport in Solids, edited by W. Van Gool (North-Holland Publ., Amsterdam, 1973), p. 35.

20. A. D. LeClaire, in Fast Ion Transport in Solids, edited by W. Van Gool (North-Holland Publ., Amsterdam, 1973), p. 51.

21. B. Dunn, R. M. Ostrom, R. Seevers, and G. C. Farrington, Solid State Ionics (to be published).

22. G. Burns, F. H. Dacol and M. W. Safer, Solid State Commun. 19, 291 (1976).

23. G. L. Bottger and A. L. Geddes, J. Chem. Phys. 46, 3000 (1967).

24. W. Jost, K. Funke, and A. Jost, Z. Naturforsch. A 25, 983 (1970).

25. P. Bruesch, S. Strassler, and H. R. Zeller, Phys. Status Solidi A 31, 217 (1975).

26. A. Fontana, G. Mariotte, M. Montagna, V. Capozzi, E. Cazzanelli, and M. P. Fontana, Solid State Commun. 28, 35 (1978).

27. G. Mariotto, A. Fontana, E. Cazzanelli, and M. P. Fontana, Phys. Status Solidi B 101, 341 (1980).

28. A. Fontana, G. Mariotto, and M. P. Fontana, Phys. Rev. B 21, 1102 (1980).

29. G. Mariotto, A. Fontana, E. Cazzanelli, F. Rocca, M. P. Fontana, V. Mazzacurati and G. Signorelli, Phys. Rev. B. 23, 4782 (1981).

30. A. Fontana, G. Mariotto, E. Cazzanelli, F. Rocca, and M. P. Fontana, Solid State Commun. (to be published).

31. E. Cazzanelli, A. Fontana, G. Mariotto, F. Rocca, V. Mazzacurati, G. Ruocco, and G. Signorelli, Solid State Ionics (to be published).

32. D. F. Shriver, G. Joy III, and D. Greig, J. Electrochem. Soc. 123, 588 (1976).

33. G. Burns, F. H. Dacol, and M. W. Shafer, Solid State Commun. 19, 287 (1976).

34. M. J. Delaney and S. Ushioda, Solid State Commun. 19, 297 (1976).

35. F. Habbal, J. A. Zvirgzds, and J. F. Scott, J. Chem. Phys. 69, 4984 (1978).

36. S. J. Allen, Jr. and J. P. Remeika, Phys. Rev. Lett. 33, 1478 (1974).

37. R. D. Armstrong, P. M. A. Sherwood, and R. A. Wiggins, Spectrochem. Acta, Part A 30A, 1213 (1974).

38. L. L. Chase, C. H. Hao, and G. D. Mahan, Solid State Commun. 18, 401 (1976).

39. C. H. Hao, L. L. Chase, and G. D. Mahan, Phys. Rev. B 13, 4306 (1976).

40. J. B. Bates and R. Frech, Chem. Phys. Lett. 50, 401 (1977).

41. J. B. Bates and R. Frech, Chem. Phys. Lett. 50, 89 (1977).

42. J. B. Bates, T. Kaneda, and J. C. Wand, Solid State Commun. 25, 629 (1978).

43. T. Kaneda, J. B. Bates, and J. C. Wand, Solid State Commun. 28, 469 (1978).

44. J. B. Bates, T. Kaneda, W. E. Brundage, J. C. Wang, and H. Engstrom, Solid State Commun. 32, 261 (1979).

45. P. Colomban and G. Lucazeau, J. Chem. Phys. 72, 1213 (1980).

46. P. Colomban and A. Novak, Solid State Commun. 32, 467 (1979).

47. J. B. Bates, R. Frech, H. Engstrom, J. C. Wang, and T. Kaneda, Solid State Ionics 1, 15 (1980).

48. A. Kvist, Z. Naturforsch. A 22, 208 (1969).

49. H. Øye, Thesis, Trondhein (1963).

50. K. Schroeder, Thesis, Göteborg (1975).

51. A.-M. Josefson and A. Kvist, Z. Naturforsch A 24, 466 (1969).

52. L. Nilsson, J. O. Thomas, and B. C. Tofield, J. Phys. C 13, 6441 (1980).

CHAPTER II

ROOM TEMPERATURE VIBRATIONAL SPECTROSCOPIC MEASUREMENTS AND MODE ASSIGNMENTS

Introduction

In order to perform a thorough temperature-dependent Raman study on $LiNaSO_4$, $LiKSO_4$, and $NaK_3(SO_4)_2$, a complete symmetry-based vibrational mode assignment for the three crystals was necessary. Polarized Raman spectroscopic studies of precisely oriented single crystals were performed. A polarized infrared reflectivity study of $LiNaSO_4$ complemented the Raman work. Normal mode assignments for the three crystals were based on these studies.

Knowledge of the space group of the crystal, the site occupancies and symmetries in the unit cell,[1] and the application of group theory techniques for crystalline systems[2-4] allowed the number of normal modes belonging to each symmetry species in the crystals to be obtained. This symmetry-based analysis was done for the internal and external modes in each crystal.

The internal or "molecular" vibrational modes in a crystal correspond to intramolecular motion of a polyatomic

group. They are usually only weakly perturbed by the crystal lattice and thus the frequency of these vibrations usually does not change very much from the solid to the gas or in solution. The free sulfate ion which has T_d point group symmetry has nine vibrational normal modes corresponding to intramolecular vibrations. The irreducible symmetry representations for these normal modes is $\Gamma_{vib} = A_1+E+2T_2$.[5] By convention ν_1 is assigned to the mode belonging to the one dimensional representation A_1, ν_2 to the mode belonging to the two dimensional representation E, and ν_3 and ν_4 to the modes of the three dimensional representation T_2. A description of the normal coordinates can be found in Herzberg.[6] The frequencies of these modes are approximately $\nu_1 = 980$ cm^{-1}, $\nu_2 = 451$ cm^{-1}, $\nu_3 = 1104$, and $\nu_4 = 613$.[6]

When a polyatomic ion is in its free state, its vibrations are dependent on symmetry restrictions based on its intrinsic point group symmetry. When this same ion is in a crystal lattice its vibrations depend on the symmetry of the potential-energy environment about it, i.e., the site symmetry. The vibrational analysis can now be based only on the symmetry of the site assuming that there is no dynamical interactions between this ion and the ones surrounding it.

The assumption that no interaction occurs between an ion occupying a site in a crystal and the ions about it is not correct for most ionic crystals, however. One must

consider all ions in the crystal in order to adequately describe the vibrational modes. In the case of Brillouin zone center modes in which all unit cells are in phase one considers the entire set of ions in just one unit cell as the vibrating unit. Thus the allowed vibrations are characterized by the symmetry operations of the unit cell. The space group of the unit cell supplies the symmetry information needed for a vibrational analysis in this case. This technique is called the factor group analysis and along with the site group analysis describes the number and symmetry of modes expected for a polyatomic ion in a crystalline environment. A combination of the site group and factor group treatment is used for the internal mode analysis of the sulfate ion in these crystal systems. This technique is described in more detail in other works.[2-4]

External Modes

External or lattice modes correspond to motions of the ions as rigid entities within the crystal lattice. In the case of the sulfate crystals being studied here, these motions would consist of a superposition of the translational motion of the lithium, potassium, sodium, and sulfate ions plus rotational motion of the sulfate ion. Because the forces holding polyatomic ions together (covalent forces) are usually stronger than the force holding ionic crystals

together (coulombic attractions), the external mode vibrational frequencies are normally much lower than those of internal vibrations, i.e., they are decoupled from the internal modes. This separation of frequencies is not always so clear cut as will be shown later, however.

The decoupling of the internal and external modes allows the external mode vibrational analysis to be conducted separately from the internal mode analysis.[7] The external mode analysis is based on the assumption that the ion is a rigid entity and that the vibrations of the ions are dependent on the symmetry of the site (site group) and the symmetry of the unit cell (factor group).

A symmetry based internal and external mode analysis was done for $LiNaSO_4$. In the case of $LiKSO_4$ and $NaK_3(SO_4)_2$ the internal mode analysis had previously been done; hence only the external modes are treated here. Raman band assignments are based on these analyses.

Experimental

Single crystals of $LiNaSO_4$, $LiKSO_4$, and $NaK_3(SO_4)_2$ were grown by slow evaporation from aqueous solutions containing equimolar proportions of the appropriate salts (reagent grade $Li_2SO_4 \cdot H_2O$, Na_2SO_4, and K_2SO_4). Lithium potassium sulfate and $NaK_3(SO_4)_2$ were grown in solutions at temperature from 32° to $42^{\circ}C$. Lithium sodium sulfate

was grown in an aqueous solution at 70°C to which sulfuric acid had been added to bring the solution to pH 2. Single crystals of $^{6}LiNaSO_4$ and $^{7}LiKSO_4$ were grown in the same manner as described above beginning with crystalline $^{6}Li_2SO_4 \cdot H_2O$ which was prepared from $^{6}LiOH$ (95% atom %) by titrating with H_2SO_4 to pH 2.5 and slow evaporation of the resulting solution.

The optic axis (c axis) for all three crystal systems was identified with a polarizing microscope allowing polarized Raman and infrared reflection measurements to be performed on crystals of known orientation. The infrared reflectivity measurements in $LiNaSO_4$ were made from a crystal face containing the c axis which was cut and polished using a slurry of 3 μ Al_2O_3 in ethanol. For the Raman studies, appropriate crystal faces were cut and polished in a similar manner. In a reflectivity measurement of the E modes in $LiNaSO_4$ the incident radiation is polarized perpendicular to the optic axis ($\varepsilon \perp C$), while in a measurement of the A_1 modes the incident radiation is polarized parallel to the optic axis ($\varepsilon \parallel C$).

The $LiNaSO_4$ infrared reflectivity spectra of the internal mode region were measured at room temperature on a Beckman IR-12 spectrometer with a reflection accessory which provided a 2 to 1 linear image reduction at an average angle of incidence of 15°. Infrared reflectivity data for the region from 500 to 150 cm^{-1} were collected on

a Fourier transform spectrometer at the Oak Ridge National Laboratory using a 6μ mylar filter and a MIR source. Raman spectra were recorded at room temperature on a Spex Ramalog 5 spectrometer with a 2 cm^{-1} spectral bandpass using the 4880 Å line of an argon in laser for excitation at 200-600 mw. The geometrical arrangement of the Raman scattering experiment is shown in Figure 2.1.

Lithium Sodium Sulfate: Infrared and Raman Data

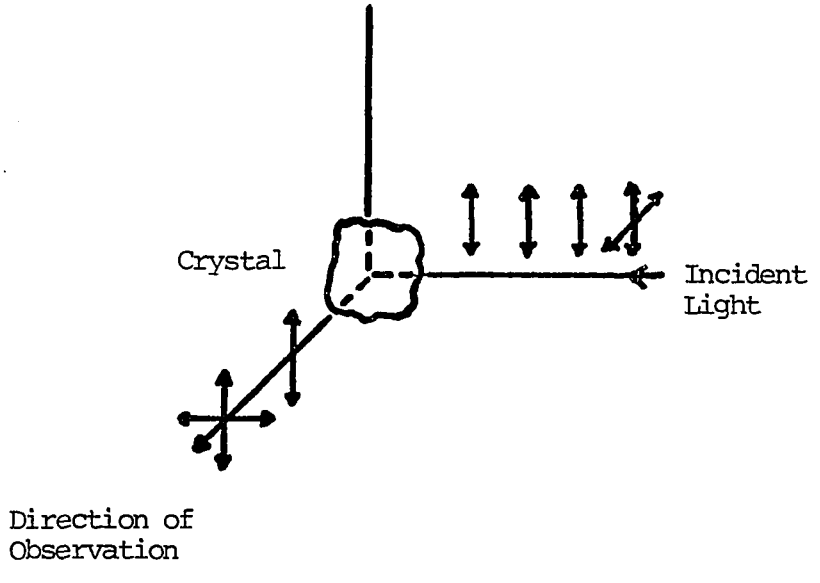
Internal Optic Modes

Lithium sodium sulfate crystallizes in the P31c space group (C_{3v}^4) with 6 molecular units in a hexagonal cell of dimension a_o = 7.627 Å and c = 9.8579 Å.[8] The important crystallographic data are listed in Table 2.1.

The correlation diagram for the internal modes using a technique reviewed by Fateley et al.[2] is given below. The irreducible representations for the sulfate internal vibrational modes are found to be $\Gamma_{int} = 9A_1 + 9A_2 + 18E$. The A_1 and E modes are both infrared and Raman active, while the A_2 are not optically observable modes.

Figures 2.2 and 2.3 show the polarized infrared reflection and Raman spectra of the ν_1 and ν_3 region of the sulfate ion internal modes. The symmetry-based vibrational analysis of this system predicts that the ν_1 region should

FIGURE 2.1. The Geometry of the Raman Scattering Experiments: A Raman scattering experiment can be described by the symbol $\alpha(\beta\gamma)\delta$ where α is the direction of the incident light, β is the polarization of the incident light, γ is the polarization of the scattered light, and δ is the direction of the scattered light. Here α,β,γ, and δ are the cartesian coordinates x,y, or z; alternatively they are the crystal axes a, b, or c.



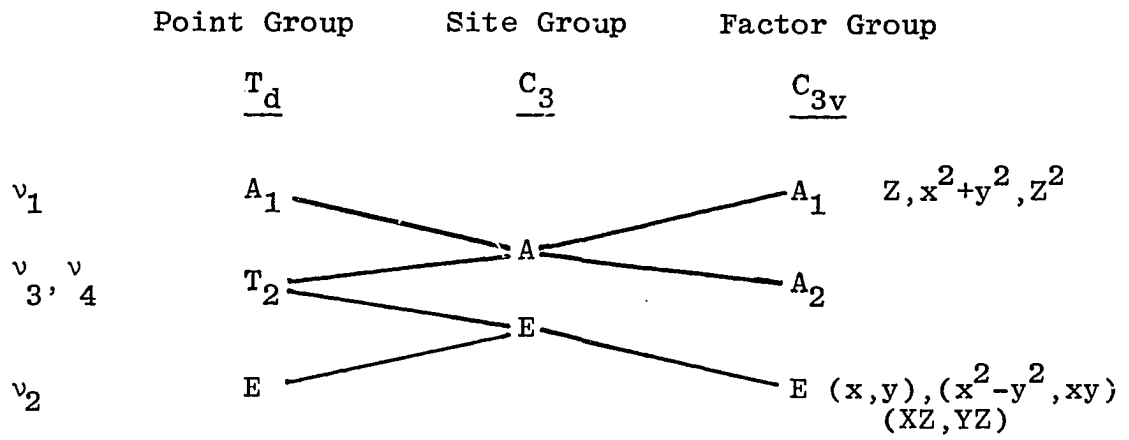


TABLE 2.1

CRYSTALLOGRAPHIC DATA FOR $LiNaSO_4$[a]

Atom	Sites Occupied[b]	Site Symmetry
Li	6c	E
Na	6c	E
S(1)	2a	C_3
S(2)	2b	C_3
S(3)	2b	C_3

[a]Reference 1.

[b]Number of equivalent sites and Wyckoff notation.

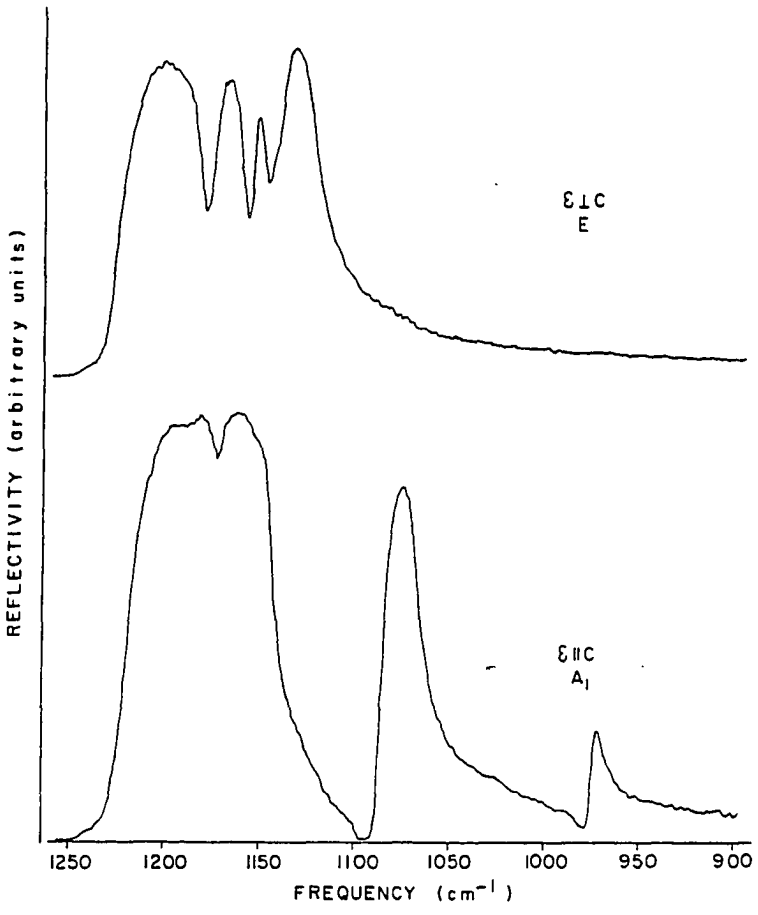


FIGURE 2.2. Near normal incidence reflectivity spectra of the internal optic modes in the ν_1 and ν_3 spectral region.

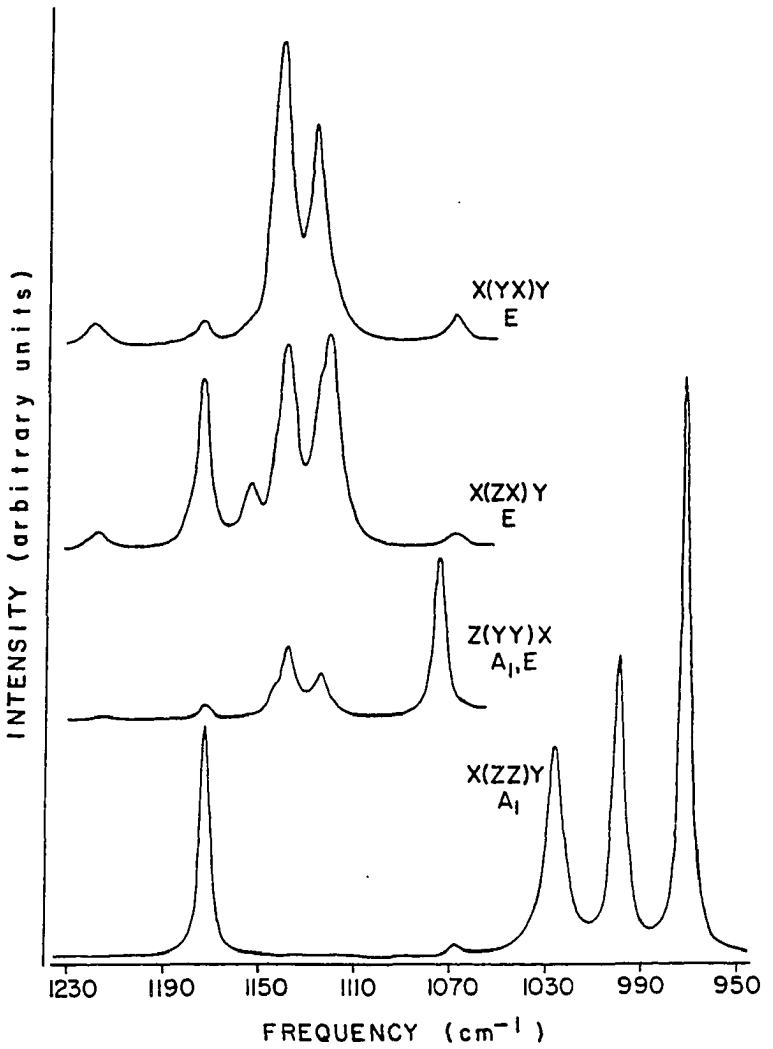


FIGURE 2.3. Raman scattering from the ν_1 and ν_3 internal optic mode region. Full scale intensity is 2×10^5 cps in the x(zz)y observation, 1×10^5 cps in z(yy)x, 1×10^4 in x(zx)y, and 2×10^4 in x(yx)y.

have three modes of A_1 type symmetry. These modes are observed at 972, 990 and 1026 cm^{-1}. A measurement with $z(xx)\bar{z}$ scattering geometry in which only longitudinal optical (LO) modes (modes whose vibrational displacement is parallel to the wave propagation in the lattice) are allowed shows modes at 974, 998 and 1026 cm^{-1}. The mode at 972 is identified as a transverse optical (TO) mode (mode whose vibrational displacement is perpendicular to the wave propagation in the lattice) while the mode at 974 is an LO mode. The modes at 998 and 1026 have no TO-LO splitting. Modes with a small or no TO-LO splitting have been observed in the ν_1 region in other sulfate crystals.[9,10] The infrared reflection spectra in this region show only one small band centered at approximately 970 cm^{-1}.

The ν_3 region should have 3 modes of A_1 symmetry and 6 modes of E symmetry. Modes in the Raman spectra at 1066, 1146 (very weak) and 1173 cm^{-1} are assigned as the ν_3 (A_1) modes. In the backscattering $z(xx)\bar{z}$ geometry a peak occurs at 1086 cm^{-1}. These frequencies correspond very closely to the inflection points observed in the infrared reflection spectra in this region. Therefore the bands at 1066, 1146, and 1173 are assigned as TO modes while the modes at 1086 is assumed to be an LO mode. The bands at 1075, 1125, 1138, 1153, and 1218 cm^{-1} in the Raman spectra are assigned to ν_3 (E) modes. The infrared spectrum shows no reflection band in the region of the 1075 cm^{-1} Raman mode; however the

three predicted $\nu_3(A_1)$ modes have been accounted for and thus the 1075 cm^{-1} mode must be assigned as a $\nu_3(E)$ mode. All the Raman bands in the 1100-1190 cm^{-1} range correspond to inflection points on the low frequency sides of infrared reflectivity bands in a rather complicated infrared spectrum for this region and are thus felt to be the TO modes. However, the frequency of the Raman mode at 1218 cm^{-1} is close to the inflection point on the high frequency side of a reflectivity band in the infrared spectrum and is assumed to be an LO mode. Therefore five of the six predicted $\nu_3(E)$ modes are identified.

The factor group multiplet resulting from ν_4 is predicted to have six E modes and three A_1 modes. Figure 2.4 shows the infrared and Raman spectra in the ν_4 region. Modes of A_1 symmetry were found at 635, 653, and 662 cm^{-1}. In Figure 2.4 the infrared reflectivity spectrum of the $\nu_4(A_1)$ modes is displayed directly above the Raman spectra of $\nu_4(A_1)$. The Raman modes match well with low frequency inflection points in the infrared spectrum and are thus identified as TO modes. Only four modes are seen in the Raman spectra of the $\nu_4(E)$ region and occur at 625, 645, 647, and 662 cm^{-1}. The 647 cm^{-1} mode is observed in an x(yx)y scattering geometry and is not shown here. The mode at 662 cm^{-1} is "leakage" from the A_1 mode at this frequency. The modes at 625 and 647 cm^{-1} are assigned as a TO mode and an LO mode, respectively, that correspond to

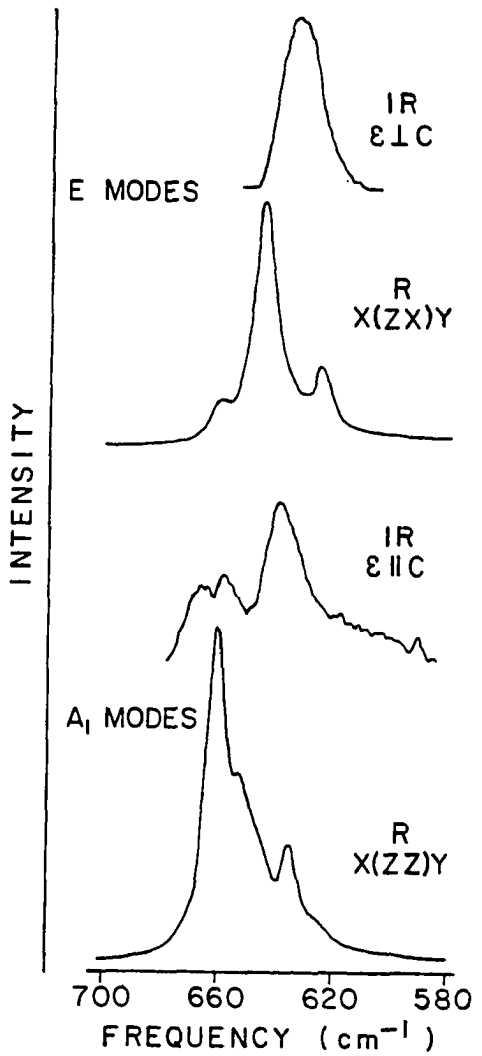


FIGURE 2.4. Raman scattering spectra and infrared near normal incidence reflectivity spectra of the internal optic modes in the ν_4 region. Full scale intensity for the Raman x(zx)y experiment is 2×10^4 cps and for x(zz)y, 5×10^4 cps.

the infrared reflectivity inflection points at 625 cm^{-1} and 650 cm^{-1} (Figure 2,4). The mode at 645 cm^{-1} in the Raman spectra is not observed in the infrared spectra. Based on the intensity of this mode as shown in Figure 2.4 it is assumed to be a TO mode. The four remaining $\nu_4(E)$ modes are not observed.

The Raman spectra for the ν_2 region are shown in Figure 2.5. Although a symmetry-based vibrational analysis predicts six modes all of E type symmetry, only one large peak at 483 cm^{-1} and a small shoulder at 476 cm^{-1} are seen. The infrared spectrum in this region which is not shown exhibits a very weak reflection band whose inflection points are 485 and 505 cm^{-1}. Thus the Raman mode at 483 is assigned as a TO mode. The shoulder at 476 is not seen in the infrared spectrum, but is believed to be a TO mode. All of the experimental data for the internal optic modes are summarized in Table 2.2.

External Optic Modes

The correlation diagram for the external modes of $LiNaSO_4$ was obtained using the same technique as described previously[2] and is shown in Figure 2.6. The irreducible representations for each ionic motion are $\Gamma_{trans}\ (Li^+) = \Gamma_{trans}\ (Na^+) = \Gamma_{trans}\ (SO_4) = \Gamma_{rot}\ (SO_4^=) = 3A_1 + 3A_2 + 6E$. The irreducible representations for all the external modes

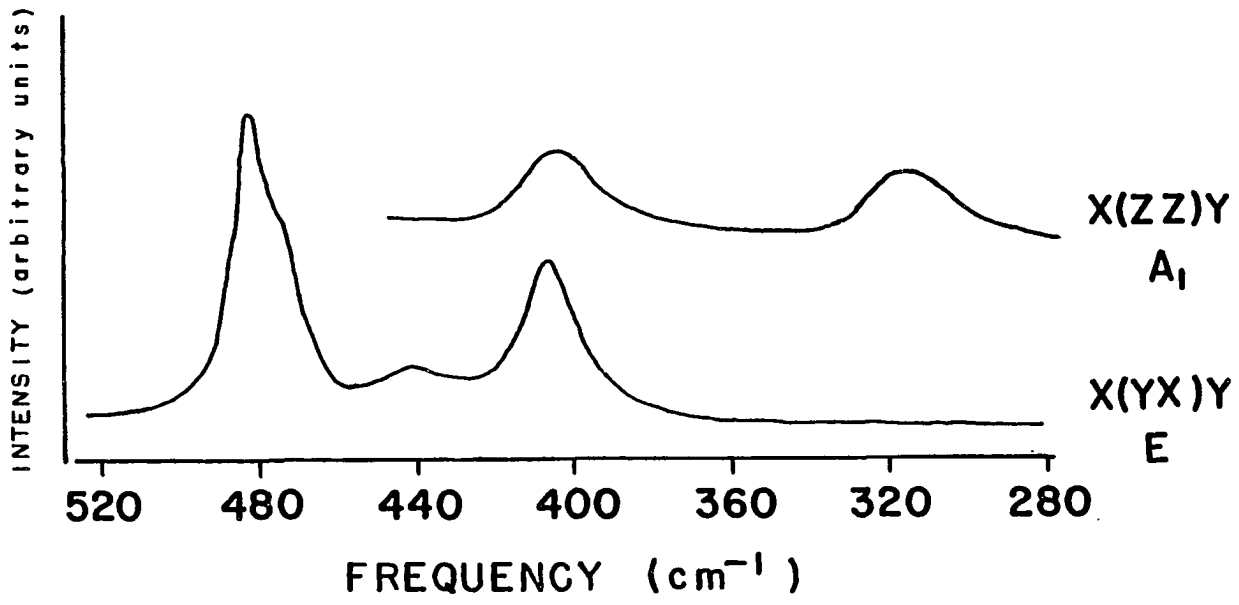


FIGURE 2.5. Raman scattering spectra from the ν_2 internal optic mode region and the high frequency A_1 and E external modes. Full scale intensity is 5000 cps.

TABLE 2.2

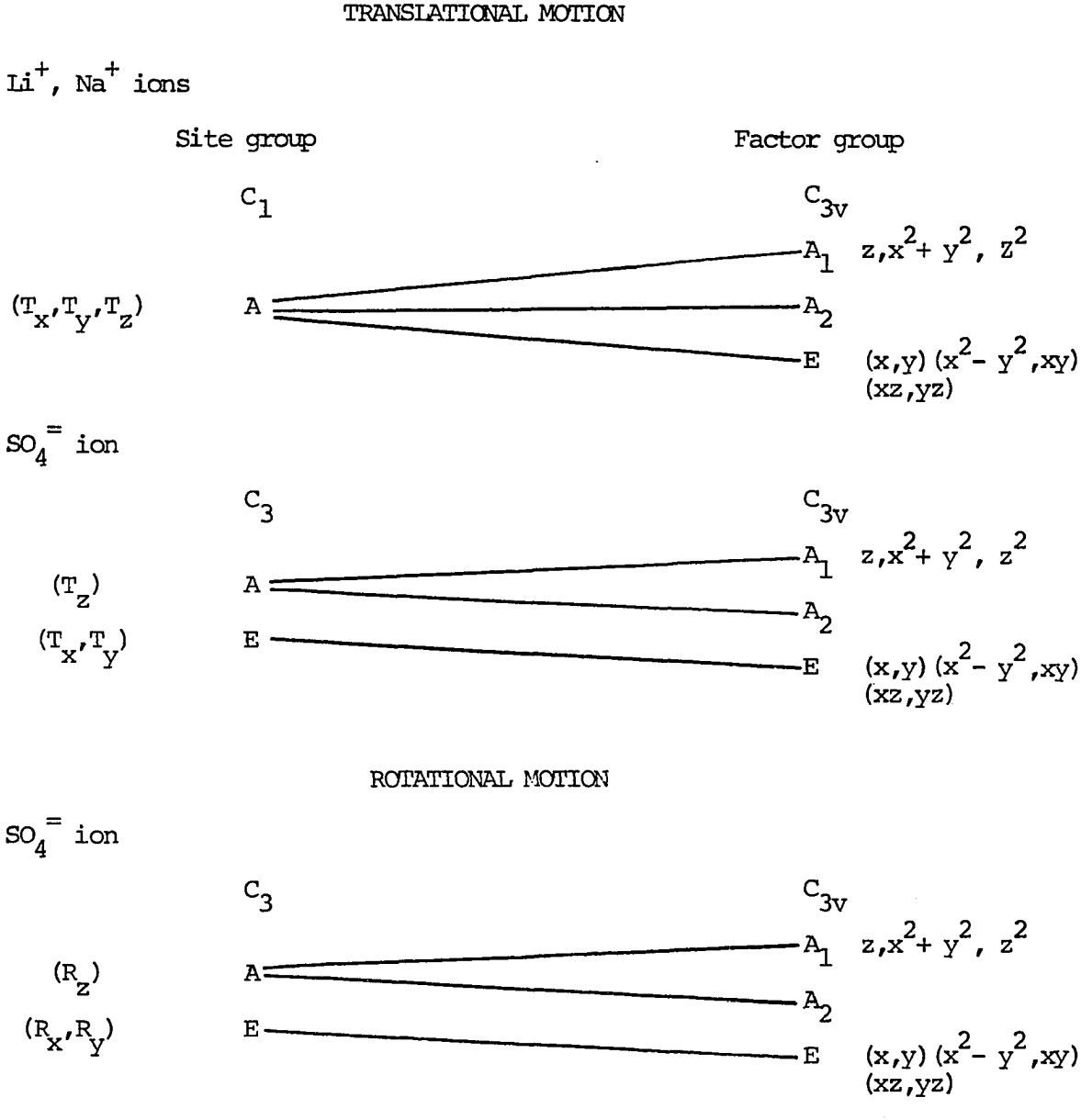
FREQUENCIES (in cm^{-1}) OF INTERNAL OPTIC MODES

Mode	Raman				Infrared	
	TO	Experimental Geometry	LO	Experimental Geometry	Transverse	Longitudinal
$\nu_1(A_1)$	972	x(zz)y	974	z(xx)$\bar{z}$	966	977
	998	x(zz)y	998	z(xx)$\bar{z}$	...	...
	1026	x(zz)y	1026	z(xx)$\bar{z}$	...	...
$\nu_2(E)$	476	x(yz)y	...		...	...
	483	x(yz)y	...		485	505
$\nu_3(A_1)$	1066	x(zz)y	1086	z(xx)$\bar{z}$	1066	1085
	1146	x(zz)y	...		...	...
	1173	x(zz)y	...		...	...
$\nu_3(E)$	1075	z(yy)x	...		...	...
	1120	x(zx)y	...		1120	1141[a]
	1125	x(yx)y	...		...	...
	1138	x(yx)y	...		1140[a]	1158[a]
	1153	x(zx)y	...		1158[a]	1180[a]
	...		1218	x(yx)y	1183[a]	1225[a]
$\nu_4(A_1)$	635	x(zz)y	...		632	665
	653	x(zz)y	...		...	...
	662	x(zz)y	...		660[a]	683
$\nu_4(E)$	625	x(zx)y	647	x(yx)y	625	650
	645	x(zx)y	...		...	...

[a]These inflection points are difficult to estimate due to the complexity of the infrared spectrum.

FIGURE 2.6. Correlation Diagram for the External modes of $LiNaSO_4$

Space group P31c (C_{3v}^4) Z = 2



must be $\Gamma_{ext} = 12A_1 + 12A_2 + 24E$. Eliminating the acoustic modes which are not optically observable one writes $\Gamma_{ext\ opt} = 11A_1 + 12A_2 + 23E$.

In Figure 2.5 one observes not only the $\nu_2(E)$ component at 483 cm^{-1} but several atypically high frequency external modes in both A_1 and E experimental geometries. The A_1 modes occur at 314 and 404 cm^{-1}. Figure 2.7 shows the Raman spectra of the lower frequency A_1 and E external modes. The A_1 mode at 109 and 155 cm^{-1} are very close in frequency to the modes at 108 and 156 which are assigned as E modes and could be attributed to "leakage." However, the discrimination between different polarizations in this particular set of measurements was quite good and it is felt that the proximity of the A and E_1 components here is due to a small factor group splitting. The reflectivity band inflection point frequencies and the Raman frequencies for the external modes are summarized in Table 2.3.

Isotopically Substituted $LiNaSO_4$

Hiraishi, Taniguchi, and Takahashi[11] observed atypically high frequency external modes in $LiKSO_4$ in the 300-450 cm^{-1} range, similar to those observed here in $LiNaSO_4$. They postulated that these modes in $LiKSO_4$ could be due to the lithium ion translational motion. To verify that these high frequency external modes in $LiNaSO_4$ were due to the lithium ions $^6LiNaSO_4$ crystals were grown and

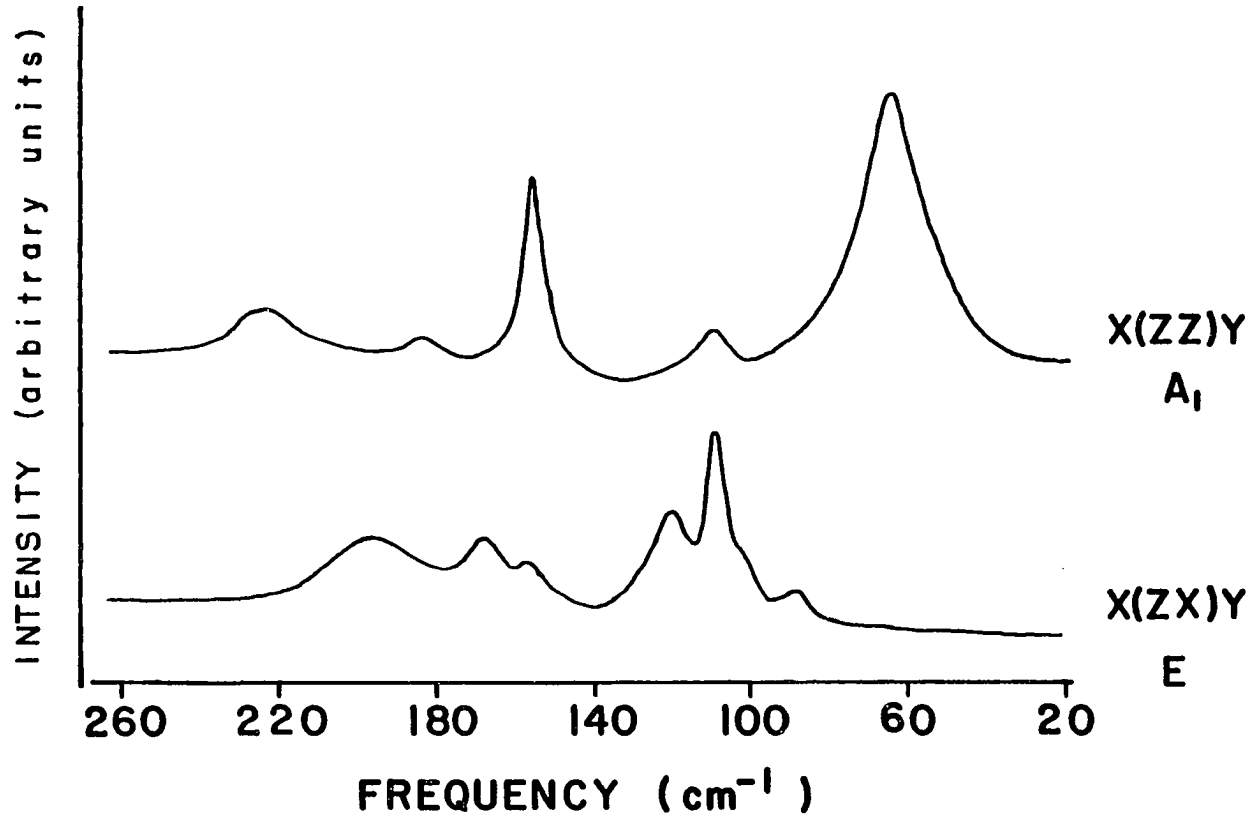


FIGURE 2.7. Raman scattering spectra from the external mode region. Full scale intensity is 5000 cps.

TABLE 2.3

FREQUENCIES (cm^{-1}) OF EXTERNAL OPTIC MODES

Mode Type	Raman Frequencies (cm^{-1}) x(zz)y Experimental Geometry	Infrared Frequencies (cm^{-1})$\varepsilon \parallel C$ TO(ifp)	LO(ifp)
A_1	63	...	...
	109	...	...
	155	...	...
	182	184	232
	223	...	...
	...	290	332
	314	...	...
	404	389	433

Mode Type	Raman Frequencies (cm^{-1}) x(zx)y Experimental Geometry	Infrared Frequencies (cm^{-1})$\varepsilon \parallel C$ TO(ifp)	LO(ifp)
E	87	...	...
	100	...	...
	108	...	...
	119	...	...
	156	...	...
	167	177	201
	196	...	...
	...	270	...
	440 (LO)	378	439
	406	...	...

spectroscopically studied. One would expect that those modes consisting primarily of lithium ion motion would shift to higher frequencies upon substitution of ^{6}Li for the naturally abundant ^{7}Li in $LiNaSO_4$. The isotopic frequency shifts confirm the higher frequency external modes as modes primarily involving motion of the lithium ion. These modes will be characterized as "lithium modes" although it should be clearly understood that vibrational decoupling is not complete, and these modes contain an admixture of various other types of ionic motion. Isotopic shifts were not observed for any other external modes. In Figure 2.8 the A_1 lithium modes at 314 cm^{-1} and 404 cm^{-1} are easily identified. The frequency assignments are given here for the naturally abundant $LiNaSO_4$ crystal. The features centered at 480 cm^{-1} originate in the ν_2 internal optic mode multiplet structure. The high frequency shoulder which appears in the $^{6}LiNaSO_4$ spectrum is due to an LO component of one of the ν_2 modes. The infrared reflectivity spectra in Figure 2.9 confirm the assignment at 404 cm^{-1} and show an additional lithium mode at 290 cm^{-1}. An E lithium mode is noted in Figure 2.10 at 406 cm^{-1}. The mode at 440 cm^{-1} is probably an LO mode since a comparison with the reflectivity spectra in Figure 2.11 shows a high frequency inflection point at this frequency. Lithium modes at 270 cm^{-1} and 378 cm^{-1} and also seen in Figure 2.11.

The irreducible representations of the lithium ion vibrational motion are $3A_1 + 3A_2 + 6E$. Thus the three A_1

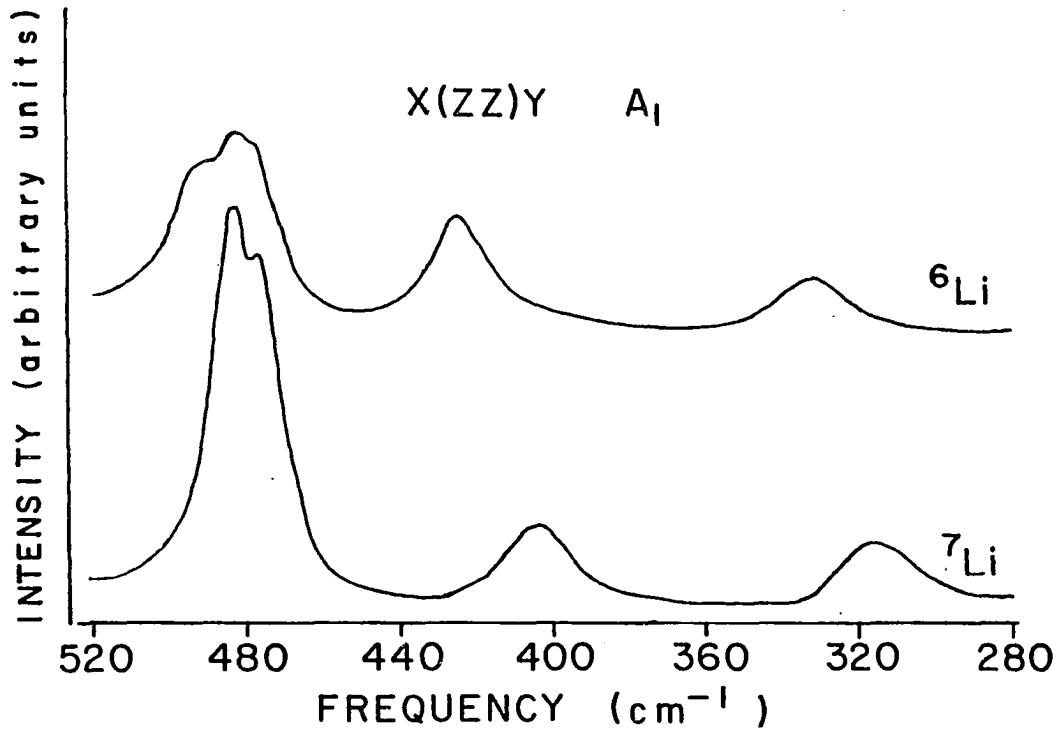


FIGURE 2.8. Raman spectra of $^{6}LiNaSO_4$ and $^{7}LiNaSO_4$ showing the isotopic shift of the lithium A_1 modes. Full scale intensity is 5000 cps.

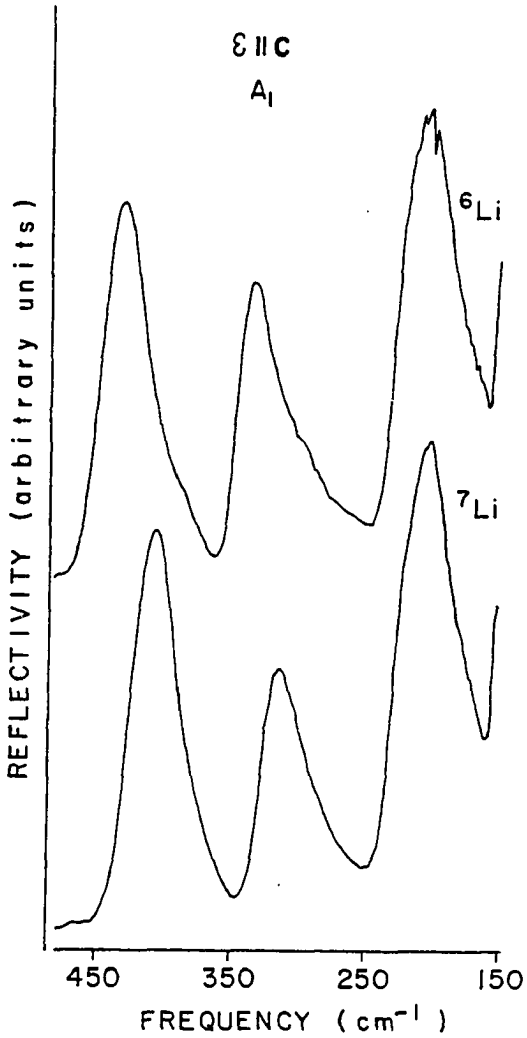


FIGURE 2.9. Infrared reflectivity spectra of $^{6}LiNaSO_4$ and $^{7}LiNaSO_4$ showing the isotopic shift of the lithium A_1 modes.

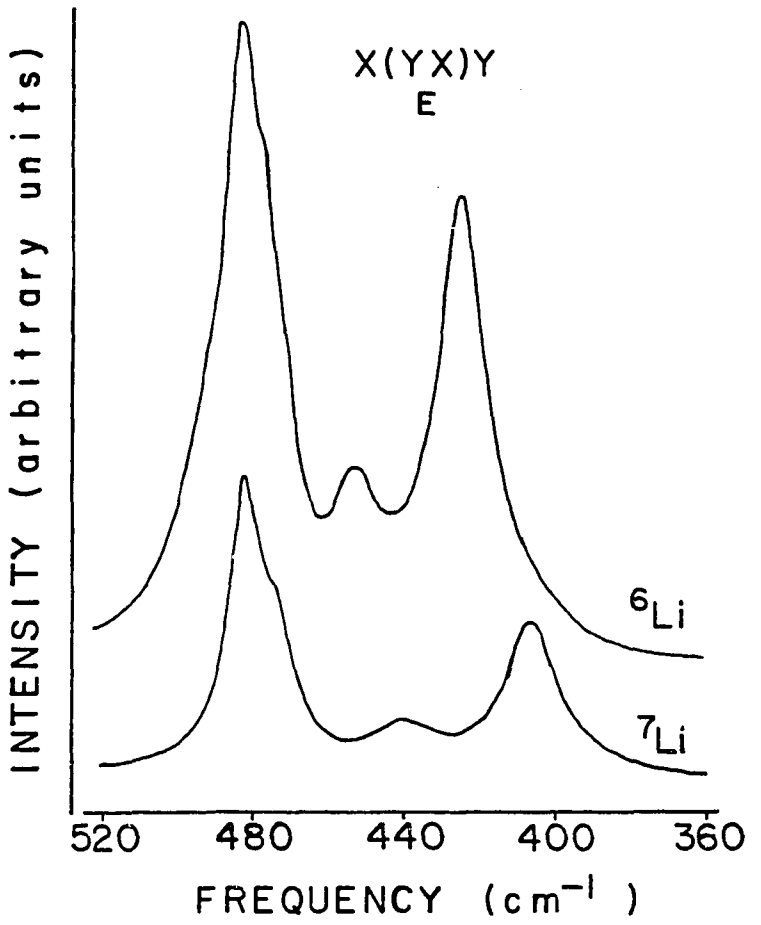


FIGURE 2.10 Raman spectra of $^6LiNaSO_4$ and $^7LiNaSO_4$ showing the isotopic shift of the lithium E modes. Full scale intensity is 5000 cps.

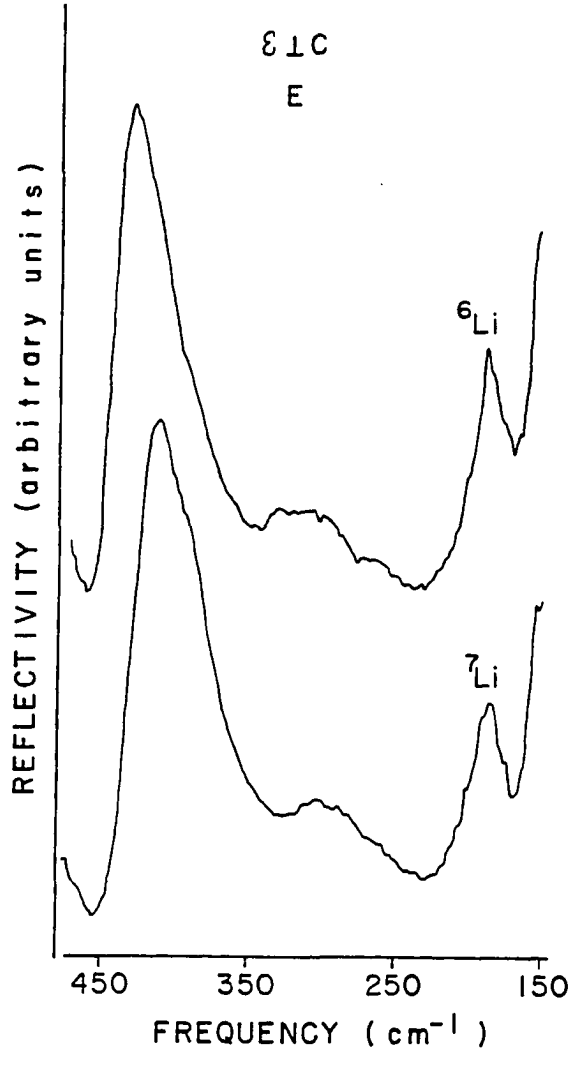


FIGURE 2.11. Infrared reflectivity spectra of $^{6}LiNaSO_4$ and $^{7}LiNaSO_4$ showing the isotopic shift of the lithium E modes.

lithium modes are found, however, only three of the expected six E lithium modes are identified. A summary of these data are presented in Table 2.4.

No internal modes shifted in frequency in the isotopically substituted crystal.

Discussion

All nine of the expected A_1 internal modes were observed in the Raman spectra while only nine of the expected eighteen E internal modes were found. The remaining E modes are probably not seen due to the small magnitudes of the polarizability derivatives and hence the scattering intensities. The infrared bands in the ν_1 and ν_2 regions are very weak which undoubtedly results from the small dipole moment derivatives. Similar behavior in the ν_1 and ν_2 regions of other sulfate crystals has been previously observed.[9]

Of the eleven A_1 and twenty-three E external modes expected, eight A_1 and ten E modes are observed in the Raman and infrared spectra. Again the absenceses of Raman modes are attributed to small polarizability derivatives while the absenceses of infrared modes are due to small dipole moment derivatives. Some of the Raman band maxima for the E modes do not match well with inflection points in the corresponding infrared reflection spectra in the external mode region. Hiraishi,

TABLE 2.4

LITHIUM MODE FREQUENCIES (in cm^{-1}) IN ISOTOPICALLY SUBSTITUTED $LiNaSO_4$ WITH CALCULATED FREQUENCY RATIOS

A_1 Modes	Raman		$\nu(^6Li)/\nu(^7Li)$	
$^7LiNaSO_4$	$^6LiNaSO_4$			
314	332		1.06	
404	425		1.05	
	Infrared			
TO(ifp) - LO(ifp)	TO(ifp) - LO(ifp)			
290 332	308 355		1.06	1.07
389 433	413 459		1.06	1.06

E Modes	Raman			
$^7LiNaSO_4$	$^6LiNaSO_4$			
406	425		1.05	
440	453		1.03	
	Infrared			
$^7LiNaSO_4$	$^6LiNaSO_4$			
TO(ifp) - LO(ifp)	TO(ifp) - LO(ifp)			
270 ...	281 ...		1.04	
378 439	395 453		1.05	1.03

Taniguchi and Takahashi[11] found that the damping constants for $LiKSO_4$ in the external mode region were relatively large. It seems reasonable to assume that the damping constants in $LiNaSO_4$ for the external mode region are also relatively large and cause the discrepancies between the TO frequencies as determined from the Raman band maxima for these E modes and the corresponding infrared reflectivity band inflection points.

The isotopic substitution experiments clearly identify the external modes in the 300-450 cm^{-1} spectral region as originating in Li^+ motion. The expected isotope shift in the harmonic approximation assuming pure Li^+ translational motion is $\nu(^6Li)/\nu(^7Li) = 1.08$. The calculated values for the frequency ratios are listed in Table 2.4 and suggest that the lithium modes are relatively decoupled from the other external modes.

Lithium Potassium Sulfate:

Raman Data

Lithium potassium sulfate crystallizes in a $P6_3$ (c_6^6) space group with two molecules per unit cell.[12] Crystallographic data of importance is listed in Table 2.5.

The internal mode symmetry based analysis and Raman band assignments have been made by several groups. Hirashi, Taniguchi, and Takahashi[11] assigned the internal

TABLE 2.5

CRYSTALLOGRAPHIC DATA FOR $LiKSO_4$[a]

Atom	Site Occupied[b]	Site Symmetry
Li	2b	C_3
K	2a	C_3
S	2b	C_3

[a]Reference 12.

[b]Number of equivalent sites and Wyckoff notation.

modes of $LiKSO_4$ and calculated damping constants for these vibrational bands. In an earlier study Mathieu, Couture, and Poulet[13] were primarily concerned with variations in intensity and frequency as a function of crystal orientation. In their assignment of internal modes, modes at 443 cm^{-1} and 402 cm^{-1} are incorrectly identified as internal optic modes. Rao et al.[10] studied the ν_1, ν_3, and ν_4 internal optic modes in $LiKSO_4$. Wu and Frech[9] also studied the internal optic modes, calculating molecular parameters from observed LO-TO splittings using a molecular dipole model. The internal mode symmetry-based analysis is not repeated here since it is given in reference nine. The irreducible representations for the internal modes are $\Gamma_{int} = 3A + 3B + 3E_1 + 3E_2$. The A and E_1 modes are Raman and infrared active while the E_2 mode is only Raman active

and the B modes are not optically observable. A summary of the internal mode frequencies is found in Table 2.6.

External Modes

The external mode assignments for $LiKSO_4$ have been made by Hiraishi et al.[11] and Mathieu et al.[13] In Mathieu's et al. work, several external modes were incorrectly assigned as internal modes. Hiraishi et al.[11] have worked out the symmetry-based vibrational mode analysis for the external vibrations. The irreducible representations for each ionic motion are $\Gamma_{trans}(Li^+) = \Gamma_{trans}(K^+) = \Gamma_{trans}(SO_4) = \Gamma_{rot}(SO_4^=) = A + B + E_1 + E_2$. The irreducible representations for the external modes after elimination of the A and E_1 acoustic modes are $\Gamma_{ext\ opt} = 3A + 4B + 3E_1 + 4E_2$. The A and E_1 modes are Raman and infrared active while E_2 is only Raman active and B modes are not optically observable. The Raman external mode spectra are shown in Figures 2.12 and 2.13. In this study all of the modes reported by Hiraishi et al.[11] were observed as well as one additional E_1 mode at 43 cm^{-1}. Three A, two E_1, and four E_2 modes are thus observed leaving only one E_1 mode unaccounted for. The frequencies for these modes agree well with Hiraishi et al. and are listed in Table 2.7.

TABLE 2.6

SUMMARY OF INTERNAL MODE FREQUENCIES (cm^{-1}) FOR $LiKSO_4$

Intramolecular Mode	Symmetry	Frequency (cm^{-1})	Reference
ν_1	A	1017	9
		1008	10
		1012	11
ν_2	E_1	465	9
		467	11
	E_2	463	9
		464	11
	A	1119	9
		1119	10
		1120	11
ν_3	E_1	1112	9
		1117	10
		1119	11
	E_2	1115	9
		1119	11
ν_4	A	626	9
		622	10
		623	11
	E_1	633	9
		634	10
		635	11
	E_2	631	9
		636	11

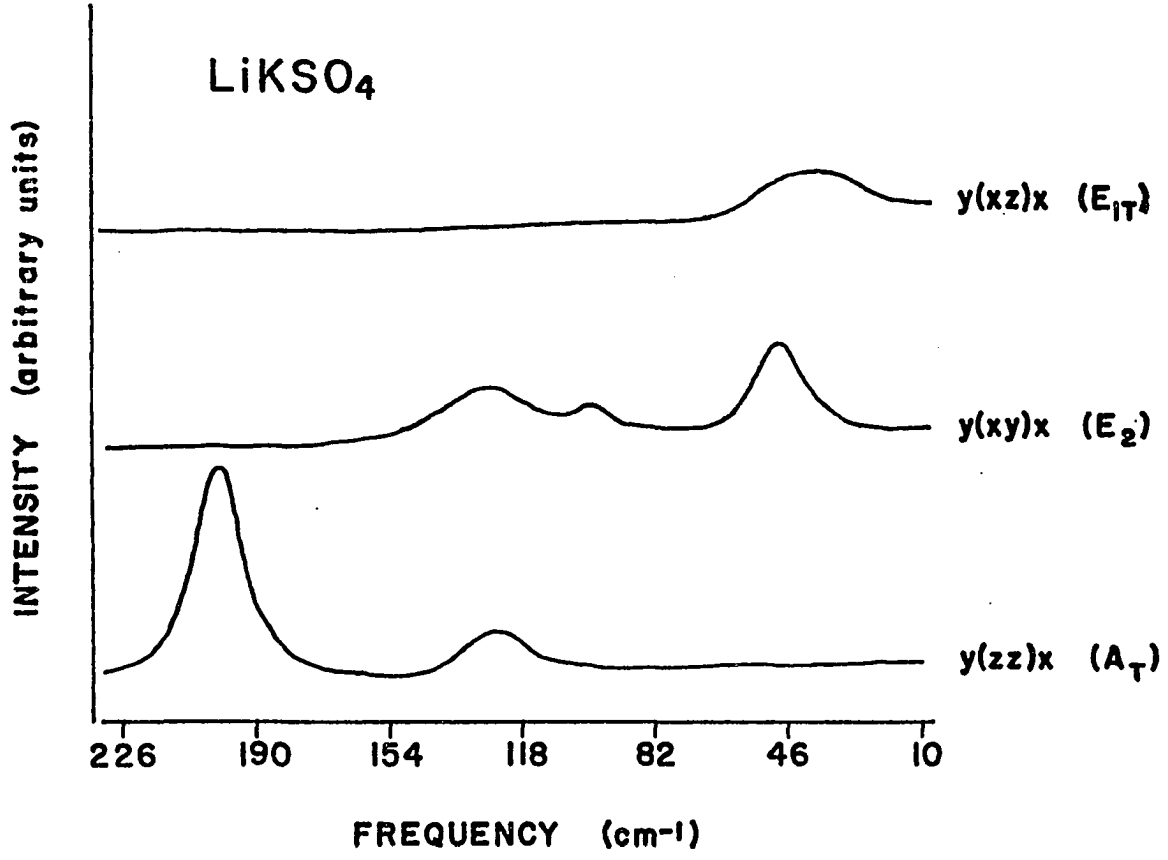


FIGURE 2.12. Raman scattering from the external mode region of $LiKSO_4$. Full scale intensity is 5000 cps.

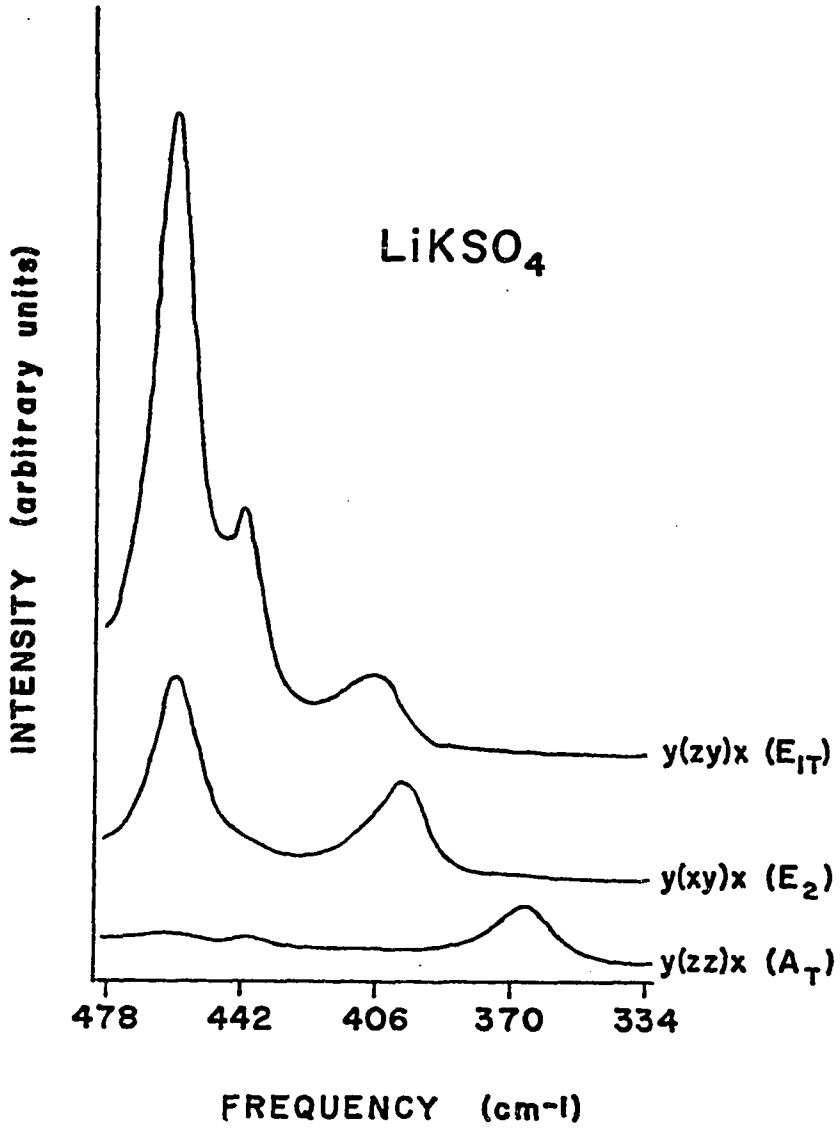


FIGURE 2.13. Raman spectra showing the atypically high frequency external modes. Full scale intensity is 5000 cps.

TABLE 2.7

EXTERNAL MODE FREQUENCIES (IN cm^{-1}) IN ISOTOPICALLY SUBSTITUTED $LiKSO_4$ WITH CALCULATED FREQUENCY RATIOS

Symmetry of Mode	Frequency (cm^{-1})		$\nu(^6Li)/\nu(^7Li)$
	$^7LiKSO_4$	$^6LiKSO_4$	(Expected $[m(^7Li)/m(^6Li)]^{\frac{1}{2}} = 1.08$)
A_T	128	128	...
	202	202	...
	370	395	1.07
E_1	43	43	...
	410	429	1.05
	445 (LO)	449	1.01
E_2	53	53	...
	103	103	...
	130	130	...
	404	421	1.04

Isotopically Substituted $LiKSO_4$

Hiraishi et al.[11] postulated that the modes around 400 cm^{-1} in $LiKSO_4$ were due to lithium ion motion. Modes in this same frequency region were also observed in $LiNaSO_4$ (see Isotopically Substituted $LiNaSO_4$, this chapter). Therefore crystals of $^6LiKSO_4$ were grown and Raman spectra of the modes in the 400 cm^{-1} region were compared with similar spectra of naturally abundant $LiKSO_4$. The spectra for $^6LiKSO_4$ and $^7LiKSO_4$ are shown in Figures 2.14 and 2.15.

The external mode frequencies of $^6LiKSO_4$ and $^7LiKSO_4$ are listed in Table 2.7. From the observed shifts, one can assume that the A mode at 370, the E_1 modes at 410 and 445 (longitudinal optic mode), and the E_2 mode at 404 cm^{-1} are primarily due to lithium ion motion. Assuming pure Li^+ translational motion and the harmonic approximation, the expected isotopic shift is $\nu(^6Li)/\nu(^7Li) = 1.08$. The calculated values of the frequency ratios are listed in Table 2.7 and indicate that these modes are relatively decoupled from the other external modes.

The ν_2 mode was the only internal vibrational band affected by the substitution of ^6Li for ^7Li in the crystal lattice. Its frequency shifted from 464 to 470 cm^{-1}. This would seem to indicate coupling between the (ν_2) asymmetric bending motion of the sulfate ion and translational motion of the lithium ions.

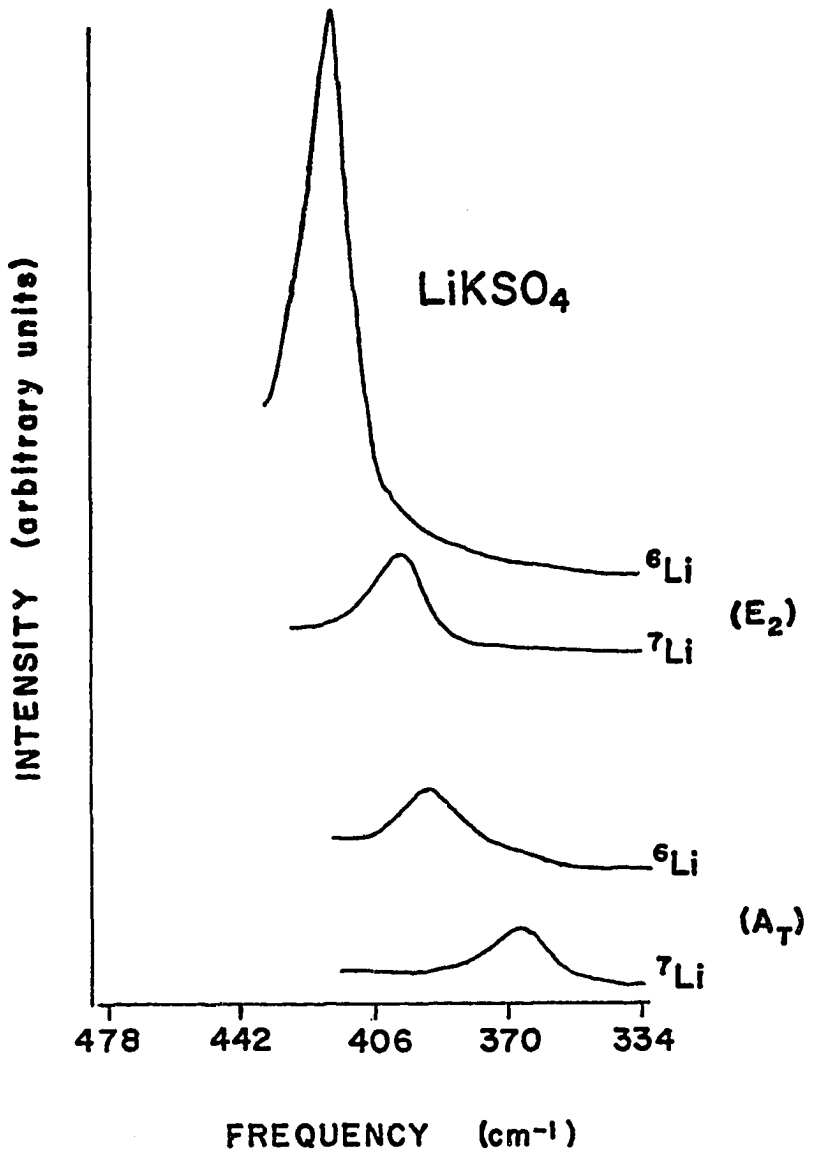


FIGURE 2.14. Raman spectra of $^{6}LiKSO_4$ and $^{7}LiKSO_4$ showing the isotopic shift of the lithium E_2 and A modes. Full scale intensity is 5000 cps.

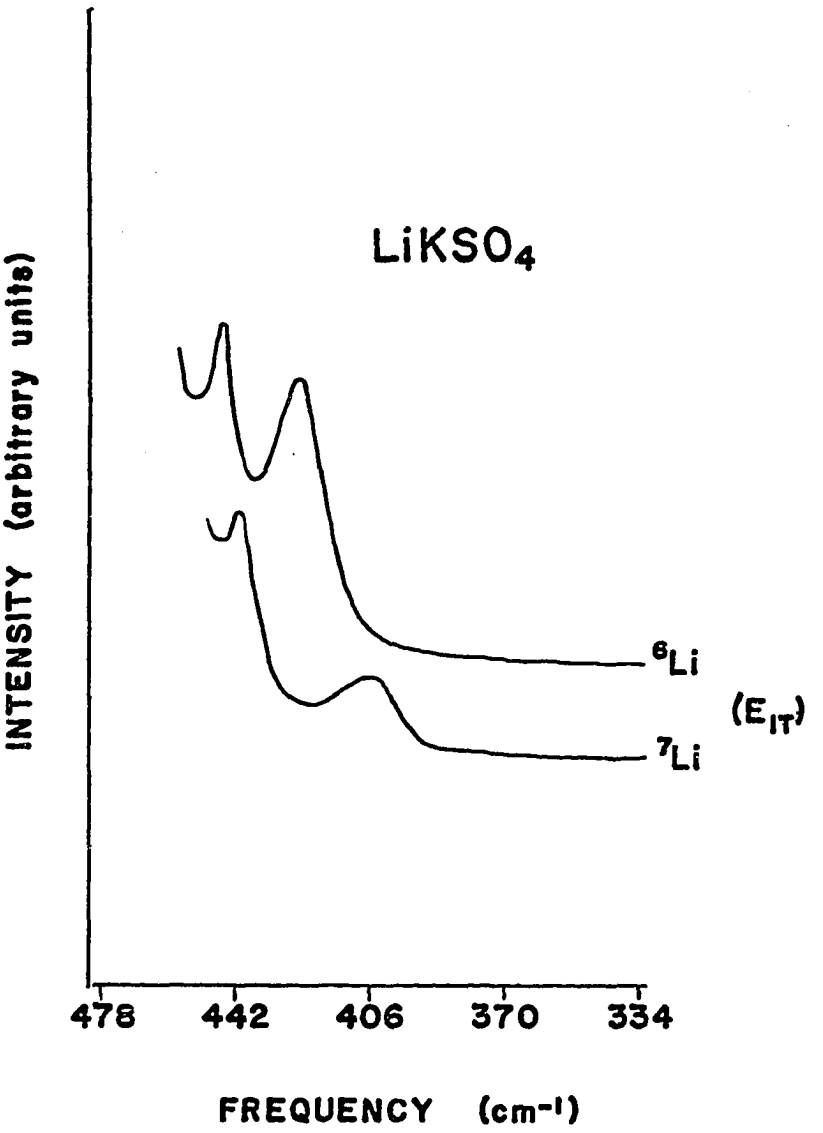


FIGURE 2.15. Raman spectra of $^{6}LiKSO_4$ and $^{7}LiKSO_4$ showing the isotopic shift of the lithium E_1 modes. Full scale intensity is 5000 cps.

Discussion

All of the internal modes of $LiKSO_4$ have been assigned in previous studies.[9,11] One additional external mode was observed in this study. One external mode of E_1 type symmetry was not observed. This is probably due to the weak scattering intensity of this mode caused by a small polarizability derivative. High frequency external modes were determined to result predominantly from lithium ion motion. From the shift observed in the ν_2 mode at 464 cm^{-1} it seems that the ν_2 asymmetric bending motion and the lithium ion translational motion are coupled to some extent. This coupling between the internal and external modes demonstrates that one must be careful in assuming that internal mode vibrations and external mode vibrations are always completely independent.

Sodium Potassium Sulfate:

Raman Data

Internal Modes

According to Hilmy[14] the salts Na_2SO_4 and K_2SO_4 will form a solid solution of the form $Na_xK_{4-x}(SO_4)_2$ where x has values from 1 to 3. The composition of the solid solution formed from slow evaporation of an aqueous solution containing Na_2SO_4 and K_2SO_4 at lower temperatures approaches

$NaK_3(SO_4)_2$.[15] This spectroscopic study also indicates that the system studied here was $NaK_3(SO_4)_2$. The space group of $NaK_3(SO_4)_2$ is $P\bar{3}m1$ (D_{3d}^3) with a = 5.6801 Å, c = 7.309 Å, and one molecule per unit cell.[16] The important crystallographic data is given in Table 2.8.

TABLE 2.8

CRYSTALLOGRAPHIC DATA FOR $NaK_3(SO_4)_2$[a]

Atom	Site Occupied[b]	Site Symmetry
K	1a	D_{3d}
K	2d	C_{3v}
Na	1b	D_{3d}
S	2d	C_{3v}

[a]Reference 16

[b]Number of equivalent sites and Wyckoff notation.

The internal mode symmetry-based vibrational analysis and Raman band assignment has been done for $NaK_3(SO_4)_2$ by Wu and Frech.[9] The irreducible representations for the internal modes are $\Gamma_{int} = 3A_{1g} + 3A_{2u} + 3E_g + 3E_u$. Only the A_{1g} and E_g modes are Raman active. The frequencies of the internal modes are listed in Table 2.9.

TABLE 2.9

INTERNAL MODE FREQUENCIES (IN cm^{-1})

$NaK_3(SO_4)_2$[a]

Intramolecular Mode	Symmetry	Frequency (cm^{-1})
ν_1	A_{1g}	996
ν_2	E_g	451[b]
ν_3	A_{1g}	1206
	E_g	1087
ν_4	A_{1g}	634
	E_g	625

[a]Reference 9.

[b]G. J. Wu, Ph.D. Dissertation, University of Oklahoma, Norman (1976).

External Modes

A symmetry-based vibrational analysis of the external modes was done and the resulting correlation diagram for $NaK_3(SO_4)_2$ is shown in Figure 2.16. The irreducible representation for each ionic motion is Γ_{trans} (Na^+) = Γ_{trans} (K^+, 1a site) = $A_{2u} + E_u$; Γ_{trans} (K^+, 2d site) = Γ_{trans} ($SO_4^=$) = $A_{1g} + A_{2u} + E_g + E_u$; Γ_{rot} (SO_4) = $A_{2g} + A_{1u} + E_g + E_u$. The total irreducible representations for the external modes are $\Gamma_{ext} = 2A_{1g} + A_{2g} + A_{1u} + 4A_{2u} + 3E_g + 5E_u$. After eliminating the acoustic modes, the irreducible representations for the optic external modes are $\Gamma_{ext.\ opt.} = 2A_{1g} + A_{2g} + A_{1u} + 3A_{2u} + 3E_g + 4E_u$. Of these modes only the $2A_{1g}$ and $3E_g$ are Raman active. Figure 2.17 shows the Raman spectra for the external mode region. All five of the external modes are observed, and the frequency data are summarized in Table 2.10.

TABLE 2.10

EXTERNAL MODE FREQUENCIES FOR $NaK_3(SO_4)_2$ (cm^{-1})

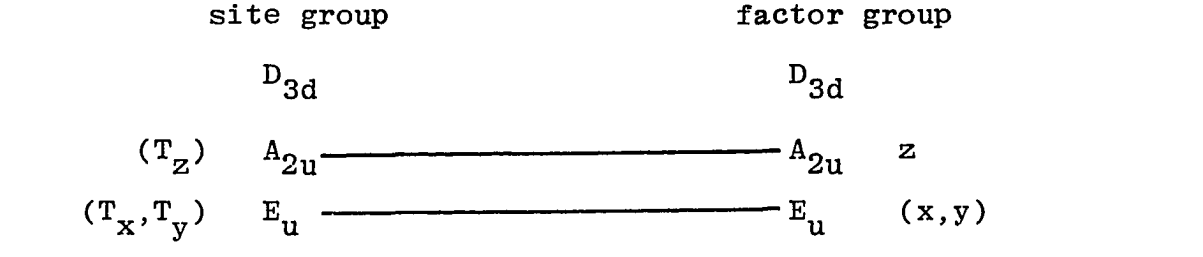
Symmetry of Mode	Frequency (cm^{-1})
A_{1g}	45
	104
E_g	71
	115
	165

Fig. 2.16. Correlation Diagram for the External Modes of $NaK_3(SO_4)_2$

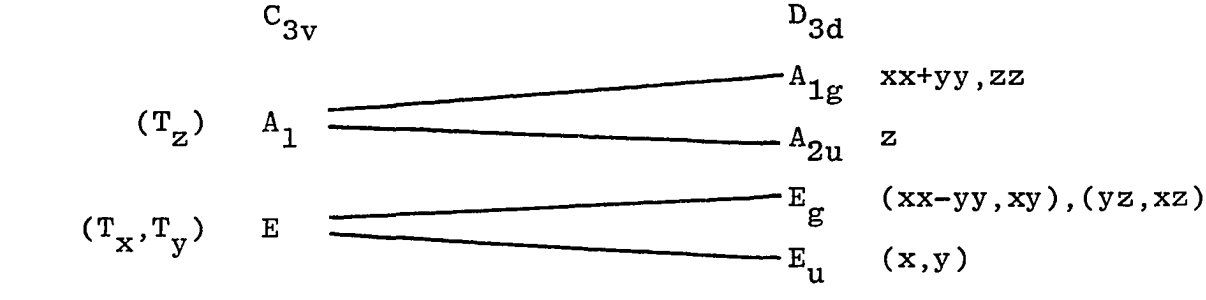
space group D_{3d}^3 ($P\bar{3}m1$) z=1

TRANSLATIONAL MOTION

K^+, Na^+ ion

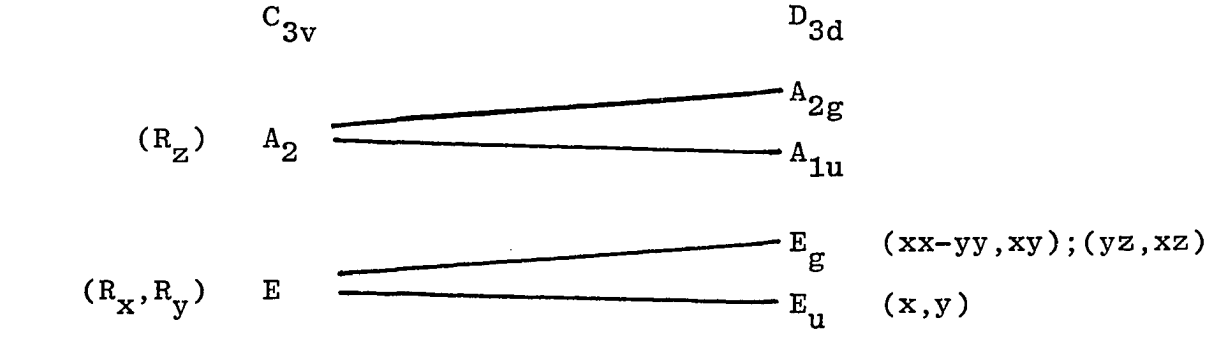


K^+,$SO_4^=$ ions



ROTATIONAL MOTION

$SO_4^=$ ion



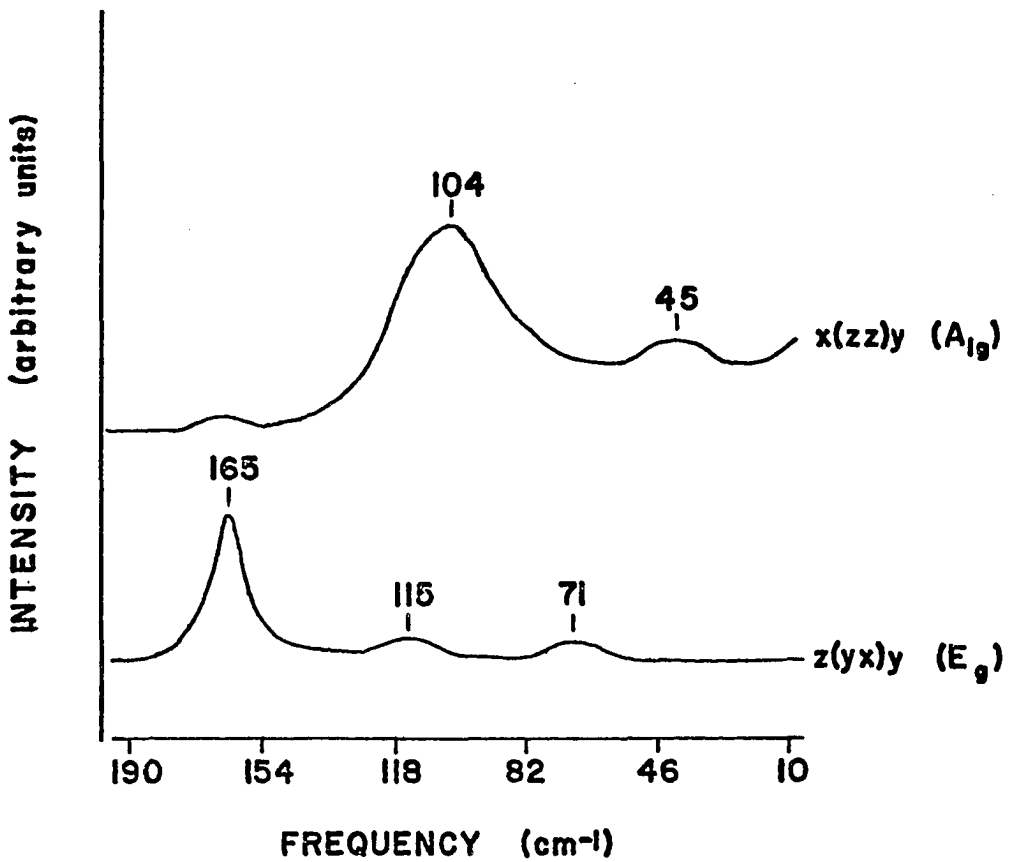


FIGURE 2.17. Raman scattering from the external mode region of $NaK_3(SO_4)_2$. Full scale intensity is 5000 cps.

Discussion

All five of the expected external modes are observed. In this system the highest frequency external mode occurs at 165 cm^{-1} since no lithium ions are present.

REFERENCES

1. International Tables for X-Ray Crystallography (The Kynoch Press, England, 1952).

2. W. G. Fately, F. R. Dollish, N. T. McDevitt, and F. F. Bentley, Infrared and Raman Selection Rules for Molecular and Lattice Vibrations: The Correlation Method (Wiley-Interscience, New York, 1976).

3. H. Poulet and J. P. Mathieu, Vibration Spectra and Symmetry of Crystals (Gordon and Breach, New York, 1976).

4. J. C. Decius and R. M. Hexter, Molecular Vibrations in Crystals (McGraw-Hill, New York, 1977).

5. E. B. Wilson, Jr., J. C. Decius, P. C. Cross, Molecular Vibrations (McGraw-Hill, New York, 1955).

6. G. Herzberg, Infrared and Raman Spectra of Polyatomic Molecules (D. Van Nostrand Company, Inc., New York, 1945).

7. G. Venkataraman and V. C. Sahni, Rev. Mod. Phys. 42, 409 (1970).

8. B. Moroson and D. L. Smith, Acta Crystallogr. 22, 906 (1967).

9. G. J. Wu and R. Frech, J. Chem. Phys. 66, 1352 (1977).

10. T. R. Rao, M. L. Bansal, V. C. Sahni, and A. P. Roy, Phys. Stat. Sol. B 75, K31 (1976).

11. J. Hiraishi, N. Taniguchi, and H. Takahashi, J. Chem. Phys. 65, 3821 (1976).

12. A. J. Bradley, Philos. Mag. 49, 1225 (1925).

13. J. P. Mathieu, L. Couture, and H. Poulet, J. Phys. Radium 16, 871 (1955).

14. M. E. Hilmy, Am. Mineral. 38, 118 (1953).

15. W. Eysel, Am. Mineral. 58, 738 (1973).

16. K. Okada and J. Ossaka, Acta Crystallogr. Sec. B B36, 191 (1980).

CHAPTER III

TEMPERATURE-DEPENDENT RAMAN STUDY OF THE LITHIUM ION MODES IN LITHIUM POTASSIUM SULFATE AND LITHIUM SODIUM SULFATE

Introduction

The binary cation sulfates $LiNaSO_4$ and $LiKSO_4$ are of particular interest in a study of fast ion conduction in sulfates since both have hexagonal room temperature unit cells with lithium ions present as one of the cations and both have a high temperature phase transition. However, only the high temperature phase in $LiNaSO_4$ displays fast ion conductivity while the high temperature phase in $LiKSO_4$ behaves as a normal ionic conductor. The room temperature structure of $LiNaSO_4$ belongs to the space group P31c (C_{3v}^4) with 6 molecules per unit cell.[1] It undergoes a structural phase transition into a body centered cubic phase[2,3] with a specific conductivity of 1.008 ohm^{-1} cm^{-1} at 563°C reported by Josefson and Kvist[4] and a value of 1.044 ohm^{-1} cm^{-1} at 570°C reported by Polishchuk and

Shurghal.[5] Lithium potassium sulfate crystallizes in a $P6_3(C_6^6)$ space group with two molecules per unit cell.[6] A phase transition occurring at approximately 436°C has been observed by measurements of the dielectric constant, dc resistivity, and pyroelectric current.[7] This phase transition has also been observed by an x-ray measurement of the thermal expansion of the unit cell,[8] by thermal analysis,[3,9] and by heat capacity measurements.[10] This high temperature phase is reported to be orthorhombic with normal ionic conductivity.[3]

One of the major problems in the study of fast ion conducting materials is to understand the dynamical behavior of the mobile ion species. In $LiNaSO_4$, the lithium ion is found to have a large diffusion coefficient in the high temperature phase[11] and is thus a mobile ion. In $LiKSO_4$ the lithium ion is apparently not mobile.[3] In both compounds vibrational modes have been observed which are due primarily to lithium ion motion. This was discussed in Chapter II. Knowing that certain modes in $LiNaSO_4$ and $LiKSO_4$ are lithium modes allows a comparative investigation of the potential energy environment of the lithium ion in a system where it becomes a mobile ion and a system where it does not. The temperature dependence of the bandwidth of these modes was investigated for $LiNaSO_4$ and $LiKSO_4$. The bandwidth data was fit to several models allowing activation energies to be calculated.

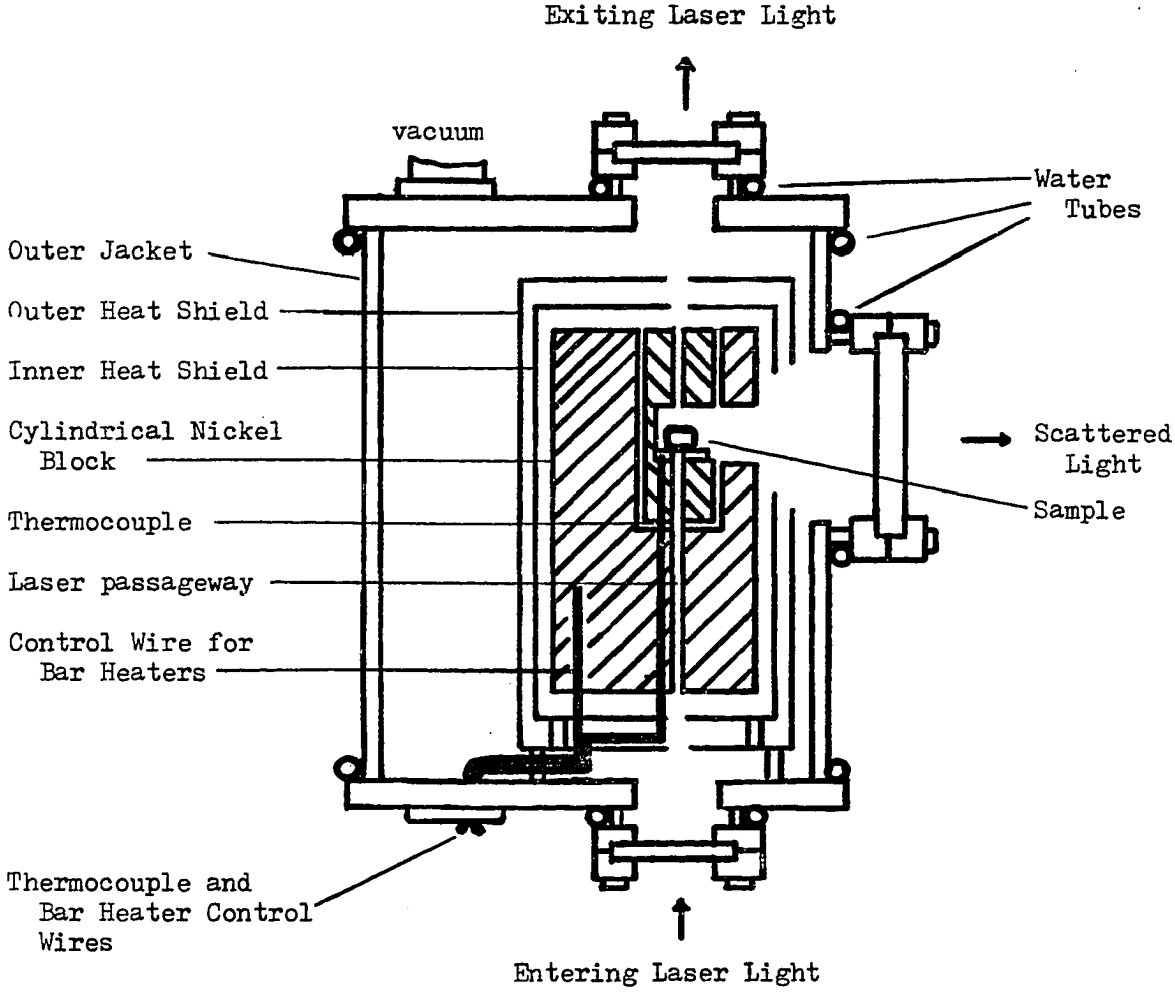
Experimental

Single crystals of $LiKSO_4$ and $LiNaSO_4$ were grown by slow evaporation as described in the experimental section in Chapter II. Raman spectra were recorded on a Spex Ramalog 5 spectrometer with a 2 cm^{-1} spectral bandpass using the 4880 Å line of an argon ion laser for excitation at 600 mw. The geometrical arrangement of the Raman is the same as shown in Figure 2.1.

The Raman spectra at temperatures below 25°C were obtained by using an Air Products displex model CSA-202E closed cycle refrigeration system equipped with a DMX-1E vacuum shroud. Temperatures could be controlled to ±.1 degree. Raman spectra at temperatures greater than 25°C were recorded with the crystal in a high temperature cell similar to that described by Quist,[12] but modified for compatibility with the optics of the Spex Raman System. Figure 3.1 shows a diagram of the high temperature cell. The temperature of the apparatus was controlled to within one degree by a LFE series 230 temperature controller.

Cracking of the crystals was a problem at higher temperatures, especially for $LiKSO_4$. This problem was solved by heating crystals of $LiKSO_4$ in an oven to a temperature slightly above the phase transition at 436°C and maintaining them at this temperature for approximately one day. The crystals then were slowly cooled back to room

FIGURE 3.1. High - temperature Raman cell.



temperature. Pieces of these crystals were then cut, polished, and used for high temperature studies. The room temperature spectrum of these annealed crystals was checked against crystals that had not been heated. Only slight changes in the frequencies were noticed.

The same procedure was attempted for crystals of $LiNaSO_4$. When the crystals were heated past the phase transition the pieces remaining were too small for proper sample preparation. In this case a crystal was placed in the high temperature cell and slowly heated to the temperatures at which spectra were to be recorded allowing ample time for equilibration. Over a two week period, temperatures from 25°C to 625°C (phase transition occurs at 518°C) were investigated.

Temperature Dependence of the Lithium Modes in Lithium Potassium Sulfate

The frequencies of the lithium modes (as determined by shifts in frequencies due to isotopic substitutions) are listed in Table 2.7. Temperature dependent polarized Raman spectra were measured for the lithium modes from 12K to 775K. Spectra for the A and E_2 lithium modes are shown in Figure 3.2. The modes generally broaden and decrease in intensity with increasing temperature, although anomalous behavior is observed in the bandwidths and discussed in

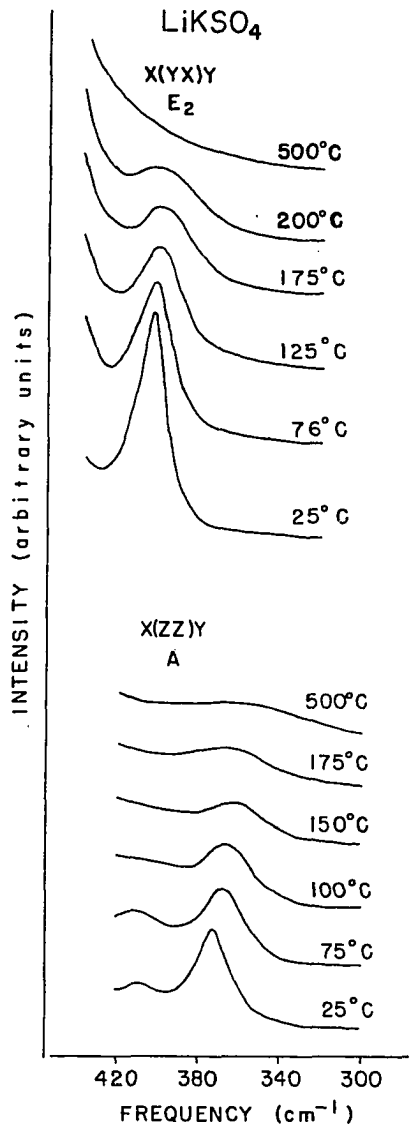


FIGURE 3.2. Temperature - dependent Raman scattering from the A and E_2 lithium modes in $LiKSO_4$. Full scale intensity is 5000 cps.

detail below. The bands were fit using a non-linear least-squares computer routine[13] to a Lorentzian curve plus an appropriate power function which accounted for the overlapping portion of the ν_2 internal mode. A typical fit is shown in Figure 3.3. The resulting bandwidth and frequency data are shown in Figures 3.4 through 3.6. Data for the E_1 lithium modes could not be obtained due to the low intensity of the mode.

The bandwidth of both the A and E_2 modes exhibits rather unusual behavior. In Figure 3.4 the bandwidth of the E_2 lithium mode increases from 12 K to about 475 K and then begins to decrease as the band "sharpens up" over a relatively narrow temperature range. At approximately 600 K the bandwidth again begins to increase. The bandwidth vs. temperature data for the A lithium mode is shown in Figure 3.5. The bandwidth increases from 12 K to about 270 K and then begins to decrease. Reliable data could not be obtained above 500 K due to the weak scattering intensity. The frequency of these modes as shown in Figure 3.6 decreases with temperature with no unusual changes apparent in the data, particularly in the temperature region of the anomalous bandwidth behavior.

Bandwidth data as a function of temperature were collected from two other crystals as a check of the reproducibility of these observations. The bandwidths of all three crystals were almost identical at temperatures below 275 K.

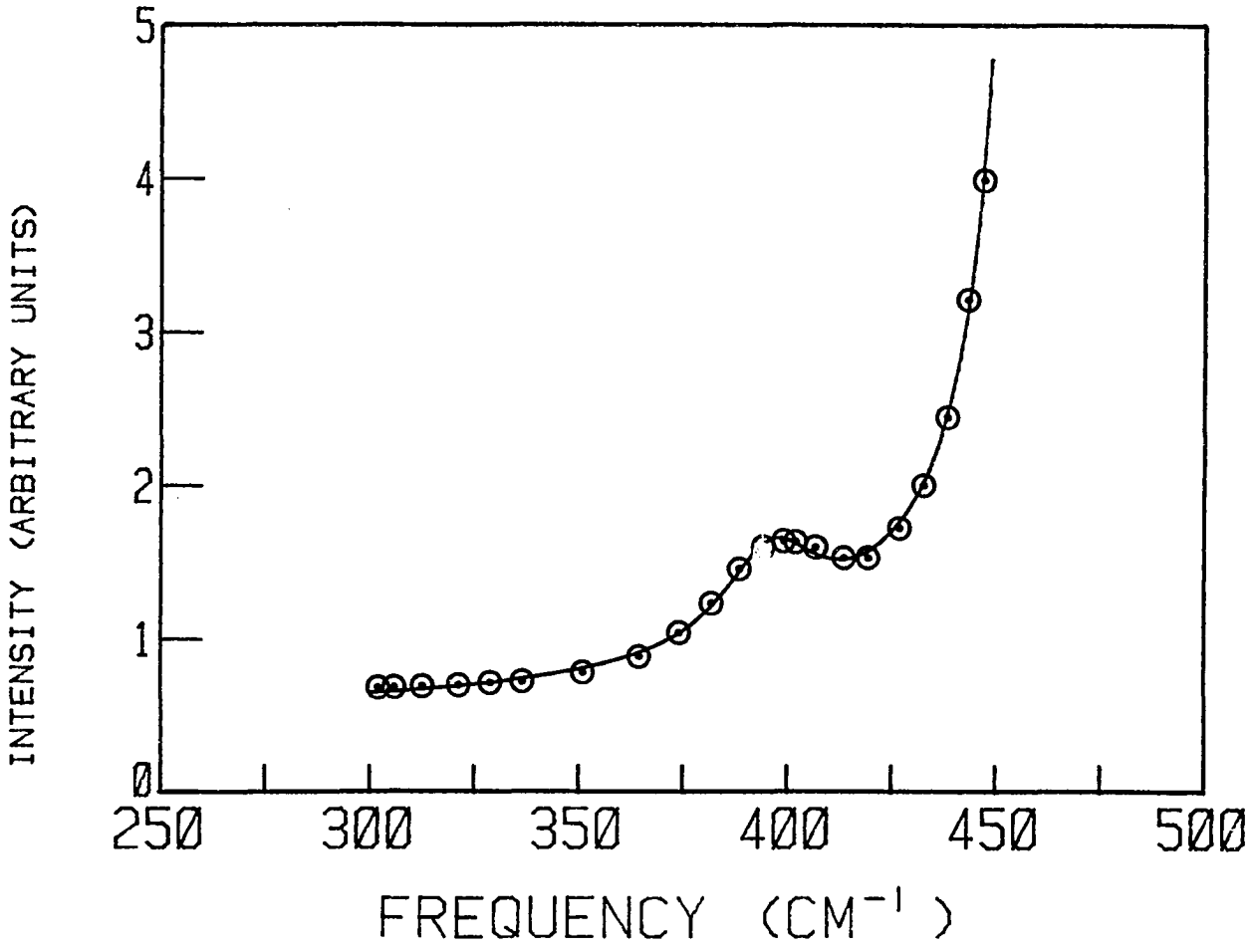


FIGURE 3.3. Graph showing a typical fit for curve resolving. Circles represent digitized Raman data points. The line shows the fit obtained by using a power function and a Lorentzian function.

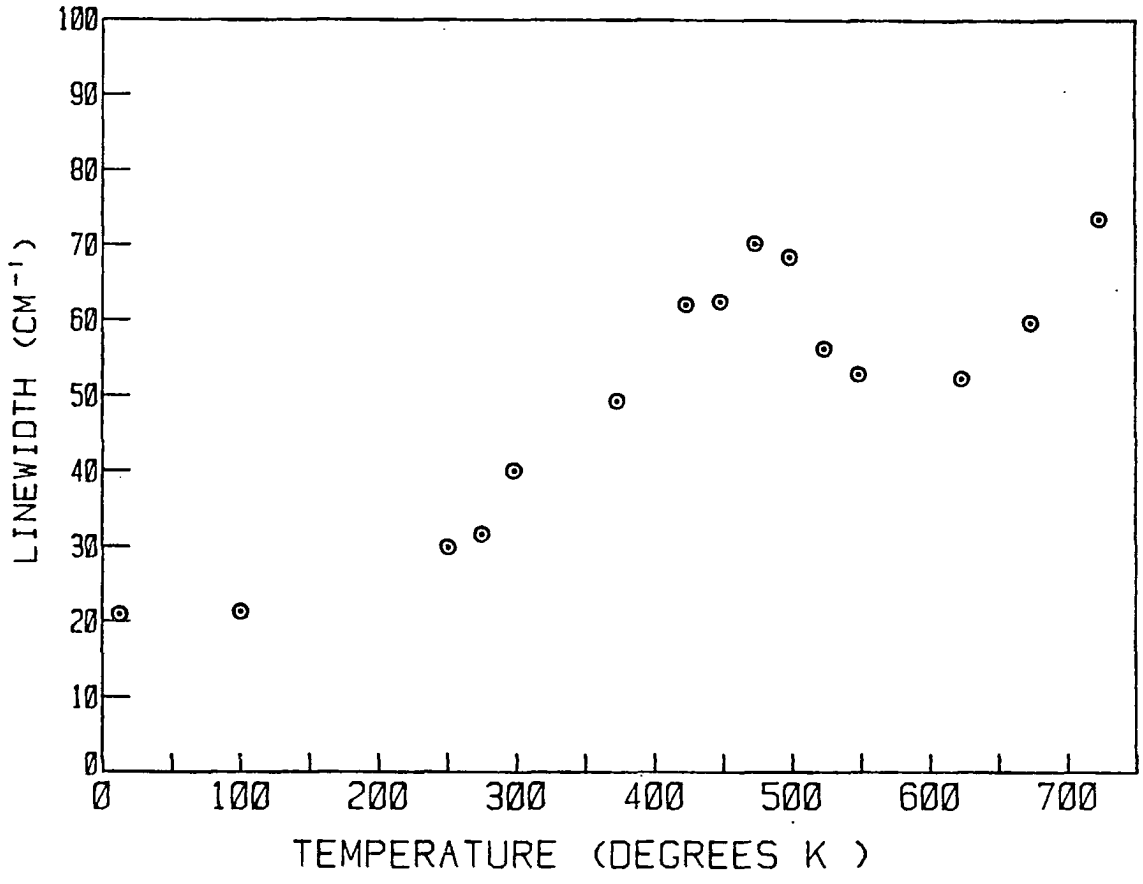


FIGURE 3.4. Graph showing temperature - dependent linewidth (FWHM). The error in the linewidth is ± 3 cm^{-1}. The maximum is observed at approximately 475 K.

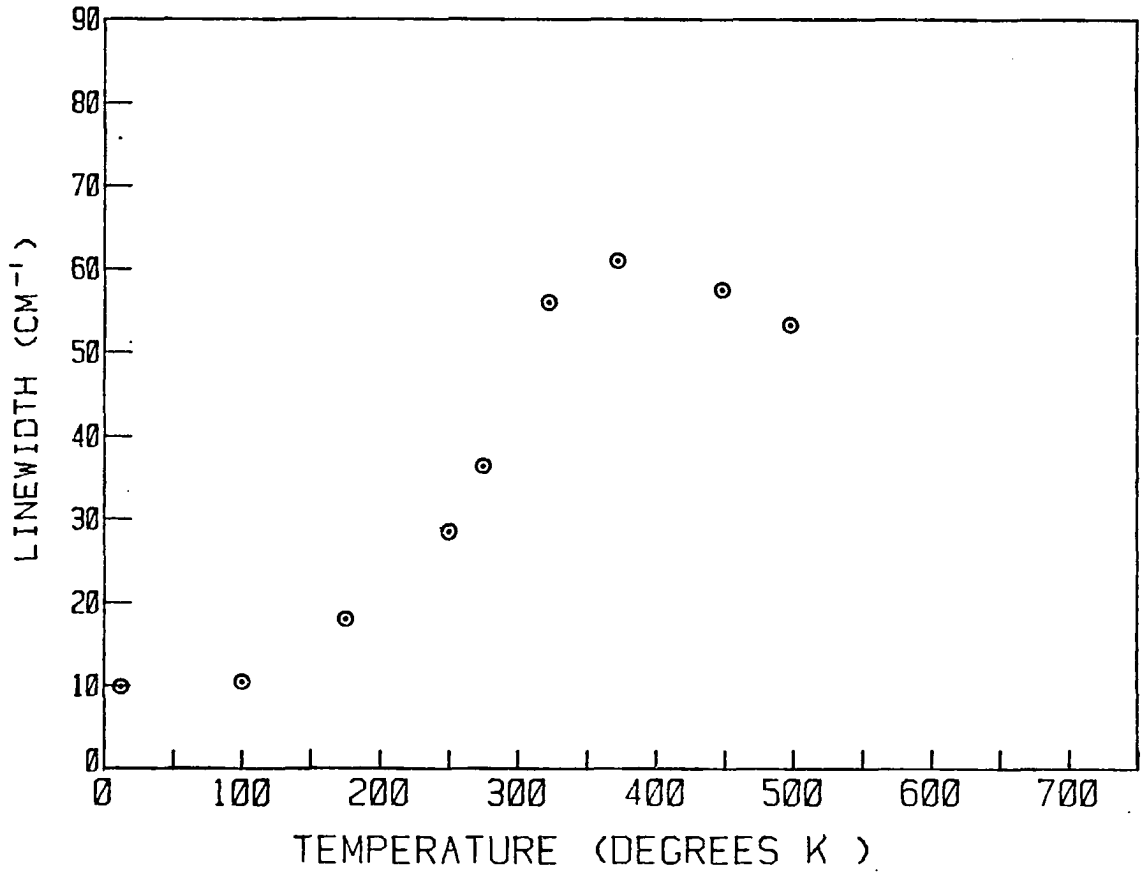


FIGURE 3.5. Linewidth (FWHM) versus temperature data for the A lithuim mode of $LiKSO_4$. The error in linewidth is approximately ± 3 cm^{-1}. The maximum is observed at approximately 375 K.

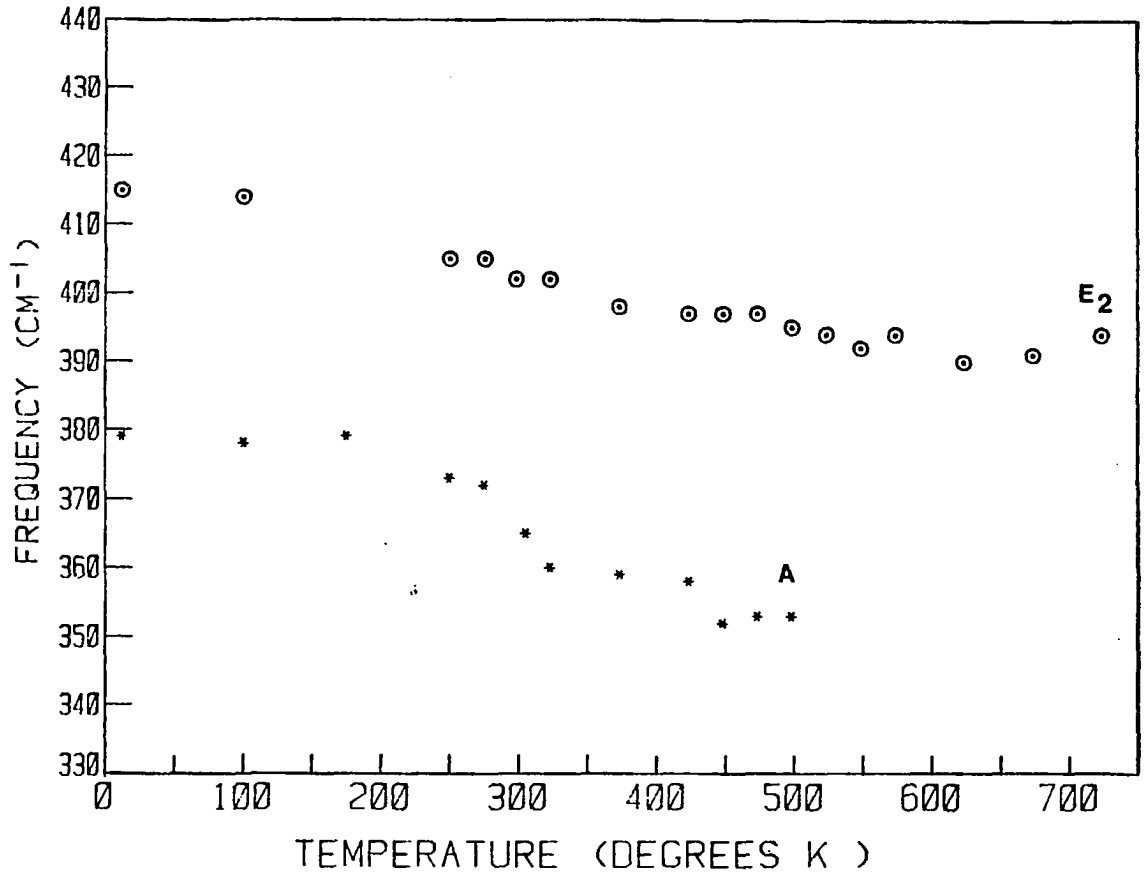


FIGURE 3.6. Temperature - dependent frequency data for the E_2 and A lithium modes in $LiKSO_4$.

Data for the E_2 mode above this temperature are shown in Figure 3.7. Curve a is the same data as shown in Figure 3.4 while b and c are from different crystals of $LiKSO_4$. Bandwidth versus temperature data for crystals b and c could not be obtained above 600 K due to weak intensity of the lithium modes at these temperatures. The maximum of curve a occurs at approximately 475 K, while curves b and c exhibit maxima at 400 K and 375 K respectively. The presence of a maximum seems to be reproducible although the temperature at which the maximum occurs apparently depends on the sample.

The bandwidth of the A mode could not be reliably measured above 500 K due to the rapidly decreasing intensity of the mode. At temperatures above the phase transition the lithium mode were very weak, and in the case of the E_2 mode, not observable.

It should also be pointed out that the maximum in the bandwidth curves occurs at different temperatures for the lithium A and E_2 modes when measured in the same crystal. Figures 3.4 and 3.5 show bandwidth data measured in the same crystal. The maximum of the E_2 mode is roughly at 475 K while the maximum of the A mode occurs at approximately 370 K.

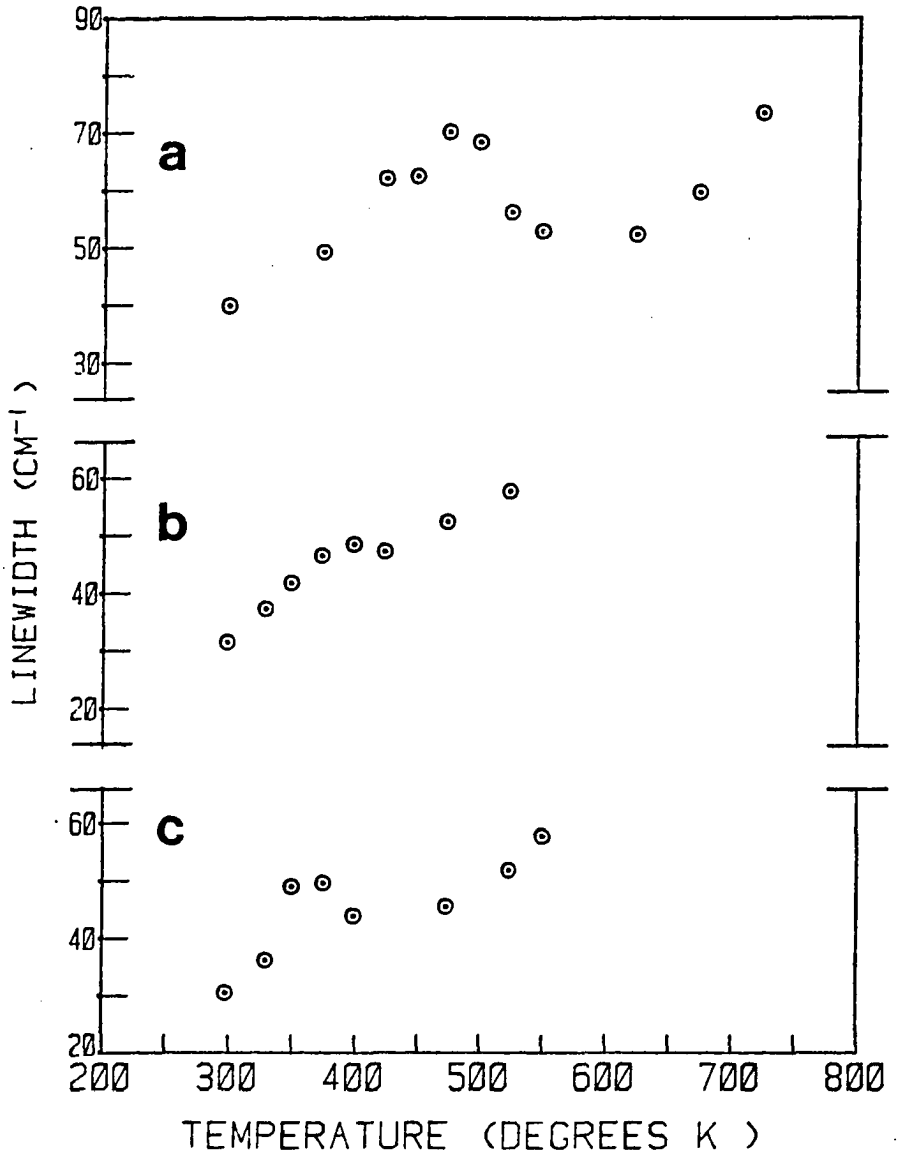


FIGURE 3.7. Temperature - dependent linewidth data (FWHM) for the E_2 lithium mode in three different crystals of $LiKSO_4$. In a the maximim occurs at 475 K, in b at 400 K, and in c at 375 K.

Discussion of the Temperature Dependence of Lithium Modes in Lithium Potassium Sulfate

The A and E_2 external modes which originate primarily in the lithium ion motion increase in bandwidth with increasing temperature in a non-linear way. Since thermal expansion of the lattice is usually assumed to cause linear increases in bandwidth,[14] it is probable that some other mechanism is occurring. A model suggested by Andrade and Porto[15,16] describes the linewidth of a phonon associated with a Brownian sublattice. This model is based on an order-disorder process of random or so-called Brownian particles whose fluctuations are due to random thermal forces. Using a Langevin formalism, Andrade and Porto were able to derive an expression for the temperature dependence of the bandwidth of a phonon. This expression is:

$$\Gamma = a + bT + C \frac{\tau_c}{1 + \omega^2 \tau_c} \qquad (3.1)$$

where a, b, and c are constants. The effect of thermal expansion of the crystal lattice on the bandwidth is assumed to be described by a term which is simply proportional to the temperature (i.e., bT in Equ. 3.1).[14] The correlation time τ_c is given by

$$\tau_c = \tau_o \exp(\Delta U/kT) \qquad (3.2)$$

In Equation 3.2, τ_o is usually assumed to obey the Eyring relation and is written $\tau_o = h/kT$ while ΔU is the activation energy necessary to go from an ordered to a disordered state (roughly the height of the potential barrier of a double well potential).

The activation energy ΔU for the two lithium modes were obtained from non-linear least squares fit[13] of bandwidth vs. temperature data using Equation 3.1. The frequencies of the lithium modes (see Figure 3.6) were fit to polynomial functions. These polynomial functions were used for ω in Equation 3.1. It is apparent in Figure 3.4 that there are two distinct regions in the bandwidth data. Therefore the portion of the curve from 12 K to the maximum at 475 K was first used, resulting in an activation energy of .04 eV. Next the best curve was drawn through the bandwidth data over the entire temperature range of 12 K to 725 K, ignoring the maximum (see Figure 3.8). The activation energy found was .6 eV. Finally the portion of the bandwidth data for the A lithium mode from 12 K to 370 K was used as shown in Figure 3.9. This resulted in an activation energy of .03 eV. If the disordering process described by Andrade and Porto is correct, the disordering must occur within a unit cell with no ionic transport between unit cells since $LiKSO_4$ has low ionic conductivity in all phases below the melting point.

A more general analysis of the bandwidth data

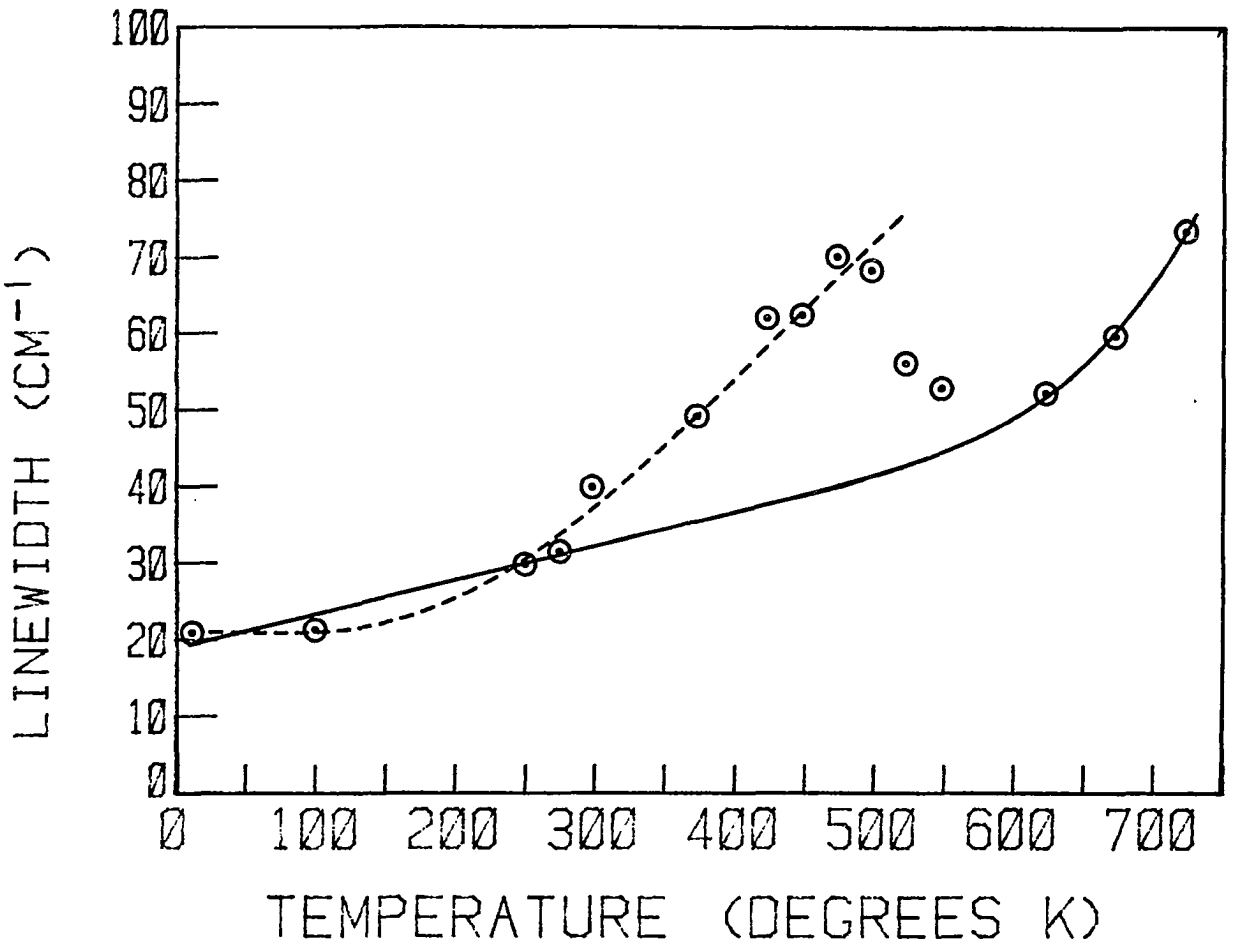


FIGURE 3.8. Curve fitting proceedure for the lithium E_2 mode linewidth data in $LiKSO_4$. The solid line is a fit of Eq. 3.1 over the temperature interval 12 K to 725 K. The dashed line is a fit of Eq. 3.1 over the interval 12 K to 475 K.

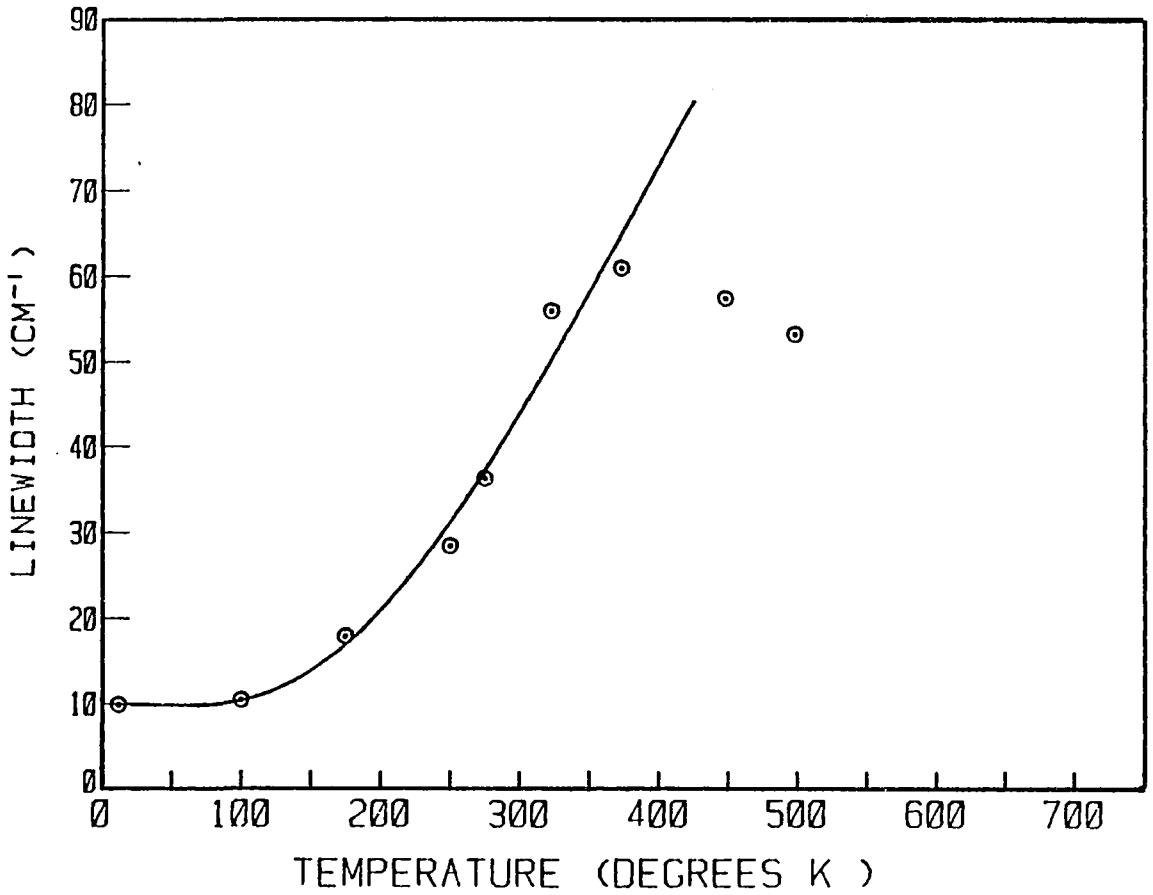


FIGURE 3.9. Curve fitting proceedure for the A mode linewidth data in $LiKSO_4$. The solid line is a fit of Eq. 3.1 over the temperature interval 12 K to 400 K.

recognizes the behavior as Arrhenius-like and fits the data to

$$\Gamma = a + bT + c \exp(-Ea/kT) \qquad (3.3)$$

In this case the data are fit over the identical temperature ranges for each mode as in the analysis using the Andrade and Porto model. The resulting activation energies are given in Table 3.1 and compared with the Andrade and Porto results. The average error in these calculated values is 40%.

TABLE 3.1

CALCULATED ACTIVATION ENERGIES

Lithium Mode	Activation Energy (eV) Equation 3.1	Equation 3.3
A	.03	.06
E_2	.04 (12-475 K)	.07 (12-475 K)
	.6 (12-725 K)	.6 (12-725 K)

The activation energies listed in Table 3.1 indicate two distinct thermally activated processes are involved in the temperature-dependent bandwidth data. The first of these has a very low activation energy of a few hundredths of an electron volt and appears to be slightly sample dependent. This could be caused by the concentration of intrinsic defects, the presence of crystal imperfections, or grain boundaries. The fact that no other external normal mode shows bandwidth anomalies in this temperature region seems to contradict these explanations. Another possible explanation is a thermally induced disordering of the

lithium ion sublattice as described by the Andrade and Porto model. In this case the weak sample dependence is more difficult to explain. In a differential thermal analysis measurement of $LiKSO_4$ by Lepeshkov et al.[9] an exothermic process was reported in the same temperature region as the anomalous bandwidth maximum. However, repeated attempts to observe thermal effects in this region using differential scanning colorimetry have been unsuccessful.

The second type of thermally activated process which has an activation energy of .6 eV is comparable with the activation energy expected for the "normal" conductivity of an ionic crystal. The lithium ion is tetrahedrally coordinated with the oxygen atoms of neighboring sulfate ions in the room temperature structure of $LiKSO_4$.[6] This interaction is so strong that an isotopic frequency shift is observed in the lowest frequency internal optic mode (ν_2) of the sulfate ion upon enrichment with ^6Li (discussed in Chapter II). Therefore the activation energy of .6 eV is probably associated with the removal of an Li^+ ion from the interior of the oxygen tetrahedron into either a vacant site or an interstitial position.

Temperature Dependence of the Lithium Modes in Lithium Sodium Sulfate

Table 2.4 lists the frequencies of lithium modes for $LiNaSO_4$. The modes studied here have room temperature frequencies at 314 and 404 cm^{-1} (A_1 modes) and 406 cm^{-1} (E mode). Temperature dependent polarized Raman spectra were measured for the lithium modes from 77°K to temperatures above the transition which occurs at approximately 790°K. Temperature-dependent spectra for the A_1 and E lithium modes are shown in Figures 3.10 and 3.11 respectively. The modes shift to lower frequency, broaden out, and eventually disappear as the temperature approaches the phase transition. The bands were fit by the same procedure as described for $LiKSO_4$. The computer resolved temperature-dependent bandwidth and frequency data are shown in Figures 3.12 and 3.13 respectively. The frequency of the lithium modes seems to generally decrease even though the low frequency A_1 mode data seems to have a slightly erratic behavior. The bandwidth data could not be obtained past 500 K due to weak intensities of the modes. Anomalies in bandwidth, much like those in $LiKSO_4$ but not as pronounced, were found in $LiNaSO_4$. These anomalies are especially observable in the two A_1 modes. The A_1 mode whose room temperature frequency is 404 cm^{-1} has a weak maximum at 275 K while the A_1 mode whose room temperature frequency is at 314 cm^{-1} has a maximum at 300 K.

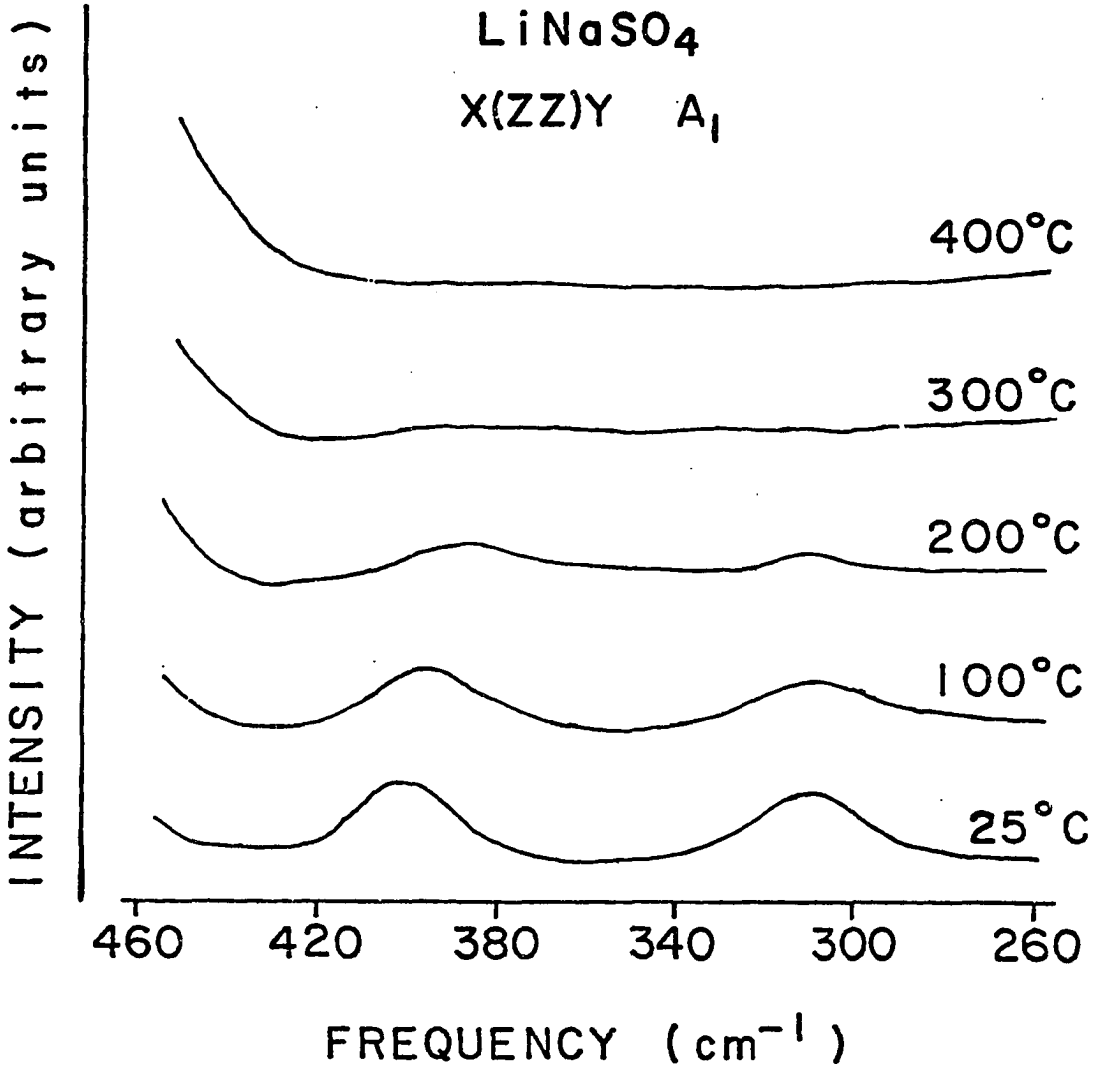


FIGURE 3.10. Temperature - dependent Raman scattering from the A_1 lithuim modes in $LiNaSO_4$. Full scale intensity is 5000 cps.

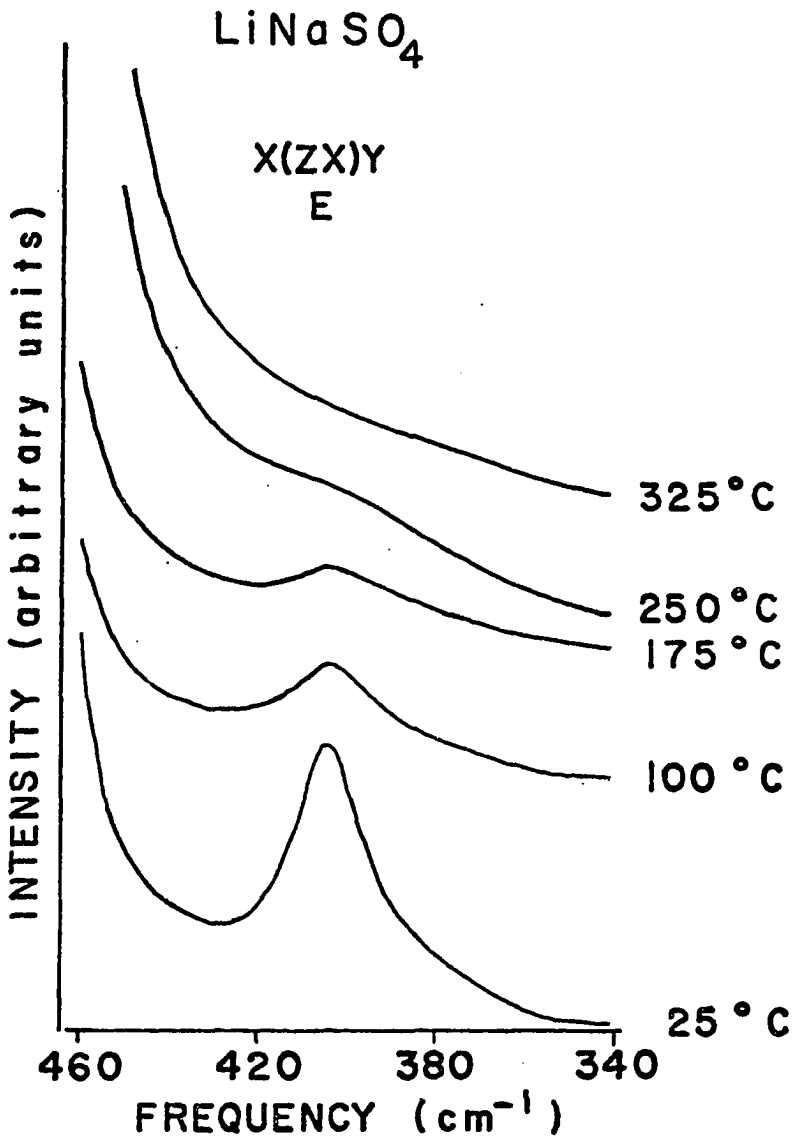


FIGURE 3.11. Temperature - dependent Raman scattering from the E lithium modes in $LiNaSO_4$. Full scale intensity is 5000 cps.

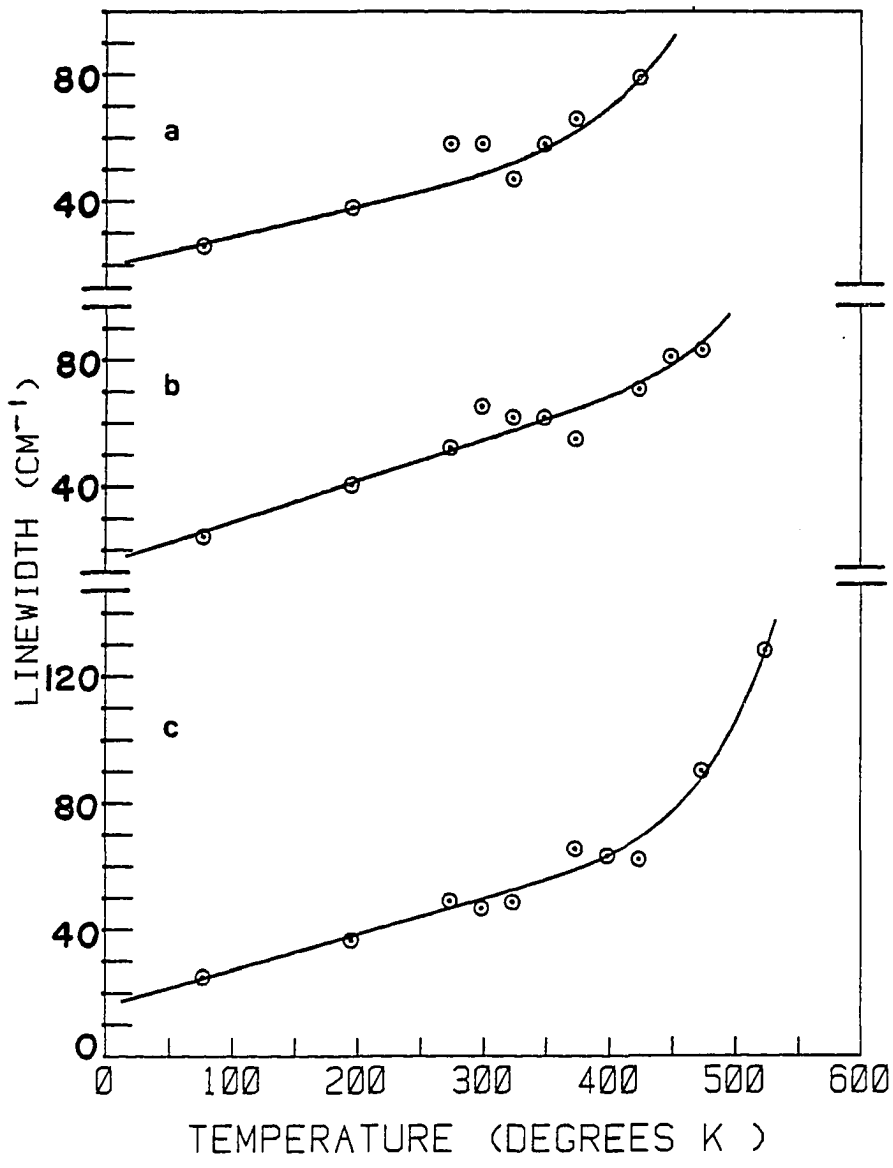


FIGURE 3.12. Normal mode linewidths of the lithium modes in $LiNaSO_4$ as a function of temperature. Data a is the A_1 mode at 314 cm^{-1}, b the A_1 mode at 404 cm^{-1}, and c is the E mode at 406 cm^{-1}. The error in the linewidth is $\pm$ 3 cm^{-1}. The solid lines are fits of Eq. 3.1 to the data.

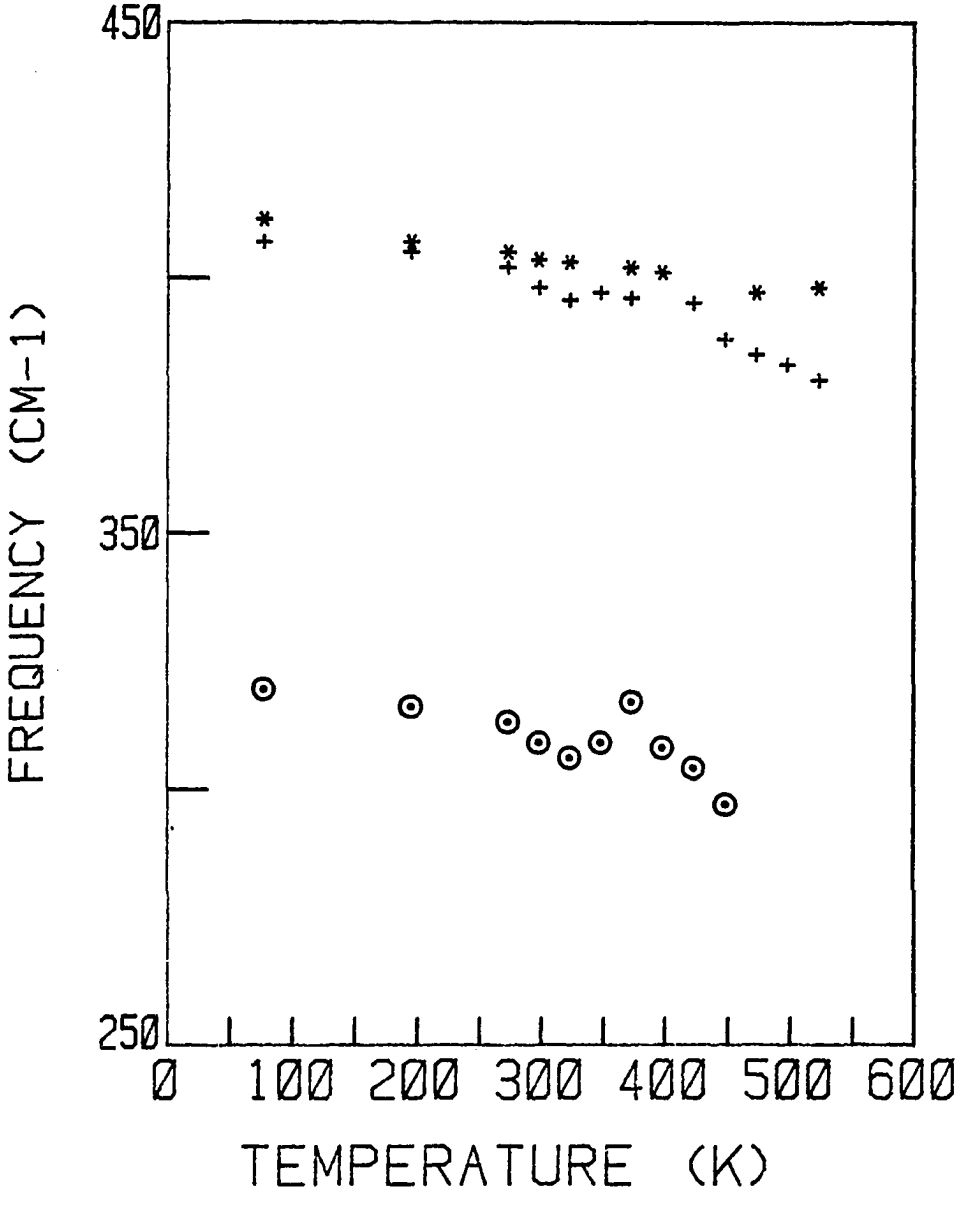


FIGURE 3.13. Normal mode frequencies of the A_2 and E lithium modes in $LiNaSO_4$ as a function of temperature. Circles and +'s are A_1 mode data points, *'s are E data points.

Discussion of the Temperature Dependence of Lithium Modes in Lithium Sodium Sulfate

The bandwidth vs. temperature data for $LiNaSO_4$ were analyzed using the Andrade and Porto model (Equation 3.1) and the more general Arrhenius-like fit (Equation 3.3). In this case the fit was over the entire temperature range ignoring the data points in the anomalous region since maxima here are not as pronounced as in the case of $LiKSO_4$. The fits using Equations 3.1 and 3.3 are very similar. The fit of Equation 3.3 is shown in Figure 3.12. The activation energies from the Andrade and Porto analysis and the Arrhenius-like equation are listed in Table 3.2. The uncertainty in the values calculated for the A_1 modes are larger than the values of the activation energies. The error is much better for the E mode.

TABLE 3.2

CALCULATED ACTIVATION ENERGIES FOR $LiNaSO_4$
ACTIVATION ENERGY (eV)

Lithium Mode	Equation 3.1	Equation 3.3
A_1 (314 cm^{-1} mode)	.2 ± .3	.2 ± .3
(404 cm^{-1} mode)	.4 ± .8	.5 ± .8
E	.4 ± .1	.4 ± .1

The activation energies given in Table 3.2 are comparable with the value of .6 eV for the E_2 mode in the range 12-725 K (see Table 3.1) for $LiKSO_4$. Like the lithium ions

in $LiKSO_4$, the lithium ions in $LiNaSO_4$ are tetrahedrally coordinated with oxygen atoms of neighboring sulfate ions in the room temperature structure.[1] The activation energies listed in Table 3.2 could be associated with the removal of an Li^+ ion from its oxygen tetrahedral coordination as was also postulated for the lithium ions in $LiKSO_4$. In $LiNaSO_4$ no isotopic frequency shift is observed in the lowest frequency internal optic mode (ν_2) as was the case in $LiKSO_4$.

Comparison of $LiNaSO_4$ and $LiKSO_4$

In $LiKSO_4$ and $LiNaSO_4$ two kinds of dynamical behavior can be distinguished. There appears to be a process involving only the lithium ion sublattice which may involve a local disordering of the lithium ions and would account for the appearance of a maximum in bandwidth vs. temperature curve. This maxima occurs in both $LiKSO_4$ and $LiNaSO_4$ even though it is not as prominent in the latter. The difference in experimental preparation of crystals for the two sulfates (see experimental section) could have some effect on the prominence of the maximum for the two systems. In the case of $LiNaSO_4$ the maximum occurs at lower temperatures, 275 and 300 K for the two A_1 modes, as compared to 370 K for the A mode and 475 K for the E_2 mode in $LiKSO_4$. This seems to indicate that if disordering of the lithium ions is taking place in these systems, it occurs at a lower temperature

in $LiNaSO_4$.

Disordering of this nature would be difficult to observe by x-ray diffraction techniques because of the inherently weak x-ray scattering intensity of the lithium ions. Scott[17] has pointed out that Raman spectroscopic measurements are much more sensitive to minute displacements of ions within a unit cell than are x-ray measurements. This could be another example of the great value of Raman spectroscopy in investigating small structural changes in the unit cell of various crystals.

The second type of dynamical process is postulated to be related to the removal of the lithium ion from its tetrahedral coordination sphere defined by the oxygen atoms of the neighboring sulfate ions. The lithium-oxygen interaction in $LiKSO_4$ seems to be very strong as indicated by the isotopic frequency shift of 6 cm^{-1} for the ν_2 internal optic mode in $LiKSO_4$. A significant shifting of internal mode frequencies upon substituting ^6Li into the crystal lattice for ^7Li is not observed in $LiNaSO_4$ or for internal modes in various other ionic crystals[18,19] where lithium is tetrahedrally coordinated. For diffusion of lithium ions to occur in the high temperature phase of $LiNaSO_4$, it would seem that the lithium ion would have to be removed from the oxygen tetrahedron. The activation energy for ionic conductivity in the high temperature phase of $LiNaSO_4$ is .37 eV.[5] The value of .37 eV compares well with

the activation energies of .4 eV for the E lithium mode (Table 3.2) which is postulated to involve removal of the lithium ion from tetrahedral oxygen coordination.

The behavior of the lithium ions in $LiKSO_4$ and $LiNaSO_4$ seems to be very similar in the two systems. Studies performed on the external modes in Chapter IV point out differences in the two systems.

REFERENCES

1. B. Morosin and G. L. Smith, Acta Crystallogr. 22, 906 (1967).

2. H. Forland and J. Krogh-Moe, Acta Crystallogr. 11, 224 (1958).

3. K. Schroeder, Thesis, Goteberg (1975).

4. A. M. Josefson and A. Kvist, Z. Natursforsch. A 24, 2045 (1968).

5. A. F. Polishchuk and T. M. Shurghal, Elektrokhimiya 9, 838 (1973).

6. A. J. Bradley, Phil. Mag. 49, 1225 (1925).

7. R. Ando, J. Phys. Soc. Japan 17, 937 (1962).

8. H. F. Fishmeister and A. Ronnquist, Ark. Kemi 15, 393 (1960).

9. I. N. Lepeshkov, N. V. Bodaleva, and L. T. Kotova, Russ. H. Inorg. Chem. 6, 864 (1961).

10. N. K. Voskresenkaya and E. I. Banashek, Izvest. Sektora Fiz.-Khim. Anal., Inst. Obshchei i Neorg. Khim., Akad. Nauk S.S.S.R. 26, 111 (1955).

11. B. Heed, A. Lunden, and K. Schroeder, Electrochim. Acta 22, 705 (1977).

12. A. S. Quist, Appl. Spectrosc. 25, 82 (1971).

13. Subroutine NLLSQ was written by Dr. E. Enwall and follows the strategy of D. W. Marquardt, J. Soc. Ind. Appl. Math. 2, 431 (1963).

14. A. Korshunov and A. Bondarev, Opt. Spectrosc. 15, 98 (1963).

15. P.d.R. Androde and S.P.S. Porto, Solid State Commun. 13, 1249 (1973).

16. P.d.R. Androde and S.P.S. Porto, Solid State Commun. 14, 547 (1974).

17. J. F. Scott, in Molecular Spectroscopy of Dense Phases, Proceedings of the 12th European Congress on Molecular Spectroscopy, edited by M. Grosmann, S. G. Elkomoss, J. Ringeissen (Elsevier, 1976), pp. 203-213.

18. P. Tarte, Spectrochim. Acta 20, 238 (1964).

19. P. Tarte, Spectrochim. Acta 21, 313 (1965).

CHAPTER IV

EXTERNAL MODE TEMPERATURE DEPENDENCE OF LITHIUM SODIUM SULFATE, LITHIUM POTASSIUM SULFATE, AND SODIUM POTASSIUM SULFATE

Introduction

The phase transition in many sulfate systems is believed to be closely related to the librational (hindered rotational) motion of the sulfate ion.[1] This motion of the sulfate ion is also postulated to enhance ionic motion in the high temperature phase of some sulfates.[2] Translational motion of the ions in the crystal lattice must also play a part in phase transitions of various sulfates.[3] Presented here is a comparative temperature-dependent Raman study of the external modes in $LiNaSO_4$, $LiKSO_4$, and $NaK_3(SO_4)_2$ as the phase transition in the three systems is approached. This study looks at the dynamical behavior of the external modes (except for lithium ion modes which are covered in Chapter III) in terms of the disorder in the systems.

Experimental

The temperature-dependent Raman experimental procedures are given in the Experimental section of Chapter III. Crystals of $LiNaSO_4$ and $LiKSO_4$ received the same type of preheating treatment as described in Chapter III. $NaK_3(SO_4)_2$ was preheated in the same manner as $LiKSO_4$. Slight differences between the room temperature frequencies given in Chapter II and those presented here are due to this preheating treatment. The geometrical arrangement of the Raman experiment is given in Chapter II.

Temperature Dependence of the External Modes in Lithium Sodium Sulfate

Lithium sodium sulfate undergoes a phase transition at approximately 518°C from a hexagonal P31c $(C_{3v}^4)^4$ to a body-centered cubic phase.[5] In this study the phase transition occurred at a temperature between 525°C and 550°C.

Table 2.3 lists the room temperature frequencies for $LiNaSO_4$. In all the polarized experiments the modes are observed to decrease in frequency and broaden as the temperature is increased. Many of them merge with other external modes or become too low in intensity to observe. Figure 4.1 is a graph of frequency vs. temperature data for the external modes of $LiNaSO_4$. The external mode of lowest frequency is observed to be very temperature

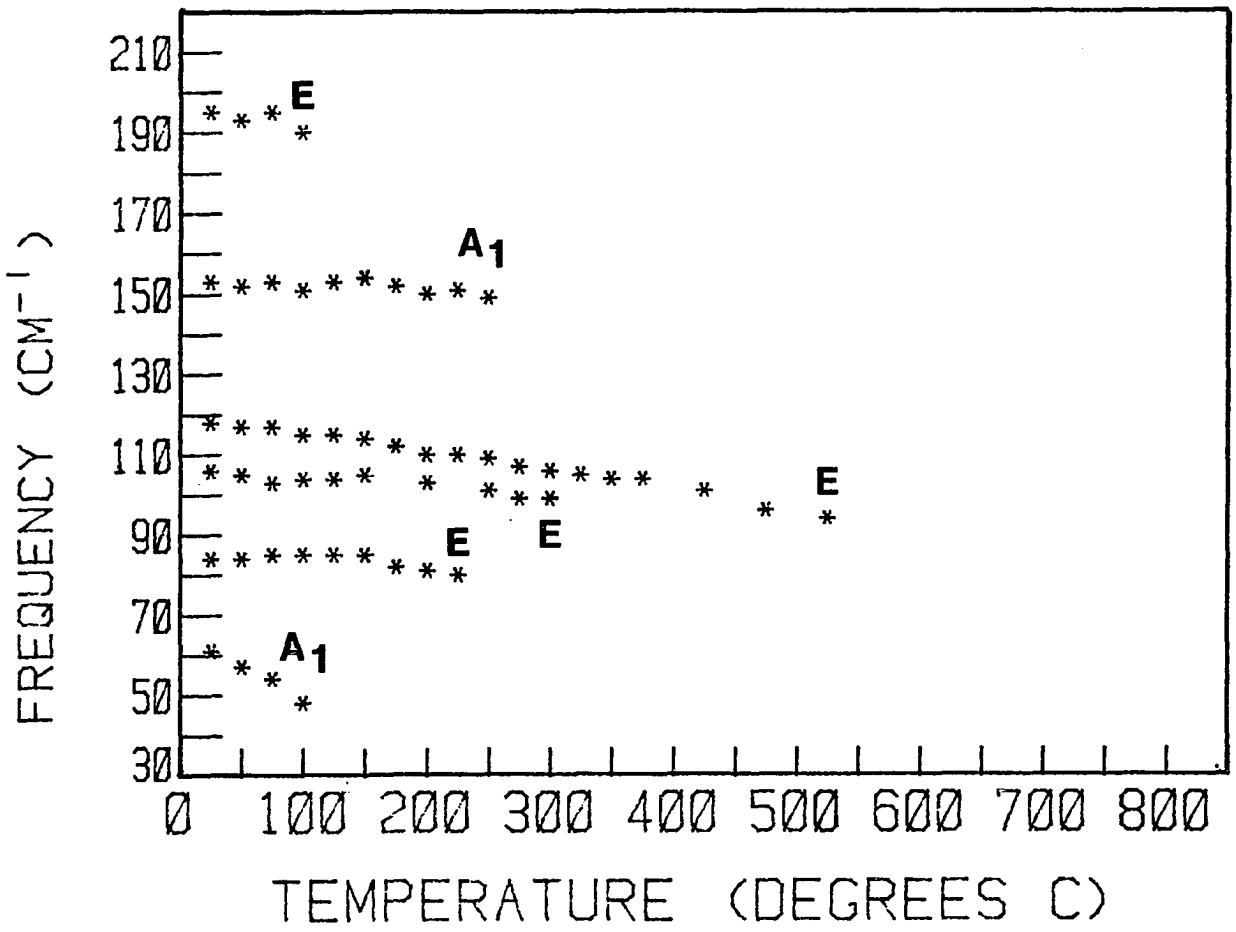


FIGURE 4.1. Temperature - dependent frequency data for the external modes in $LiNaSO_4$. The phase transition occurs between 525 and 550 K.

dependent. The temperature-dependent spectra of this A_1 mode are shown in Figure 4.2. As the temperature is increased it eventually disappears at about 100°C into the broad "wing" that emerges from the excitation line. At temperatures above the phase transition no external modes are observed. Instead a broad asymmetric band structure is attributed to a density of states is seen as a broad wing of the laser excitation line. Figure 4.3 shows spectra above and below the phase transition.

Discussion of the Temperature Dependence of the External Modes in Lithium Sodium Sulfate

The external modes of $LiNaSO_4$ as expected generally broaden and decrease in frequency as the temperature is elevated. The A_1 mode at 63 cm^{-1} is particularly interesting since it is by far the most temperature sensitive of all the external modes.

It is well known that Li_2SO_4 has a phase transition at 573°C into a face-centered cubic phase and that this phase is considered a fast ion conductor.[6] Nilsson, Thomas, and Tofield[2] have postulated that this is a so-called plastic phase caused by rotational disorder of the sulfate group. Plastic phases are associated with large volume changes at the transition together with a larger heat of transition than the heat of fusion. Polishchuk and

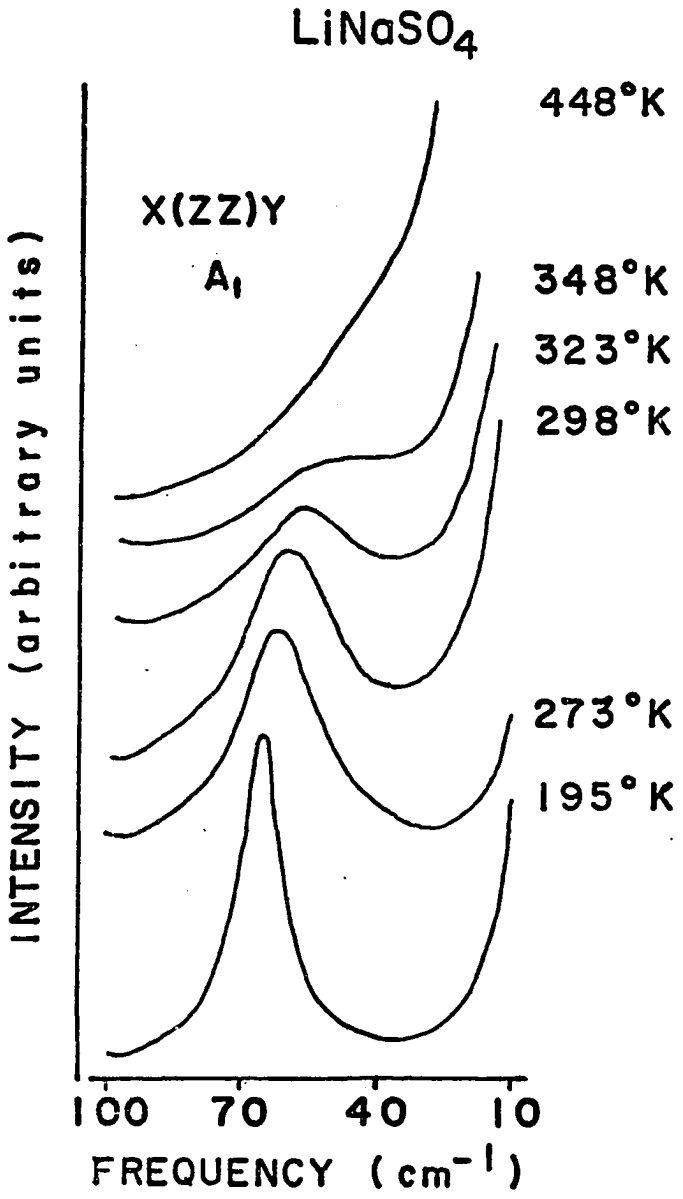


FIGURE 4.2. Temperature - dependent Raman scattering from the A_1 normal mode centered at 63 cm^{-1} (room temperature) in $LiNaSO_4$. Full scale intensity is 5000 cps.

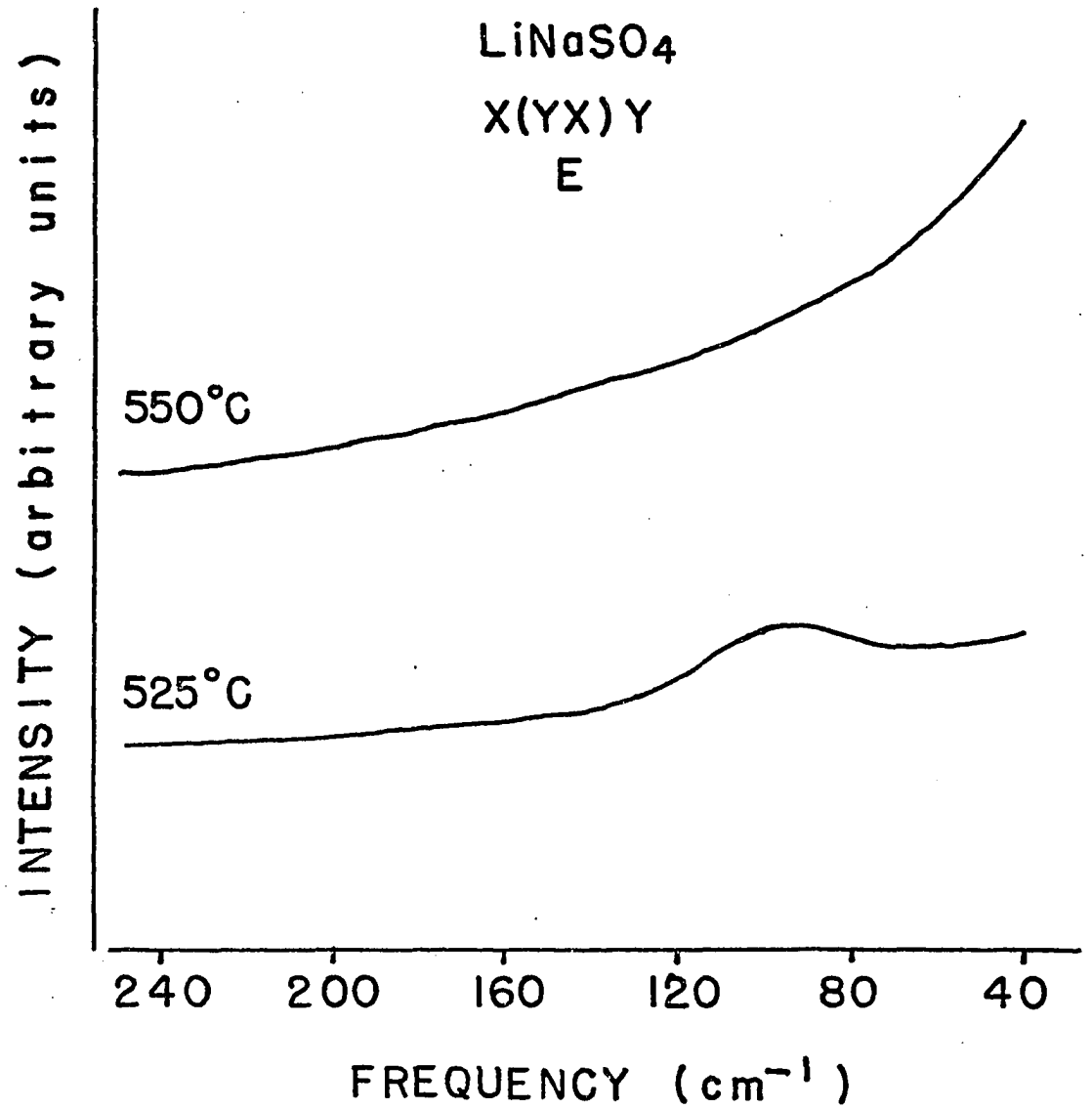


FIGURE 4.3. Raman scattering at temperatures just below and above the phase transition in $LiNaSO_4$. The broad density of states wing is observed at temperatures above the transition. Full scale intensity is 5000 cps.

Bogdanova[7] suggested that the high temperature phase of $LiNaSO_4$ could also be a plastic phase. They reported values for the heat of transition and heat of fusion for $LiNaSO_4$ of 5380 cal $mole^{-1}$ and 760 cal $mole^{-1}$, respectively, indicating a plastic phase. Jansson and Sjoblom[8] reported a value of 2.70 cm^3 $equivalent^{-1}$ for the change in volume at the phase transition. This value can be compared to a value of 1.16 cm^3 $equivalent^{-1}$ for Li_2SO_4 with its plastic phase and .06 cm^3 $equivalent^{-1}$ in $LiKSO_4$,[8] which does not have a plastic phase.

If the phase transition in $LiNaSO_4$ is associated with rotational motion of the sulfate ion as is the case in several sulfate crystals[1] and if the rotational motion of the sulfate ion is even greater after the phase transition, one might expect a mode that is due to sulfate ion rotational motion to be the most affected by temperature. A symmetry-based vibrational analysis for the external modes (see Chapter II) shows that the rotational motion of the sulfate ion about the c axis is of A_1 symmetry. One must not forget the A_1 external modes will be a mixture of the various motions of appropriate symmetry, but it is possible that one mode could be due primarily to sulfate librational motion.

A simple relationship for the frequency of such a librational mode is

$$\bar{\nu} = \frac{1}{2\pi c}\left(\frac{k}{I_{rot}}\right)^{\frac{1}{2}} \tag{4.1}$$

where I_{rot} is the moment of inertia for rotation and k is the force constant. If this describes vibration in a periodic potential of the following form

$$V(\alpha) = \tfrac{1}{2}V_o(1-\cos n\alpha) \tag{4.2}$$

where α is the angular coordinate describing the rotation and n is the periodicity, then V_0 may be viewed as a potential barrier which would have to be overcome for rotation into the next potential energy minimum. Identifying

$$k = \left(\frac{d^2V}{d\alpha^2}\right)_{\alpha=0} = \frac{n^2V_o}{2} \tag{4.3}$$

one then has

$$\bar{\nu} = \frac{1}{2\pi c}\left(\frac{V_o n^2}{2I_{rot}}\right)^{\frac{1}{2}} \tag{4.4}$$

Using the A_1 mode frequency value of 63 cm^{-1}, n=3, and calculating I_{rot} by the use of crystallographic data,[4] one obtains a value of .3 eV for V_o. Polishchuk and Bogdanova[7] have postulated that the .37 eV calculated activation energy for fast ion conduction in $LiNaSO_4$[8] contains a contribution from the activation energy associated with the sulfate ions' rotation. This activation energy and the calculated

potential energy barrier compare very well. This supports the idea that the A_1 mode at 63 cm^{-1} contains a large contribution from sulfate rotational motion.

The rapidly decreasing frequency of this mode is also of interest. In some solids a so-called "soft mode" is observed. A soft mode is a vibrational mode whose frequency goes towards zero as the temperature approaches the phase transition temperature, i.e., the normal mode frequency decreases in anticipation of the new structure. These modes are usually associated with structural phase transitions.

The 63 cm^{-1} A_1 mode could possibly be a soft mode associated with some structural order parameter in the crystal. However, overdamping of this mode could also cause the decreasing frequency with increasing temperature. The intensity of a Raman mode can be described by

$$I_{Ram}(\omega) = k \frac{\Gamma}{(\omega^2-\omega_o^2)^2 + \Gamma^2\omega^2} \qquad (4.5)$$

where k is a constant, ω_o is the harmonic frequency of the mode, and Γ is the damping constant. With increasing temperature the vibrational amplitude of the crystal becomes larger and anharmonicity becomes more important. This results in a large damping constant which affects the observed frequency.

To determine if the mode softens or is primarily overdamped, use was made of reduced Raman intensities.

The reduced Raman intensity I_{Red} is calculated from the Raman spectrum using the equation

$$I_{Red} = \frac{\omega}{1 + n\ (\omega,T)}\ I_{Ram}\ (\omega,T) \qquad (4.6)$$

where I_{Ram} is the experimentally observed Stokes Raman data scattering intensity, ω is the frequency, and $n(\omega,T)$ is the Bose-Einstein factor which is

$$n = (\exp \frac{\hbar\omega}{kT} - 1)^{-1} \qquad (4.7)$$

As Habbal, Zvirgzds, and Scott[10] have explained, the I_{Red} reaches a maximum at the harmonic frequency of vibration ω_o regardless of the size of the damping constant Γ.

The A_1 mode was resolved from the laser excitation wing by using a non-linear least squares program[11] to fit experimental intensity data at various temperatures. Appropriate combinations of Lorentzian and power functions were used for the A_1 mode shape and the laser wing respectively. The Lorentzian curves representing the A_1 mode were then converted to reduced Raman intensities using Equation 4.6. The reduced Raman intensities for the A_1 mode at various temperatures are shown in Figure 4.4. Figure 4.5 shows the Raman and reduced Raman frequencies. If the mode was overdamped instead of softening the reduced Raman frequency would not decrease. Figure 4.5 shows that at higher temperatures the Raman frequency decreases faster

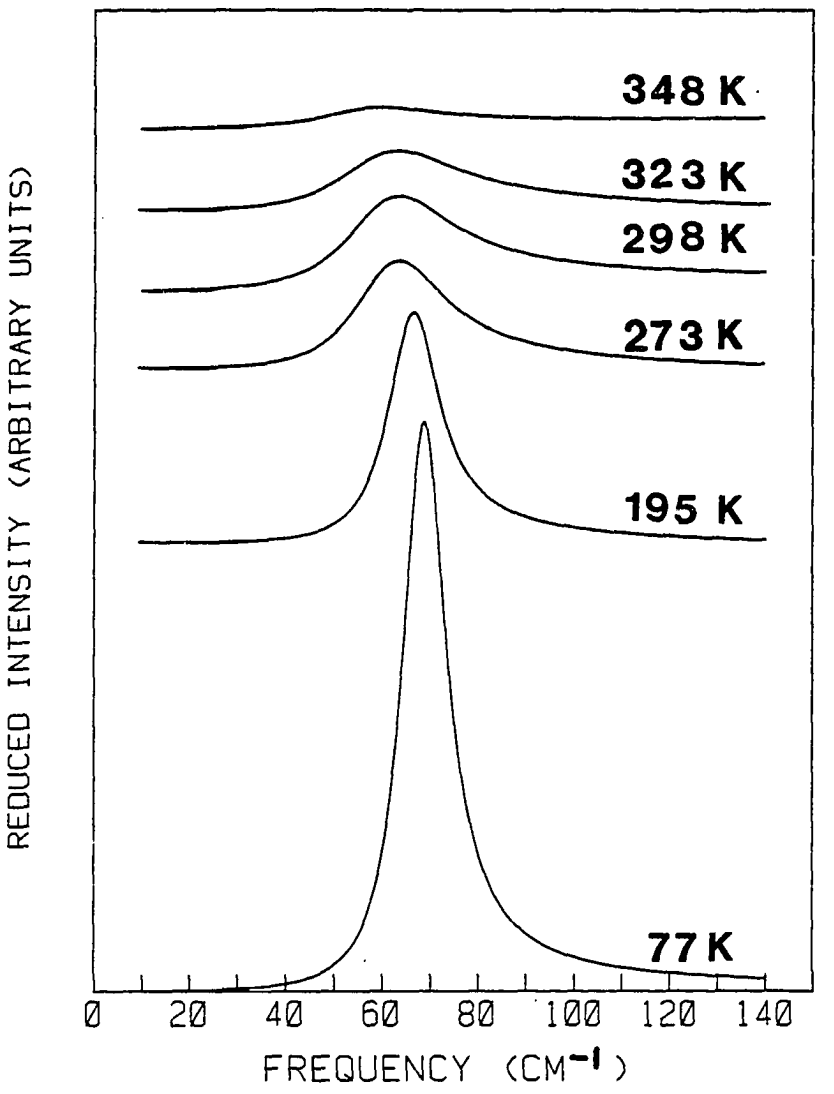


FIGURE 4.4. Reduced Raman spectra of the resolved 63 cm^{-1} (room temperature) A_1 mode in $LiNaSO_4$ at various temperatures.

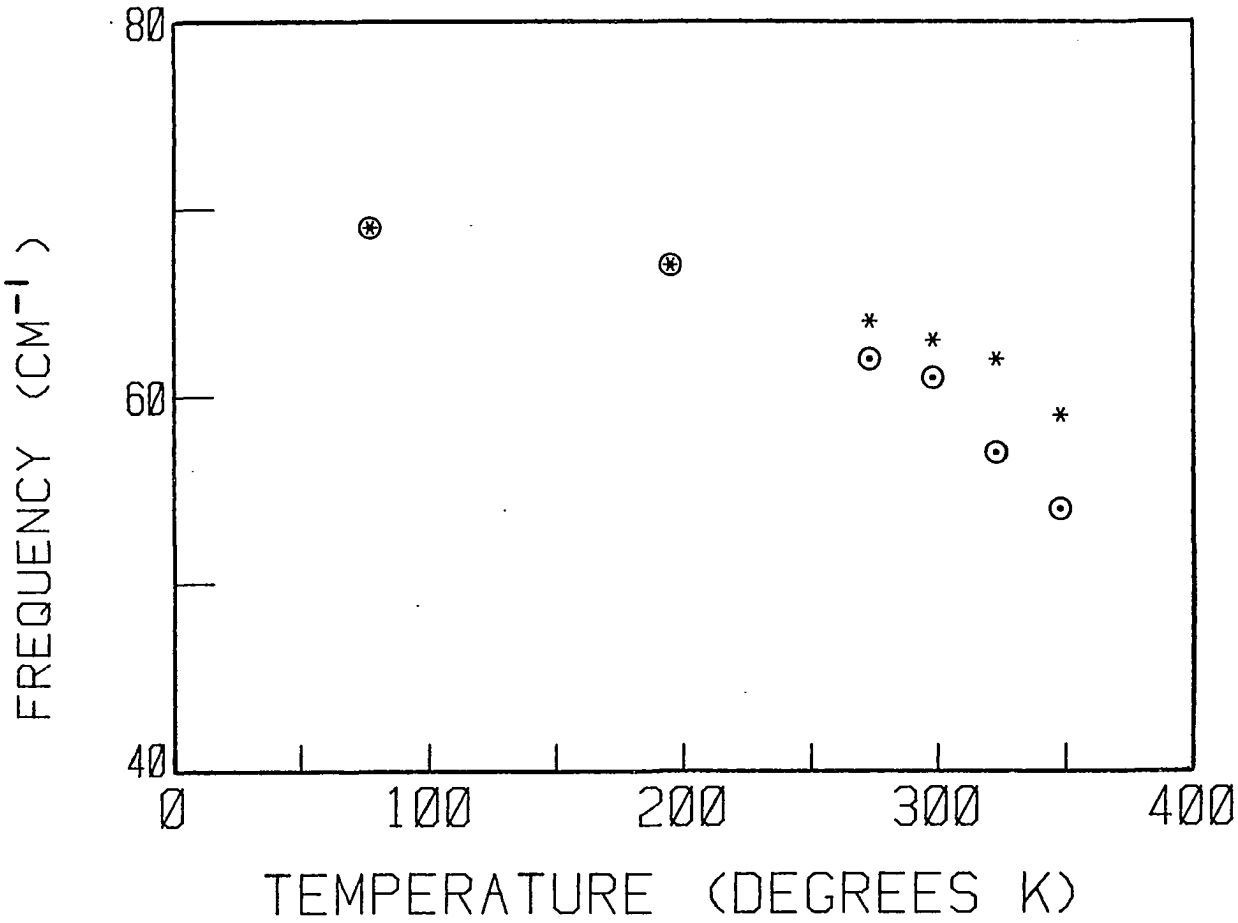


FIGURE 4.5. Temperature dependence of the low frequency A_1 mode band maximum in $LiNaSO_4$. The circled points are the maxima in in the observed Raman intensities, while the asterisks denote frequency maxima of I_{red} calculated according to Eq. 4.6.

as the temperature is increased than the reduced Raman frequency does indicating that overdamping does become more important at higher temperatures. Since the reduced Raman also decreases in frequency one must assume that this mode is also softening and that it can be associated with a structural parameter in the crystal.

If some rotational motion of the sulfate ion is involved in the A_1 mode at 63 cm^{-1} it would be interesting to investigate the contribution that this motion makes to the bandwidth. One can assume that at low temperatures the bandwidth results from an essentially harmonic vibrational mode. As the temperature increases a large librational contribution to the bandwidth could be expected especially in the case of a sulfate rotational mode. Rakov[12] has derived an expression for the bandwidth in terms of vibrational and orientational contributions. This expression is

$$\Gamma = \Gamma_{vib} + B \exp \frac{-A}{RT} \qquad (4.8)$$

The second term on the right above represents the orientational contribution to bandwidth while Γ_{vib} is the constant vibrational width contribution. The A corresponds to an activation energy. The computer resolved A_1 modes were corrected for thermal population of vibrational levels by using the Bose-Einstein factor (Equation 4.6). These corrected modes are shown in Figure 4.6. Temperature-

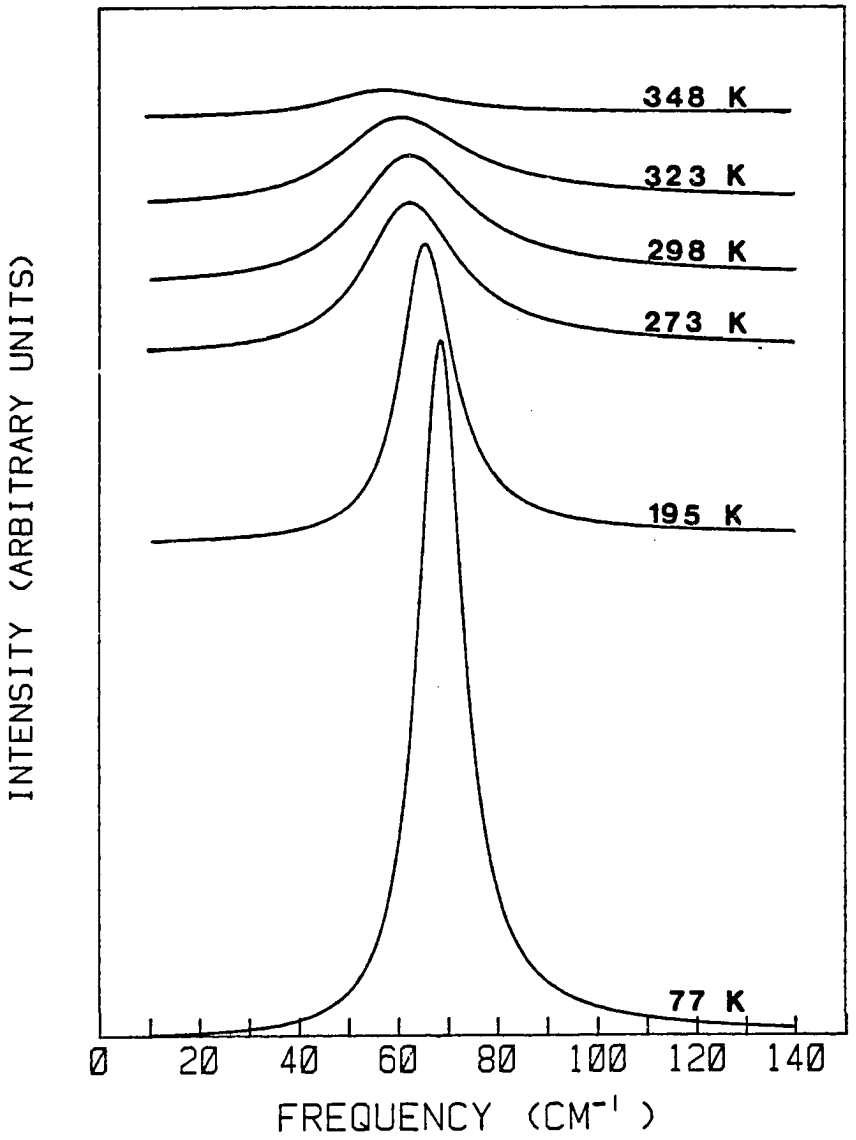


FIGURE 4.6. Raman spectra of the low frequency A_1 mode in $LiNaSO_4$ at various temperatures corrected for thermal population effects by using the Bose factor (Eq. 4.7).

dependent bandwidth data from these corrected modes were fit to Equation 4.8. The data and experimental fit are shown in Figure 4.7. The activation energy for orientational contributions is found to be .09±.01 eV. which is relatively low. This indicates that orientational contributions to bandwidth are very important especially as the temperature is increased.

Temperature Dependence of the External Modes of Lithium Potassium Sulfate

Lithium potassium sulfate has a room temperature structure of $P6_3$ (C_6^6).[13] A phase transition into an orthorhombic phase has been reported to occur at approximately 436°C.[14] The temperature of the phase transition was found to be approximately 450°C in this study.

The room temperature frequencies of the external mode of $LiKSO_4$ (excluding the lithium ion external modes) are given in Table 2.7. As expected the external modes broaden as the temperature increases. The E_2 mode at 103 cm^{-1} (room temperature frequency) merges with the mode of the same symmetry at 130 cm^{-1} (room temperature frequency) at approximately 300°C. The rest of the external modes are observable up to the phase transition. The frequency dependence of these modes is shown in Figure 4.8. The two lowest frequency E_1 and E_2 modes at 43 cm^{-1} and 53 cm^{-1}

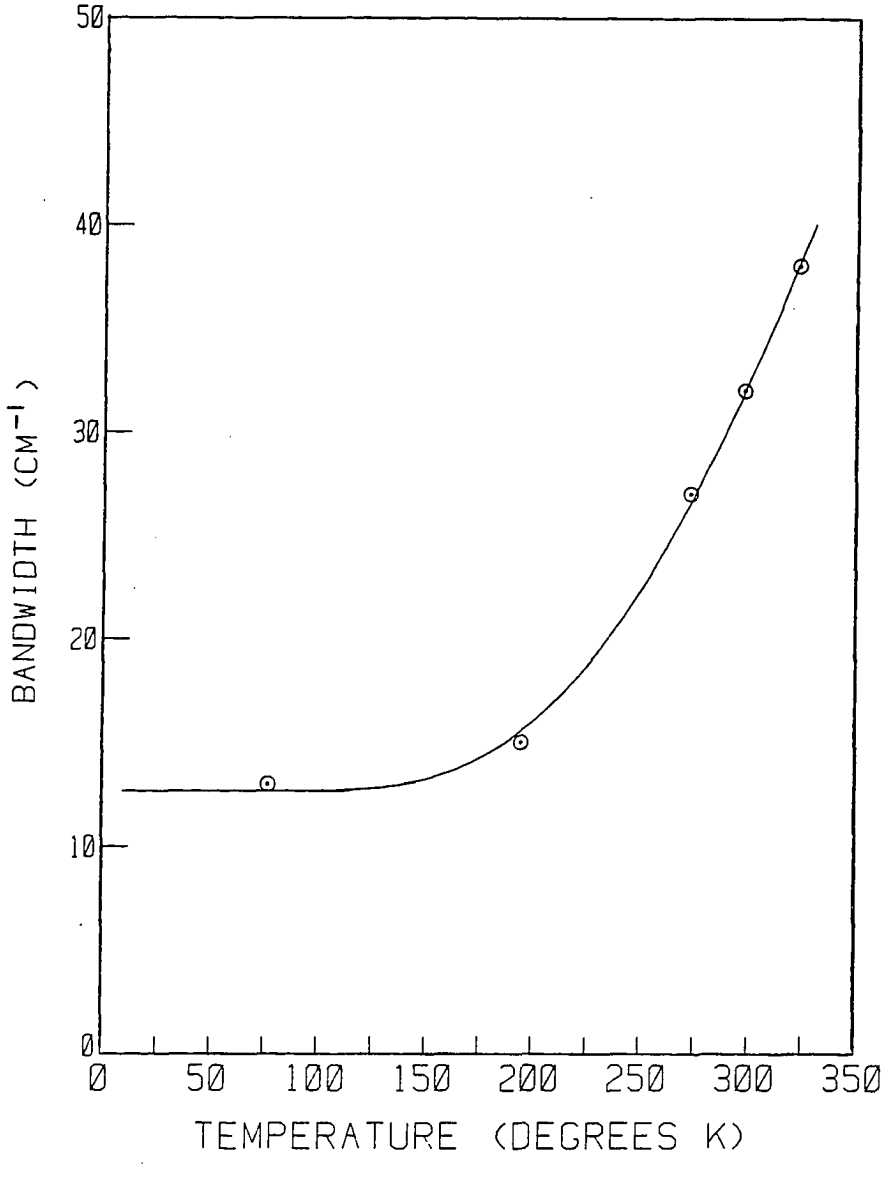


FIGURE 4.7. Orientational contribution to the Bandwidth of the low frequency A_1 mode in $LiNaSO_4$. The solid line is the best fit to Eq. 4.8.

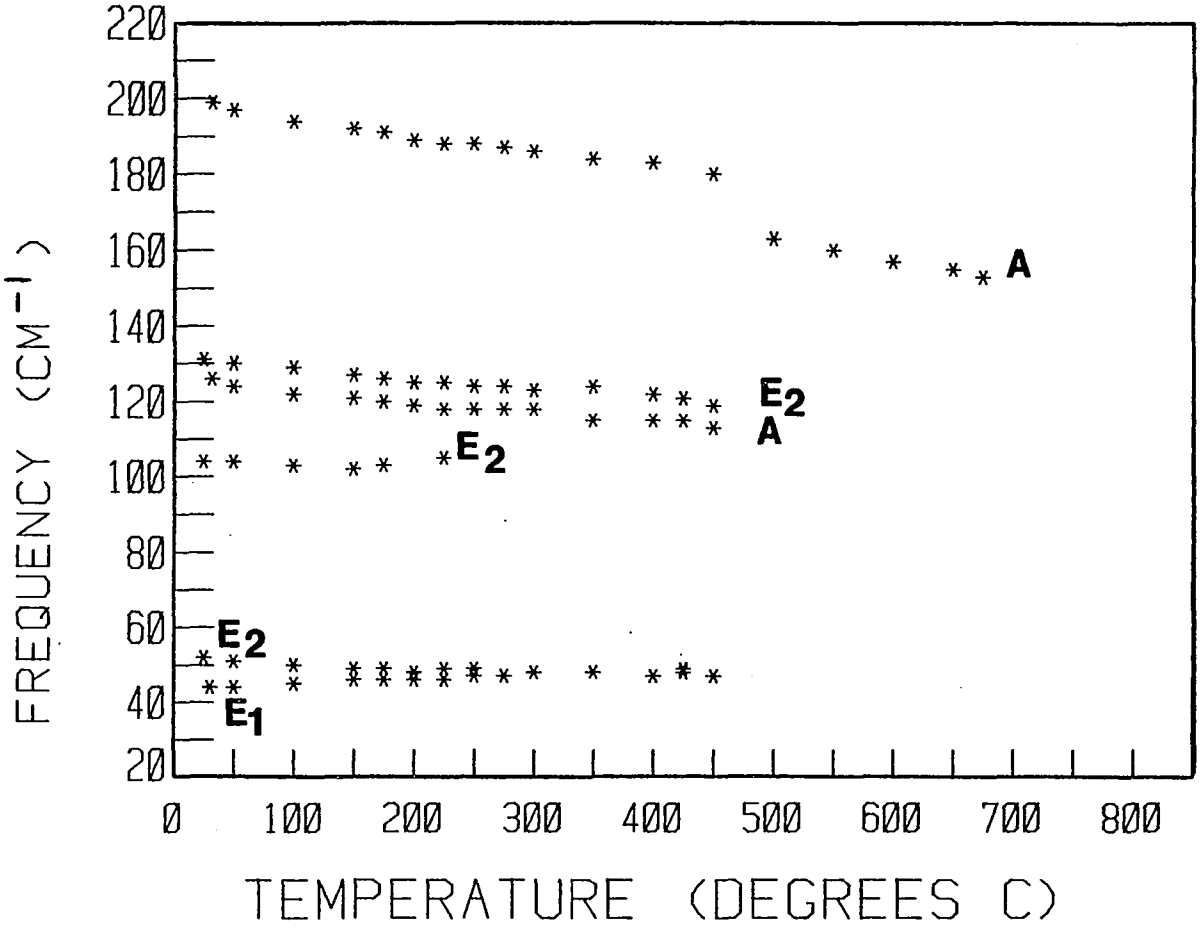


FIGURE 4.8. Temperature dependence of the external mode frequencies in $LiKSO_4$ from room temperature to 700° C. The phase transition occurs at approximately 450° C.

change only a few wavenumbers with increasing temperature, merging to a frequency of 47 cm^{-1} at 450°C. This behavior differs from that observed for the low frequency A_1 mode in $LiNaSO_4$. The rest of the external modes decrease in frequency as the temperature is increased. After the transition only one external mode is observable at 163 cm^{-1} in an x(zz)y experiment. In all other experimental geometries only a broad density of states extending from the side of the laser excitation line is observed. The density of states after the transition is shown in Figure 4.9.

The A mode at 202 cm^{-1} increased in bandwidth to a greater extent than any other external mode in $LiKSO_4$. Temperature-dependent spectra for this mode are shown in Figure 4.10 including the 163 cm^{-1} mode at 500°C.

Discussion of the Temperature Dependence of the External Modes in Lithium Potassium Sulfate

The A mode originating at 202 cm^{-1} is of special interest. Hiraishi, Taniguchi, and Takahashi[15] assign this mode as a sulfate rotational mode based on infrared reflection and Raman intensities. The frequency of 202 cm^{-1} along with I_{rot} calculated by using appropriate crystallographic data[16] were used in Equation 4.4 to calculate a potential barrier for rotation. The value obtained was 3.0 eV which is much higher than that calculated for the low frequency mode in $LiNaSO_4$. H. Takahashi,

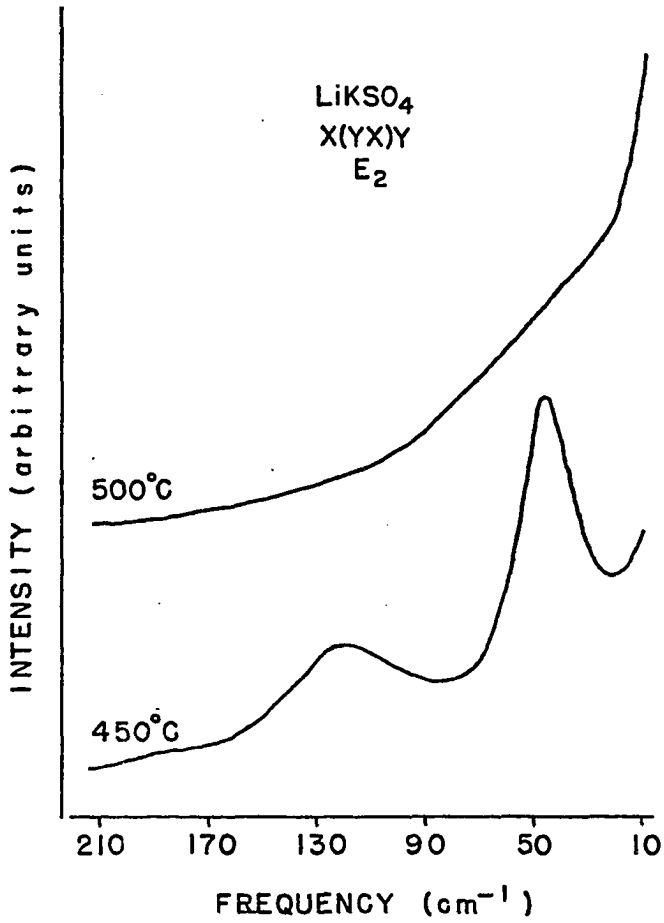


FIGURE 4.9. Raman spectra at temperatures just above and below the phase transition in $LiKSO_4$. The external modes are replaced by a broad density of states wing after the phase transition. Full scale intensity 5000 cps.

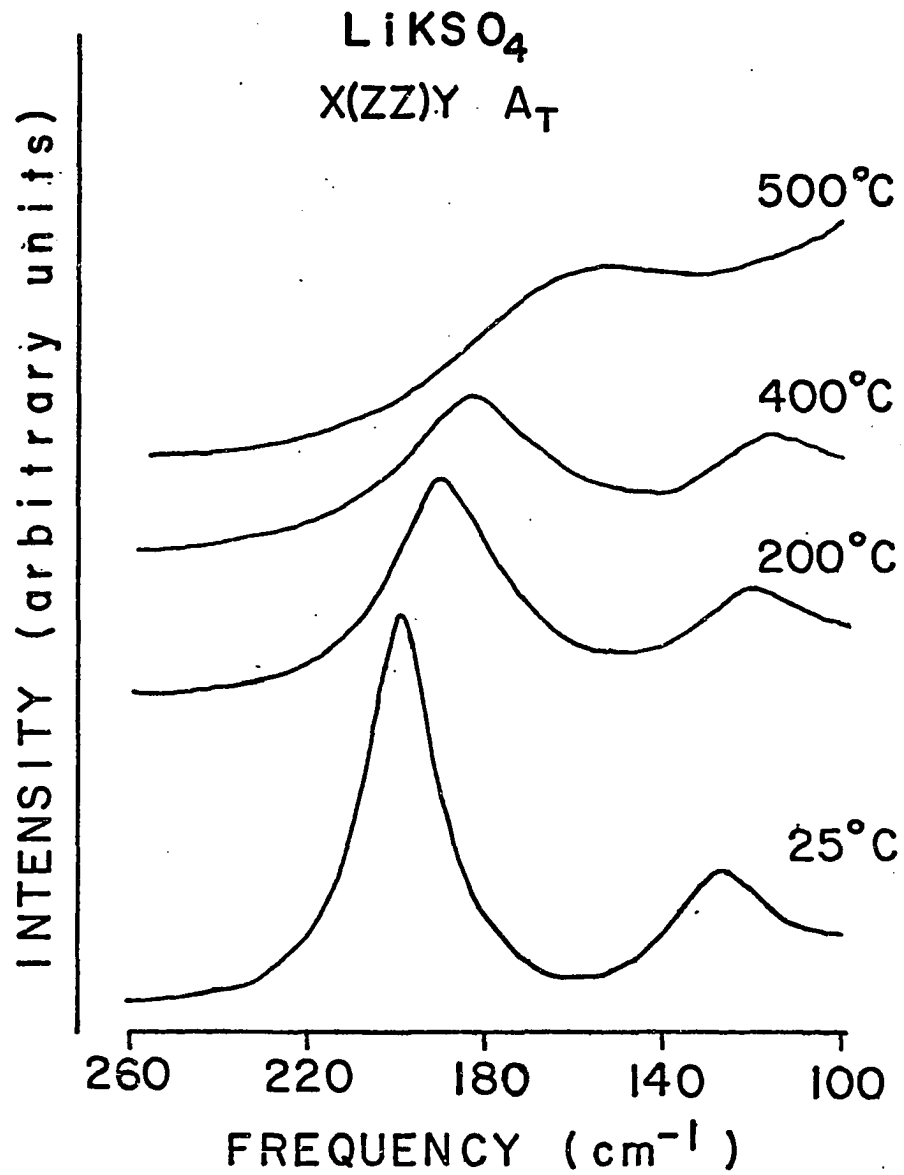


FIGURE 4.10. Raman spectra of the A mode at 202 cm^{-1} (room temperature frequency) in $LiKSO_4$ at various temperatures. Full scale intensity is 5000 cps.

Meshitsuka, and K. Higasi[17] have postulated that the potential barrier for rotation should be approxumately .3 eV in alkali metal sulfates. The high value calculated here for the A mode of $LiKSO_4$ could mean that other kinds of ionic motion (i.e., translational motion) contribute extensively. Translational motion of the potassium ion and sulfate ion could be involved. Takahashi et al.[17] in their infrared work on various sulfates have assigned the highest frequency external mode as resulting from metal-sulfate relative (translational) motion. In the mixed cation sulfate, $LiKSO_4$, there are two vibrational modes involving mainly lithium ion motion which have already been identified in the spectral region of roughly 400 cm^{-1} (Chapter II) and are the highest frequency external modes. The external mode of next highest frequency in $LiKSO_4$ is the A mode at 202 cm^{-1}, suggesting significant potassium ion motion in this normal mode. Therefore it seems likely that this mode contains translational motion of the ionic species as well as rotational (librational) motion.

Reduced Raman curves were calculated for computer resolved bands of the 202 cm^{-1} mode at various temperatures. The Raman frequencies and the reduced Raman frequencies are plotted vs. temperature in Figure 4.11. The frequency of the reduced Raman is seen to decrease in frequency almost as much as the Raman frequency does as the temperature is increased. Therefore this mode seems to soften more than

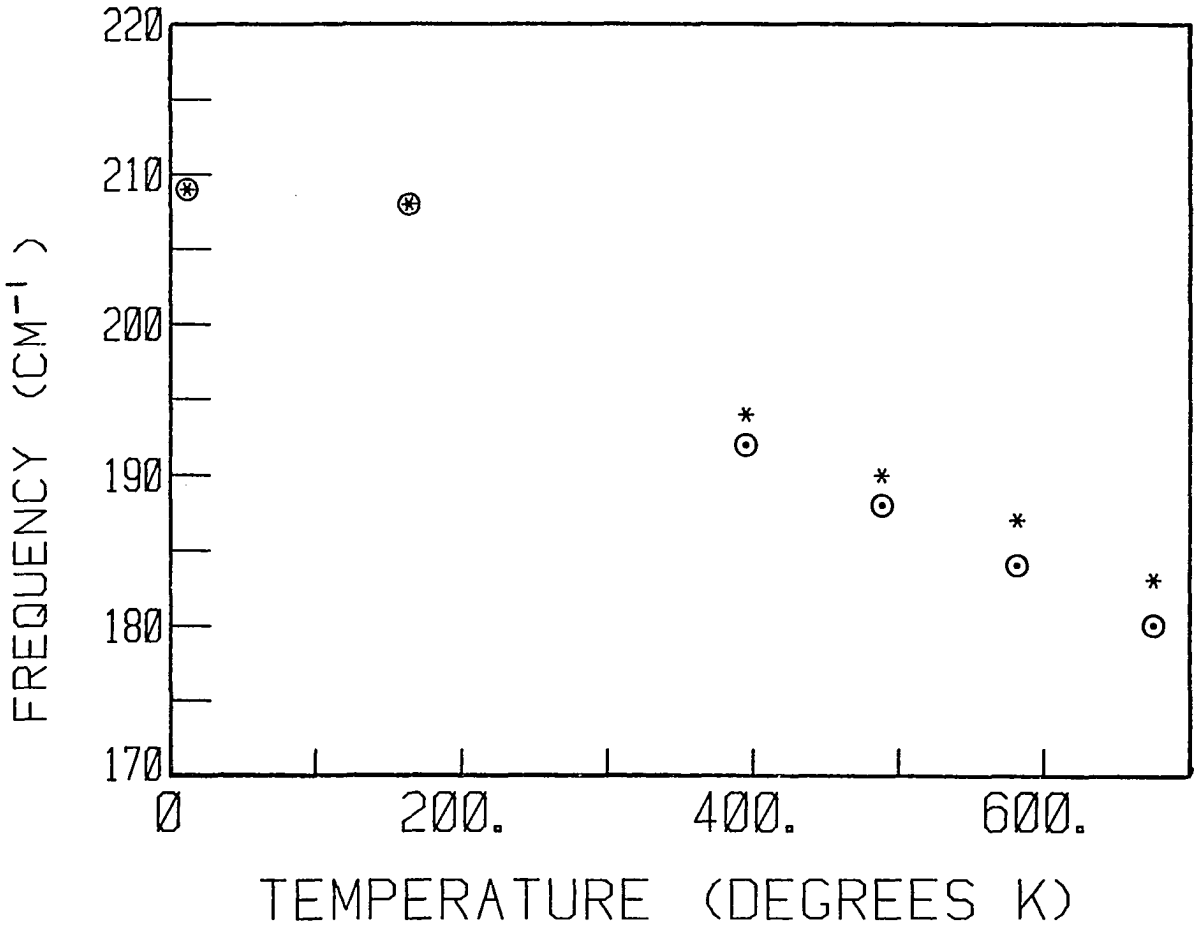


FIGURE 4.11. Temperature dependence of the A mode (202 cm^{-1}, room temperature value) band maximum in $LiKSO_4$. The circled points are the maxima in the observed Raman intensities, while the asterisks denote frequency maxima of I_{red} calculated according to Eq. 4.6.

the 63 cm^{-1} mode in $LiNaSO_4$, strongly suggesting that the mode is associated with a structural change occurring in the unit cell.

Since the exact nature of this mode is more in doubt than the low frequency A_1 mode in $LiNaSO_4$, the $LiKSO_4$ 202 cm^{-1} A mode was fit to the more general Arrhenius-like function given by Equation 3.3. A plot of the experimental data points and the calculated fit is shown in Figure 4.12. The activation energy obtained is .06±.01 eV.

Temperature Dependence of the External Modes in Sodium Potassium Sulfate

Sodium potassium sulfate has a room temperature structure of $P\bar{3}m1$ (D_{3d}^3)[18] and exhibits a phase transition at 440°C into a $P6_3mc$ (C_{6v}^4) phase.[19] The transition in this study was observed to occur between 450 and 500°C.

Table 2.10 lists the room temperature frequencies for $NaK_3(SO_4)_2$. The external modes decrease slowly in frequency as the temperature is increased as shown in Figure 4.13. The A_{1g} mode at 45 cm^{-1} is the lowest frequency external mode and, like the lowest frequency external mode in $LiKSO_4$, changes only slightly in frequency with increasing temperature. The broad A_{1g} mode at 104 cm^{-1} (room temperature value) seems to be the most affected by temperature as its frequency decreases the fastest. At

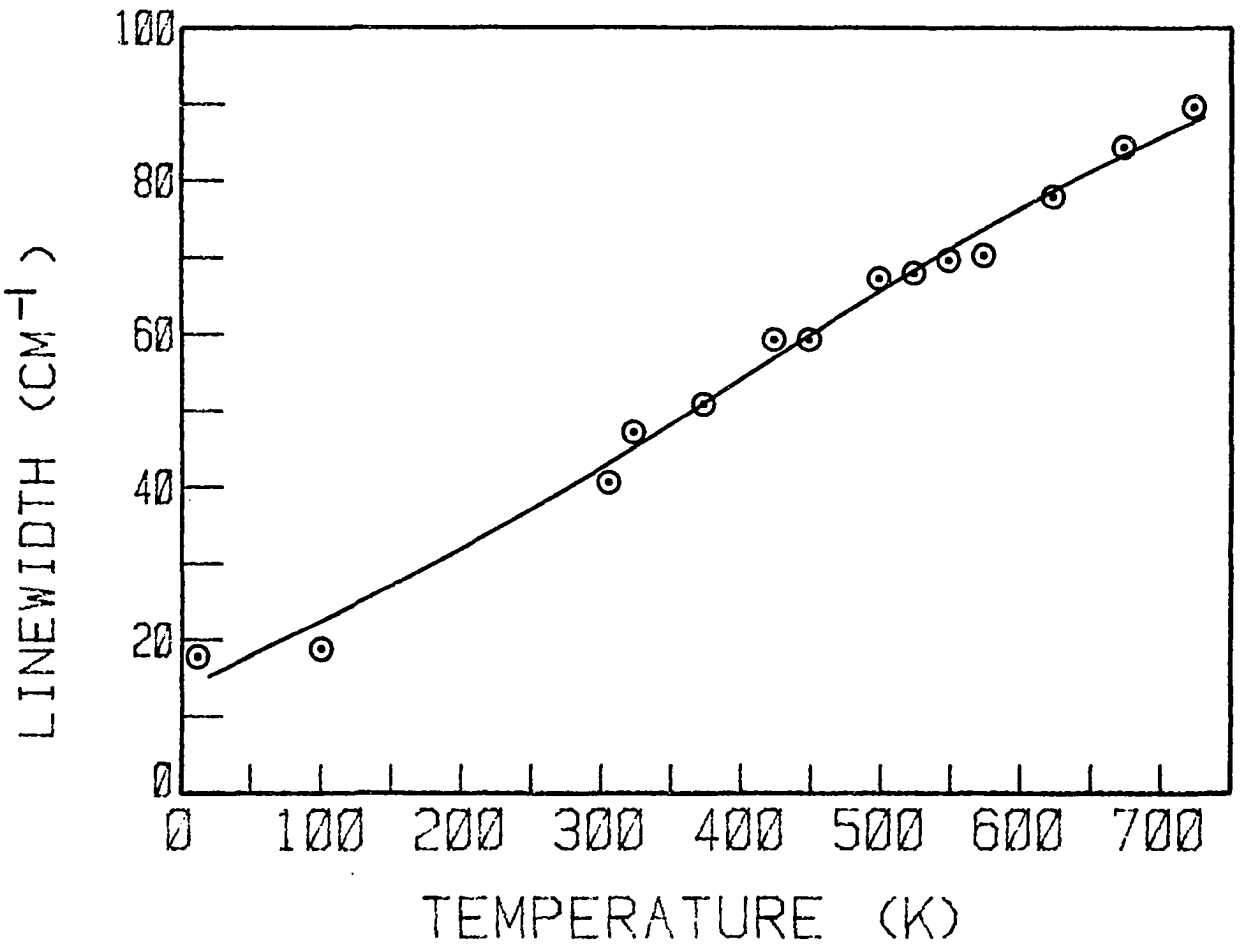


FIGURE 4.12. Temperature - dependent linewidth data for the A mode at 202 cm^{-1} (room temperature value). The solid line is the best fit to Eq. 3.3.

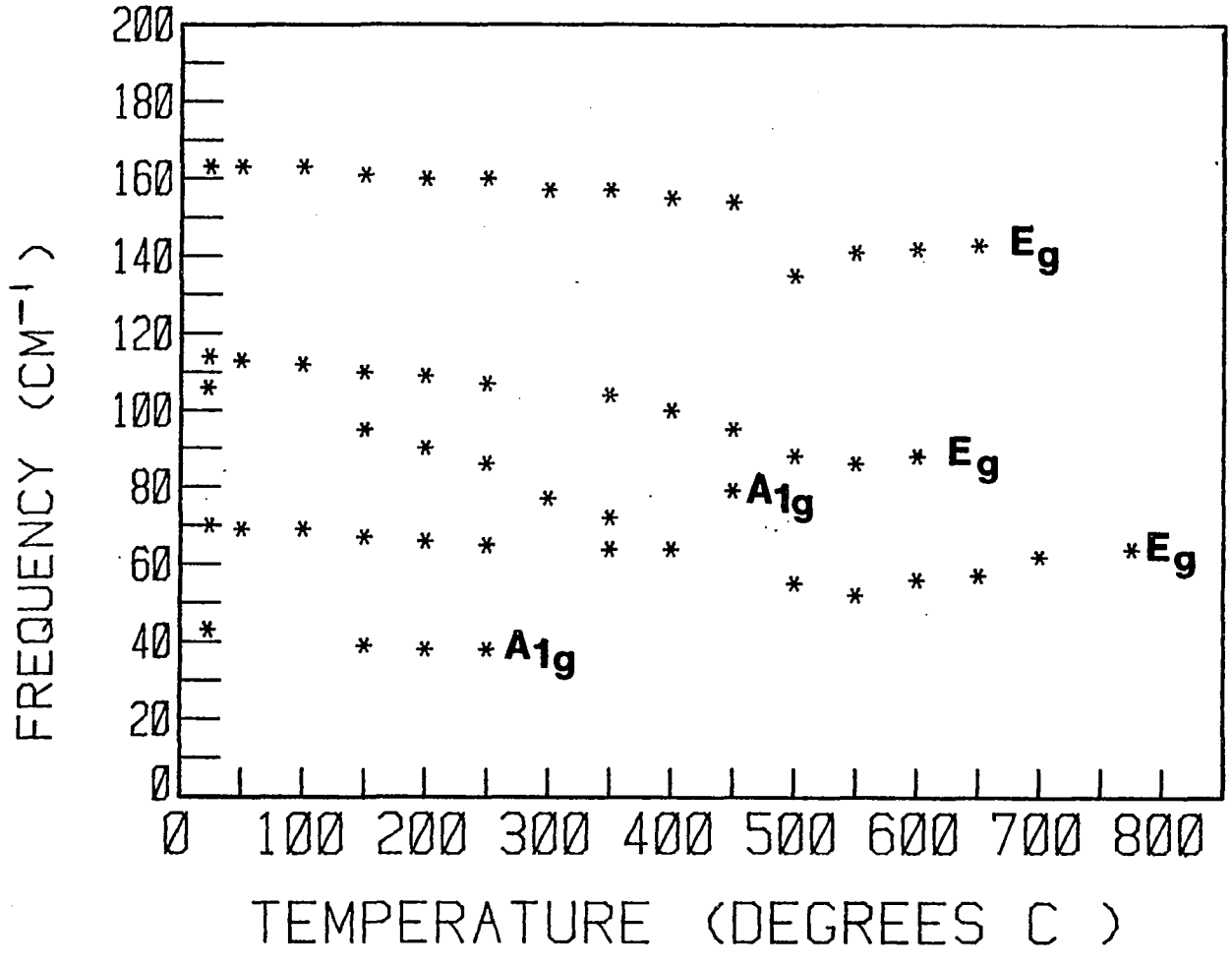


FIGURE 4.13. Temperature - dependent frequency data for the external modes in $NaK_3(SO_4)_2$. The phase transition occurs between 450 and 500° C.

300°C a broad wing appears next to the laser line making many of the external modes unobservable. At 350°C some external modes reappear. This is shown in Figure 4.14. Strange behavior is also noticed in the internal mode region at approximately this temperature (Chapter V). The phase diagram given by Eysel[18] for the system Na_2SO_4-K_2SO_4 indicates that the solid solution $NaK_3(SO_4)_2$ can coexist with a phase of K_2SO_4 at temperatures where the disappearance of the peaks occurs. It is possible that at 300°C the K_2SO_4 phase is first appearing, causing disorder in the system. At higher temperatures both $NaK_3(SO_4)_2$ and K_2SO_4 exist and contribute external mode bands.

Several external modes are observable after the phase transition. Unlike $LiNaSO_4$ and $LiKSO_4$ the formation of a density of states type wing next to the excitation line does not wipe out the external modes. This is shown in Figure 4.15. No further analysis was done on the external mode due to the possible existence of the K_2SO_4 phase.

Conclusions

The temperatures at which the phase transitions occurred in this study seem to be slightly higher than those previously reported. This is probably due to error associated with determining the temperature of the crystal in the high temperature cell. It should be mentioned that the transition

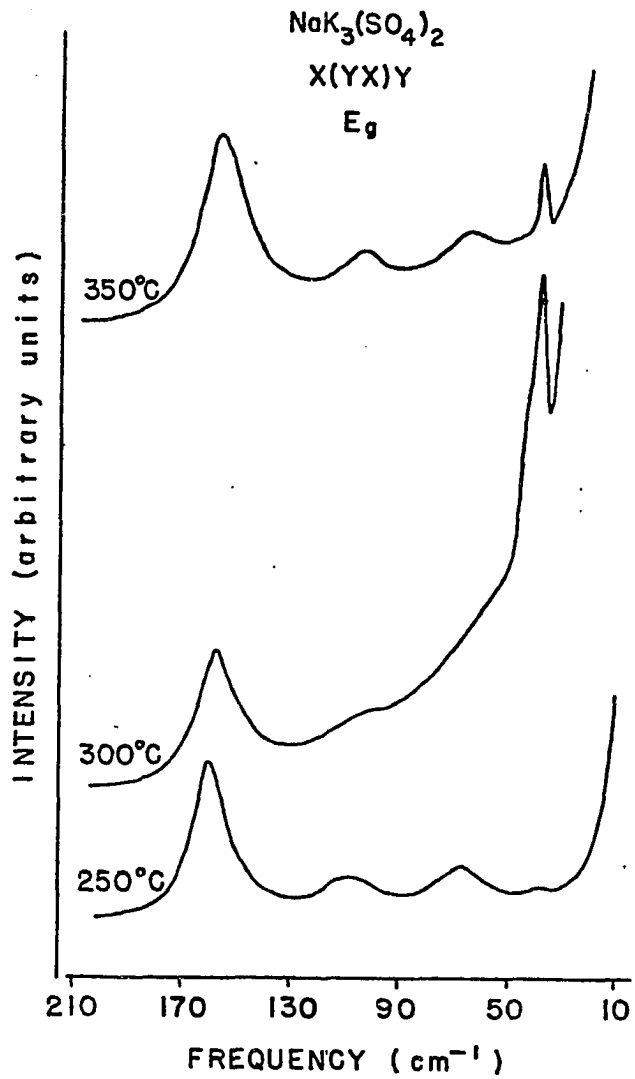


FIGURE 4.14. Raman spectra showing the appearance of a density of states wing at 300° C and reappearance of external modes at 350° C in $NaK_3(SO_4)_2$. Full scale intensity is 5000 cps.

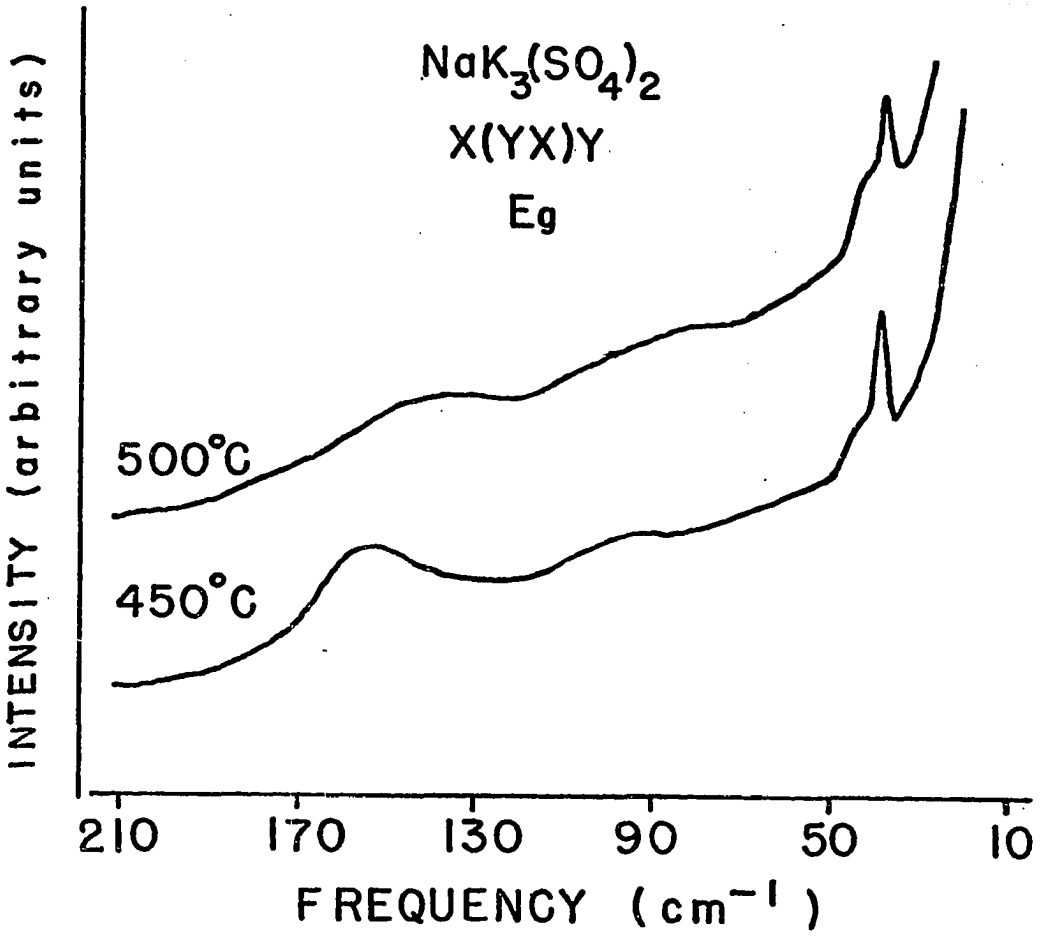


FIGURE 4.25. Raman spectra at temperatures just above and below the phase transition in $NaK_3(SO_4)_2$. External modes are still observable after thr phase transition in this sulfate. Full scale intensity is 5000 cps.

temperature of $NaK_3(SO_4)_2$ is somewhat dependent on the potassium ion concentration[19] and that Ando[20] has reported a value of 445°C for the phase transition in $LiKSO_4$ which is closer to the value observed here.

Each of the three sulfates appears to have at least one external mode whose behavior with increasing temperature is unique among the normal modes of that particular crystal. Lithium sodium sulfate has a low frequency mode at 63 cm^{-1} which appears to soften with temperature and seems to be related to sulfate rotational motion. Lithium potassium sulfate has a relatively high frequency mode at 202 cm^{-1} that broadens faster than its other external modes. It appears to soften indicating a close relationship to a structure parameter. An A_{1g} mode at 104 cm^{-1} in $NaK_3(SO_4)_2$ decreases in frequency at a greater rate than other external modes in this system.

The existence of this density of states type wing after the phase transition in the three sulfate systems has been seen in other crystals after a phase transition.[10,21,22] This is generally attributed to disorder in the system and hence the breakdown of Raman selection rules. It can be postulated that more disorder exists in $LiNaSO_4$ since no external modes are observable and that $NaK_3(SO_4)$ is the most ordered since several external modes can be seen at temperatures above the phase transition.

It is possible that the transition in $LiNaSO_4$ involves

rotational motion of the sulfate ion to a greater extent than $LiKSO_4$. Low frequency modes in $LiKSO_4$ change only slightly in frequency while the low frequency mode in $LiNaSO_4$ is very temperature sensitive. The external mode that is the most temperature-sensitive in $LiKSO_4$ seems to have a great deal of translational contribution indicating that translation of the ions in $LiKSO_4$ is very important in the phase transition in this system.

References

1. K. J. Rao and C. N. R. Rao, J. Mater. Sci. 1, 238 (1966).

2. L. Nilsson, J. O. Thomas, and B. C. Tofield, J. Phys. C 13, 6441 (1980).

3. A. F. Polishchuk, Russ. J. Phys. Chem. 47, 1088 (1973).

4. B. Morosin and D. L. Smith, Acta Crystallogr. 22, 906 (1967).

5. J. Forland and J. Krogh-Moe, Acta Crystallogr. 11, 224 (1958).

6. A. Kvist, Z. Naturforsch. A 22, 208 (1969).

7. A. F. Polishchuk and A. K. Bogdanova, Russ. J. Phys. Chem. 51, 1195 (1977).

8. B. Jansson and C.-A. Sjoblom, Z. Naturforsch. A 25. 1115 (1970).

9. A. F. Polishchuk and T. M. Shurzhal, Elektrokhimiza 9, 838 (1973).

10. F. Habbal, J. A. Zvirgzde, and J. F. Scott, J. Chem. Phys. 11, 4984 (1978).

11. Subroutine NLLSQ was written by Dr. E. Enwall and follows the strategy of D. W. Marquardt, J. Soc. Ind. Appl. Math. 2, 431 (1963).

12. A. V. Rakov, Tr. Fiz. Inst., Akad. Nauk SSSR 27, 111 (1964).

13. A. J. Bradley, Phil. Mag. 49, 1225 (1925).

14. K. Schroeder, Thesis, Göteborg (1975).

15. H. Hiraishi, N. Taniguchi, H. Takahashi, J. Chem. Phys. 65, 3821 (1976).

16. H. Schultz and R. Frech (Unpublished results).

17. H. Sakahashi, S. Meshitsuka, and K. Higasi, Spectrochem. Acta, Part A 31A, 1617 (1975).

18. K. Okada and J. Ossaka, Acta Crystallogr. Sec. B B36, 919 (1980).

19. W. Eysel, Am. Mineral. 58, 736 (1973).

20. R. Ando, J. Phys. Soc. Japan 17, 937 (1962).

21. G. Burns, F. H. Dacol, and M. W. Shafer, Solid State Commun. 19, 287 (1976).

22. G. Burns, F. H. Dacol, and M. W. Shafer, Solid State Commun. 19, 291 (1976).

CHAPTER V

INTERNAL MODE TEMPERATURE DEPENDENCE OF LITHIUM SODIUM SULFATE, LITHIUM POTASSIUM SULFATE, AND SODIUM POTASSIUM SULFATE

Introduction

An investigation of the internal modes provides an additional opportunity for a comparative vibrational spectroscopic study in $LiNaSO_4$, $LiKSO_4$ and $NaK_3(SO_4)_2$. This study provides information about potential energy environment of the sulfate ion and the changes of that environment with temperature in the three sulfates. The internal modes have a much larger Raman scattering intensity than the external modes in these sulfate crystals and are easily observable at temperature above the phase transitions, in contrast to the external modes (see Chapter IV). The comparison between the internal modes of the three systems also provides additional information about the phase transitions.

The crystals were prepared in the same manner as

described in the experimental section in Chapter II. The geometrical arrangement of the Raman scattering experiment and the room temperature vibrational mode assignments and frequencies are also given in that chapter. The room temperature internal mode frequencies of $LiNaSO_4$, $LiKSO_4$, and $NaK_3(SO_4)_2$ are given in Tables 2.2, 2.6 and 2.9 respectively. In some cases the frequency values reported in these tables may differ slightly from the room temperature values presented here. These small changes in frequency are due to the heating pretreatment which is described in the experimental sections in Chapters III and IV. The high temperature spectra were obtained using the same cell and procedure as described in Chapter III's experimental section.

Lithium Sodium Sulfate: Temperature Dependence of Internal Modes

A phase transition into a body centered cubic phase occurs in $LiNaSO_4$ at approximately 520°C.[1,2] In this study the transition was observed between 525°C and 550°C. Reasons for the higher temperature of the phase transition here are given in Chapter IV.

The ν_1 Region

The ν_1 region has three modes of A_1 symmetry whose initial frequencies are 970, 999, and 1028 cm^{-1} at room temperature. The temperature-dependent spectra are shown in Figure 5.1. The modes are seen to broaden with increasing temperature. The frequency of the 970 cm^{-1} mode increases to a value of 977 cm^{-1} just before the phase transition. The mode at 999 cm^{-1} changes very little in frequency, slowly decreasing to a value of 995 by 525°C. The 1028 cm^{-1} mode is the most temperature-dependent, decreasing to a value of 1009 at 425°C. At this temperature the 1028 cm^{-1} mode has merged with the rather broad band due to the modes originating at 970 cm^{-1} and 999 cm^{-1} and can no longer be distinguished. The mode originating at 970 cm^{-1} decreases somewhat in intensity relative to the mode originating at 998 cm^{-1} just below the phase transition. After the phase transition occurs one broad band at 990 cm^{-1} is observed that changes only slightly in temperature up to 625°C. The temperature-dependent frequency data is shown in Figure 5.2.

The ν_2 Region

In this region only the mode whose room temperature frequency was 483 cm^{-1} was investigated. The mode generally broadens with temperature and the frequency decreases from 483 cm^{-1} to 465 cm^{-1} just below the phase transition. After

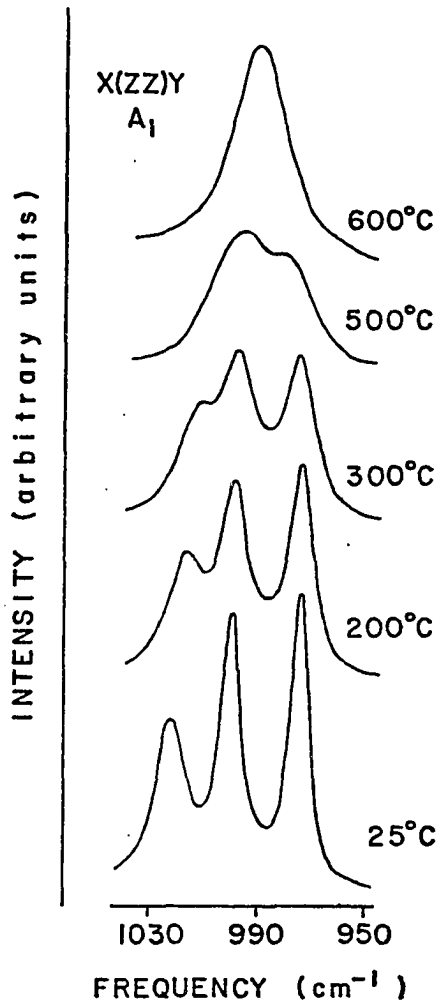


FIGURE 5.1. Temperature - dependent spectra of the ν_1 region in $LiNaSO_4$. Full scale intensity at 25° C is 2 x 10^5 cps, at all other temperatures 1 x 10^5 cps.

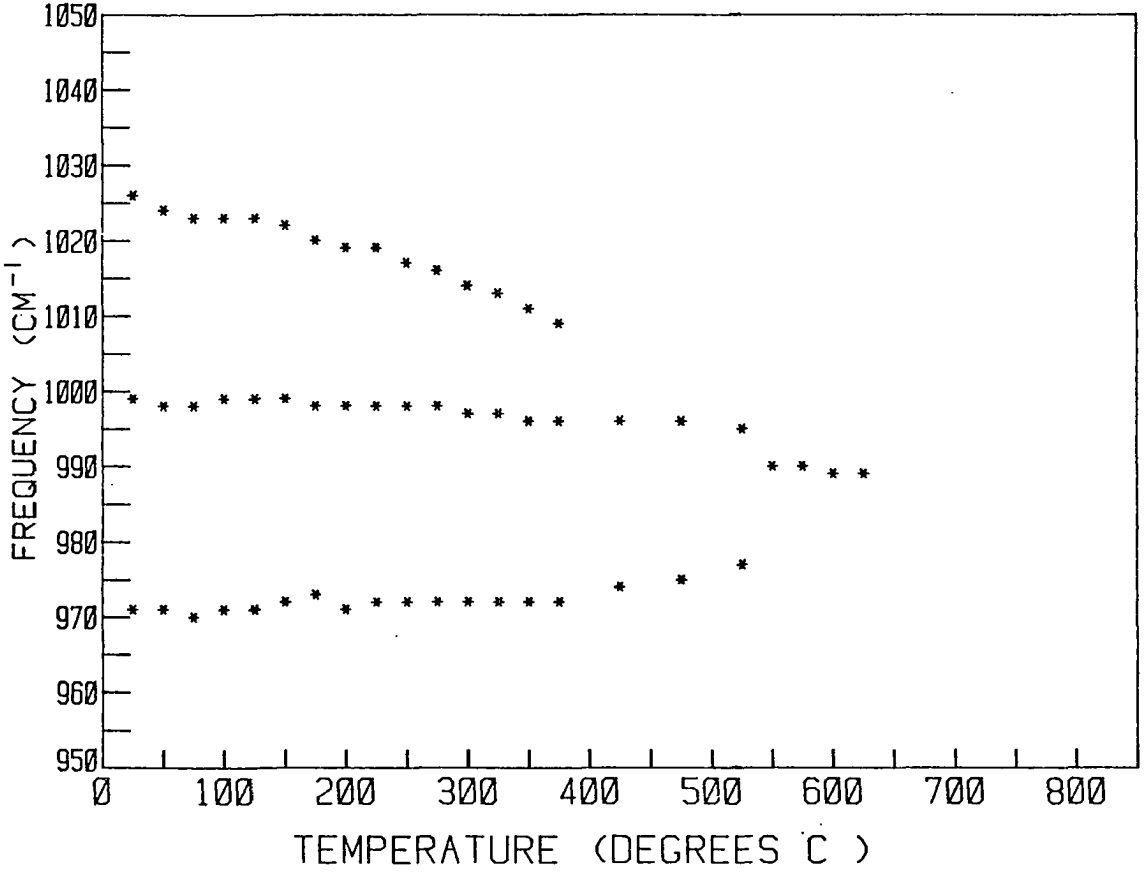


FIGURE 5.2. Temperature - dependent frequency for the A_1 modes in the ν_1 region in $LiNaSO_4$.

the phase transition occurs the ν_2 band broadens further and decreases in frequency to 455 cm^{-1} at 550°C. The frequency increases slightly to a value of 458 cm^{-1} at 625°C. A graph of this data is shown in Figure 5.3.

The ν_3 Region

The ν_3 region has modes of both A_1 and E symmetry. The room temperature frequency of these modes is given in Table 2.2. Figure 5.4 shows temperature-dependent spectra for the 1172 cm^{-1} A_1 mode while Figure 5.5 has spectra of the E components. Many of the bands are weak in this region and are difficult to observe. Others broaden out and merge with more intense modes. The A_1 mode originating at 1172 broadens out and decreases in intensity as the temperature is increased. Its frequency decreases from 1172 to 1159 cm^{-1} at the phase transition. The E mode originating at 1119 cm^{-1} decreases in frequency until it is contained in a very broad asymmetric band centered at 1114 cm^{-1} at 525°C. After the phase transition an extremely broad, weak asymmetric band centered at 1108 cm^{-1} is observed which does not seem to exhibit polarization properties. Frequency data are shown in Figure 5.6.

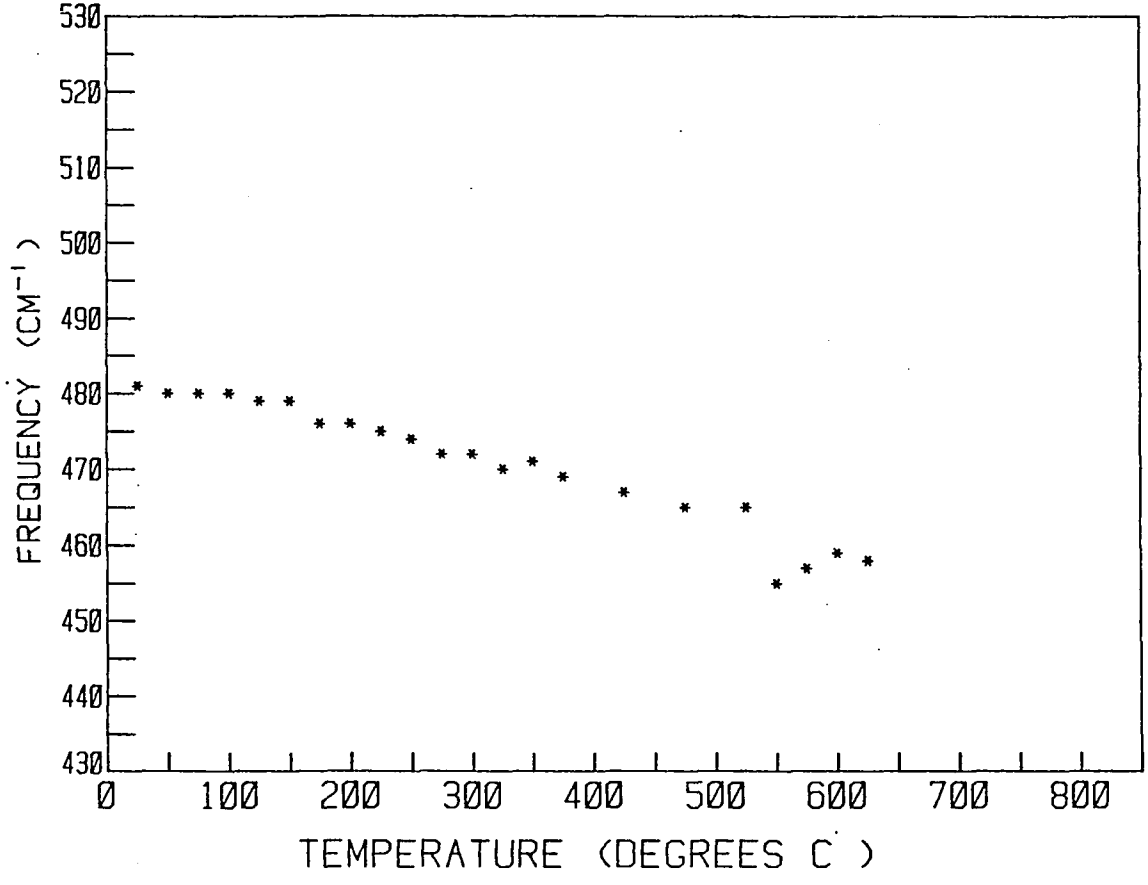


FIGURE 5.3. Temperature - dependent frequency of the ν_2 region E mode in $LiNaSO_4$.

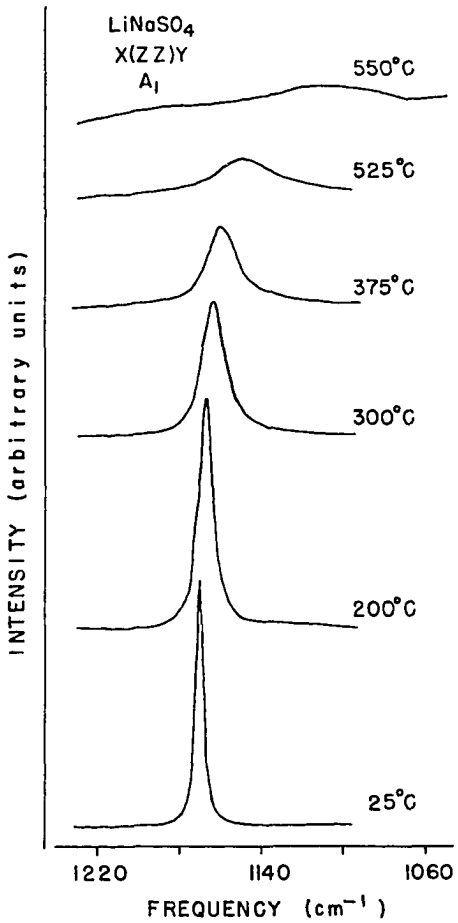


FIGURE 5.4. Temperature - dependent Raman Spectra of the A_1 modes in the ν_3 region in $LiNaSO_4$. The full scale intensities are: 25° C, 1 x 10^5 cps; 200 - 525°C, 5 x 10^4 cps ; and 550° C, 2 x 10^4 cps.

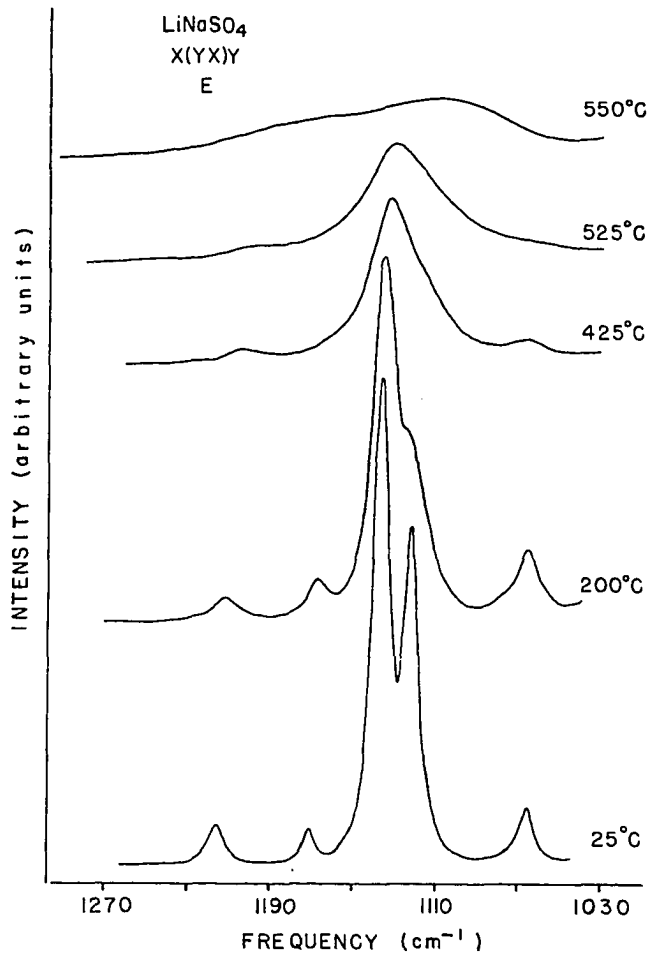


FIGURE 5.5. Temperature - dependent Raman spectra of the E modes in the ν_3 region of $LiNaSO_4$. Full scale intensity is 1×10^4 cps.

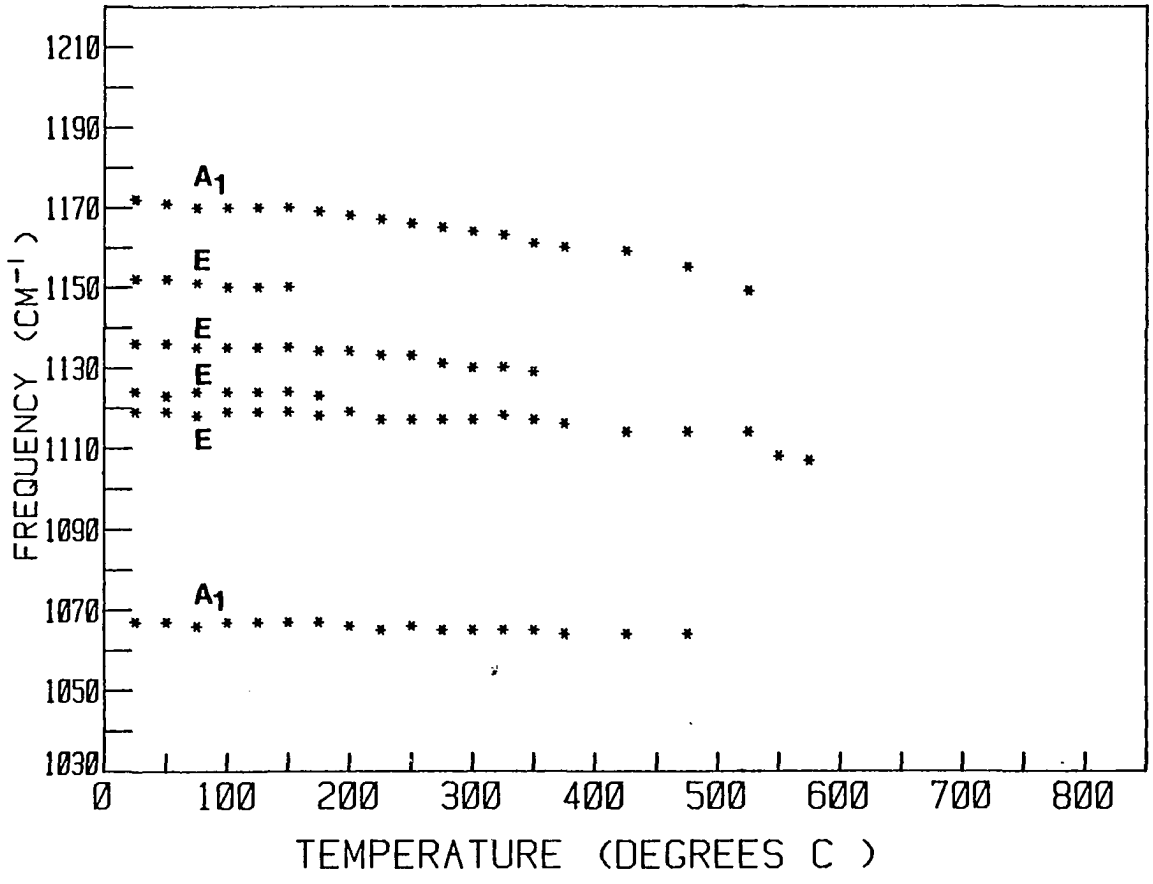


FIGURE 5.6. Temperature-dependent frequency data for the ν_3 region in $LiNaSO_4$

The ν_4 Region

The ν_4 region also has components of A_1 and E symmetry (Table 2.2) which broaden and merge together as the temperature is increased. The A_1 mode whose frequency at 25°C is 660 cm^{-1} displays the greatest relative decrease in frequency, shifting to 644 cm^{-1} by 525°C. After the phase transition a broad symmetrically shaped mode is observed in all polarizations with a frequency of 629 cm^{-1} up to 625°C. Figure 5.7 is a graph of frequency vs. temperature for the modes of the ν_4 region.

Lithium Potassium Sulfate: Temperature Dependence of Internal Modes

Lithium potassium sulfate has a reported phase transition at 436°C into an orthorhombic phase.[2] The transition was observed in this study at approximately 450°C.

The ν_1 Region

One mode at approximately 1013 cm^{-1} is observed in the ν_1 region. Temperature-dependent spectra are shown in Figure 5.8. The band broadens and decreases in frequency to a value of 996 cm^{-1} at 450°C with no abrupt change in frequency at the phase transition as was observed in $LiNaSO_4$. Above the phase transition the frequency continues

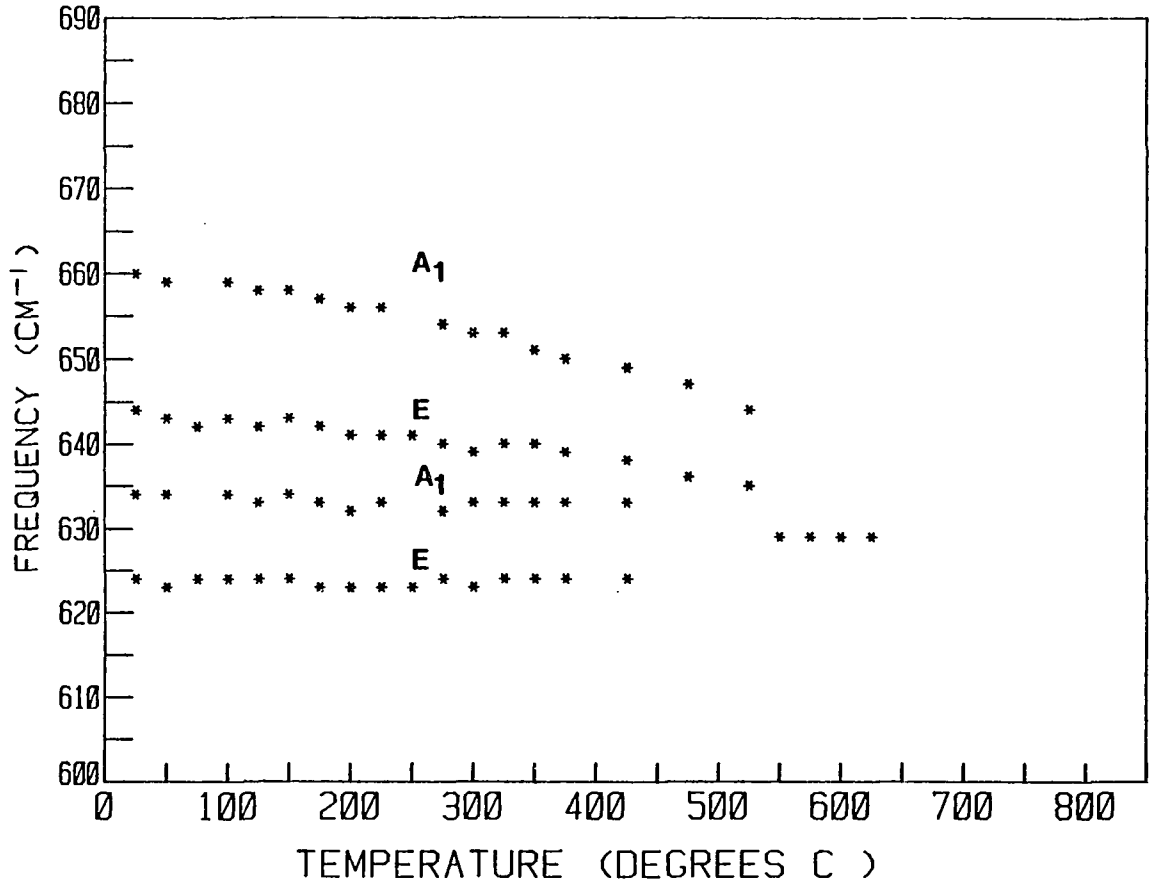


FIGURE 5.7. Temperature-dependent frequency data for the ν_4 region in $LiNaSO_4$.

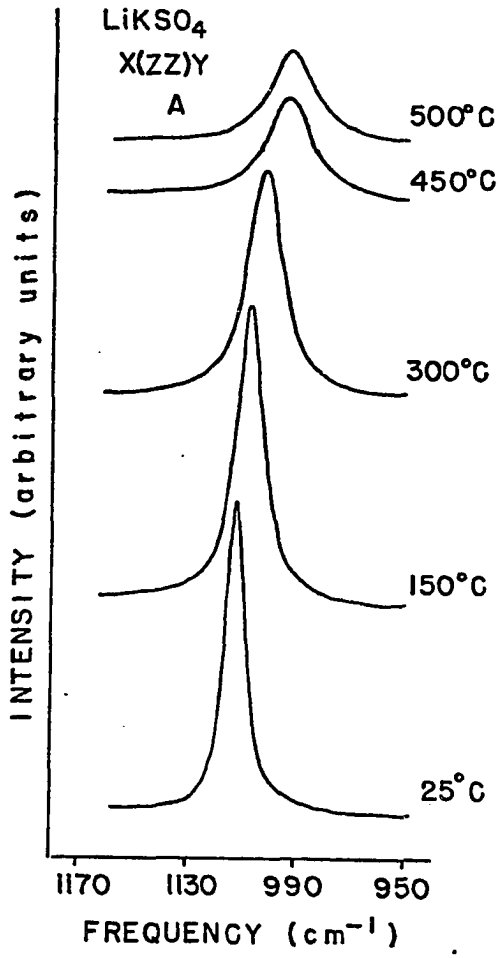


FIGURE 5.8. Raman spectra at various temperatures for the A mode in the ν_1 region in $LiKSO_4$. Full scale intensity is 2×10^4 cps.

to decrease to a value of 986 cm^{-1} at 708°C. This is shown in Figure 5.9.

The ν_2 Region

The ν_2 region has one E_1 mode at approximately 463 cm^{-1} which also broadens and decreases in frequency as the temperature is increased. At 425°C it has a value of 452 cm^{-1} which increases after the phase transition to a value of 457 cm^{-1} at 500°C. The band broadens throughout the entire temperature range. Figure 5.10 is a frequency vs. temperature plot for this mode.

The ν_3 Region

This region has an A, E_1, and E_2 mode, all very close to a value of 1119 cm^{-1}. The temperature-dependent behavior of these modes is almost identical up to the phase transition, decreasing to a frequency of approximately 1108 cm^{-1} at 400°C. At this temperature the modes are very broad. After the transition occurs two very broad asymmetric bands are observed, one centered at 1124 in an x(zz)y experiment and the other centered at approximately 1109 cm^{-1} in an x(yz)y experiment. Figures 5.11 and 5.12 show temperature-dependent spectra and frequency data for this region.

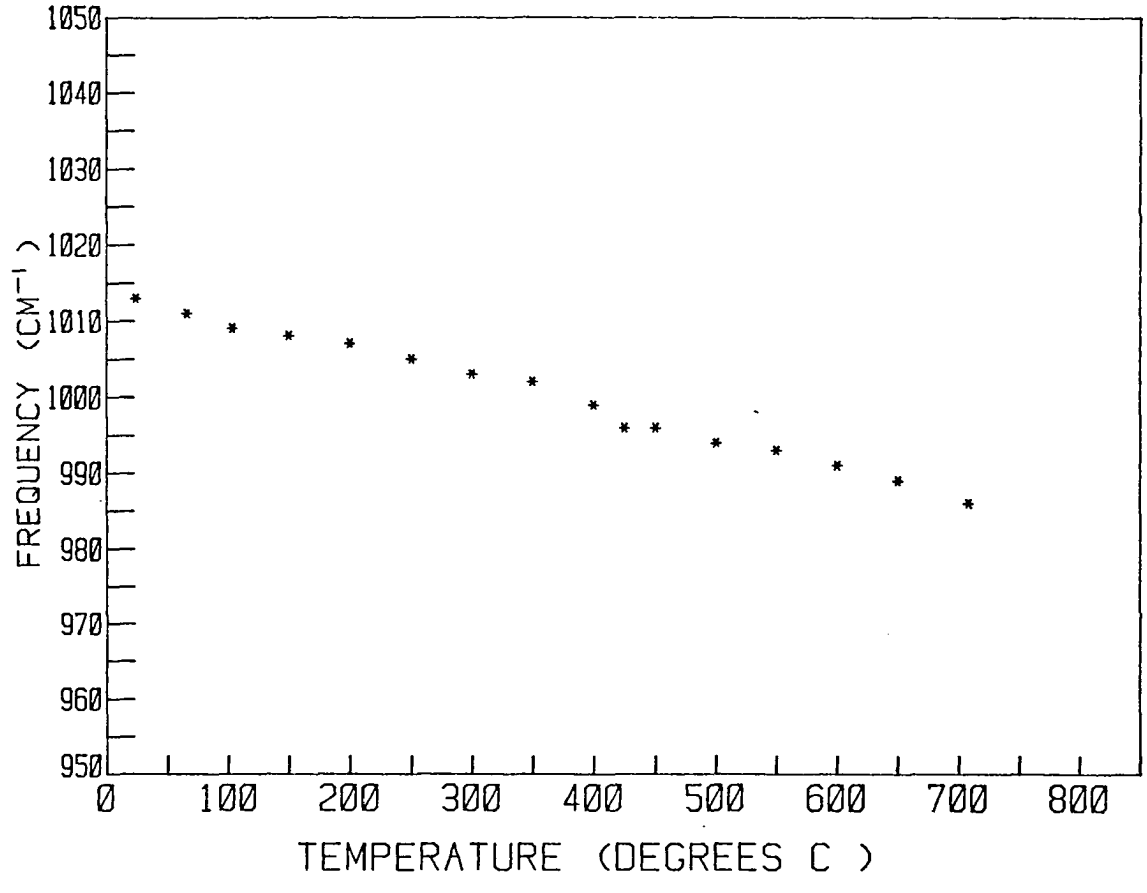


FIGURE 5.9. Temperature - dependent frequency data for the band maximum of the A mode in the ν_1 region in $LiKSO_4$.

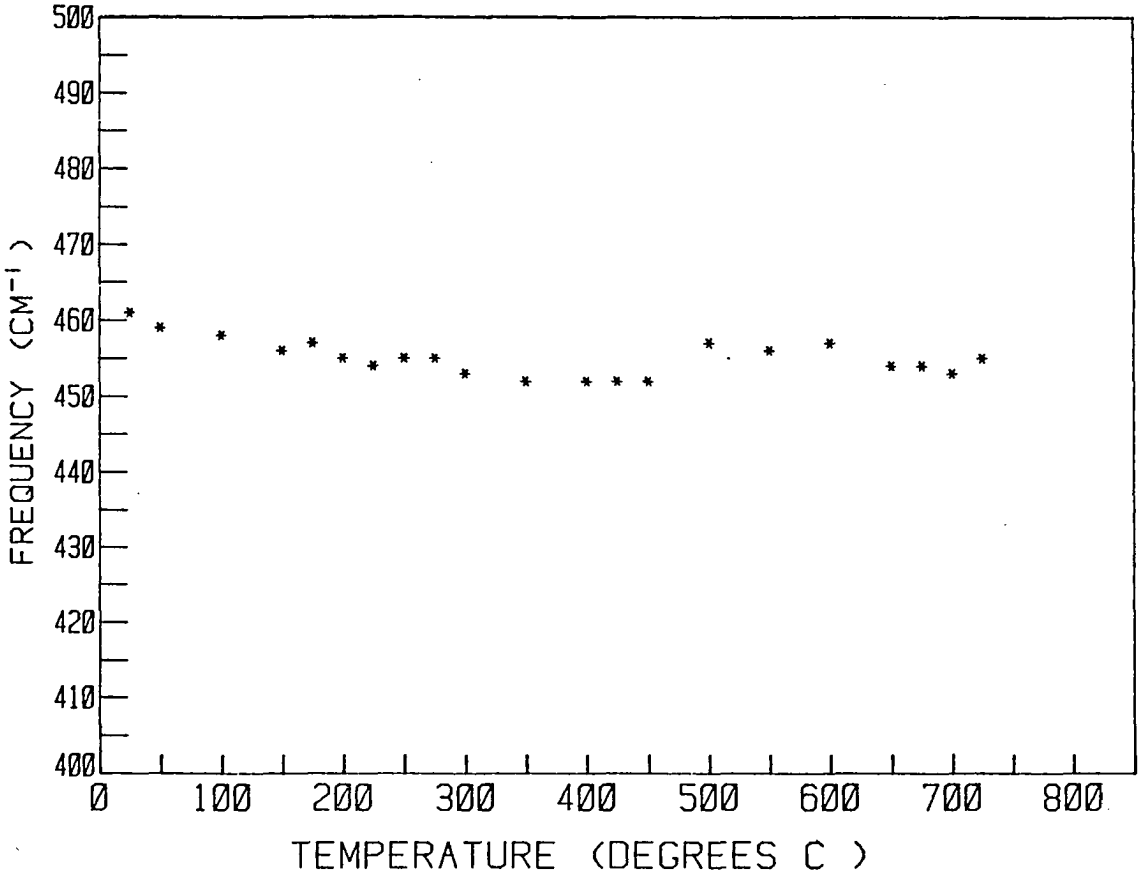


FIGURE 5.10. Temperature - dependent frequency data for the band maximum of the E_1 mode in the ν_2 region in $LiKSO_4$.

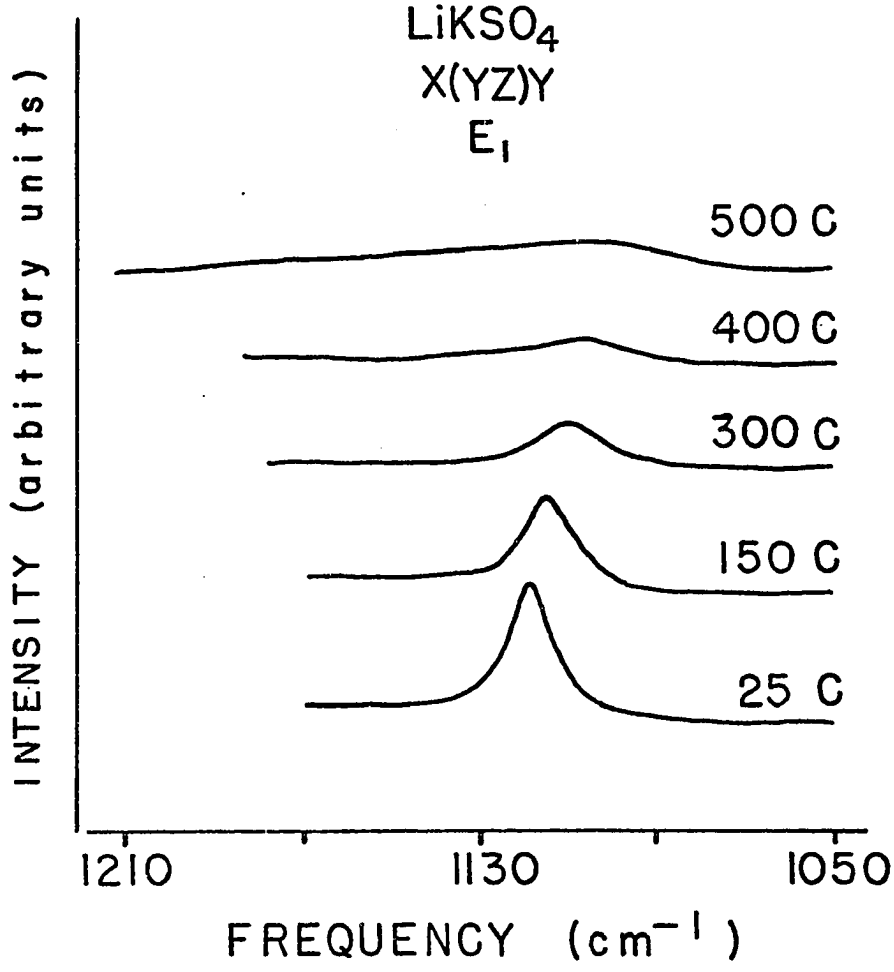


FIGURE 5.11. Temperature-dependent Raman spectra of the E_1 mode in the ν_3 region in $LiKSO_4$. Full scale intensity in 2×10^4 cps.

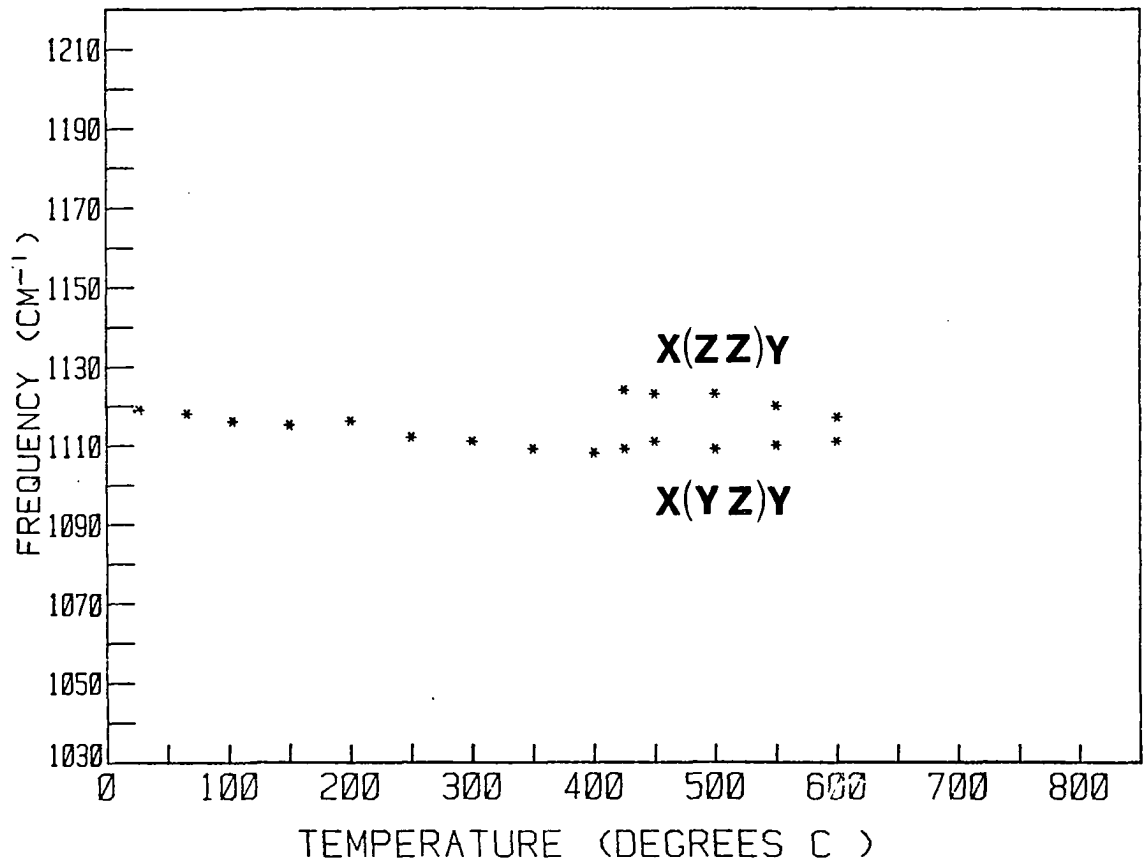


FIGURE 5.12. Temperature - dependent frequency data for the ν_3 region in $LiKSO_4$. The frequencies for all the modes have almost identical values until the phase transition when different experimental geometries show two broad modes differing in frequency.

The ν_4 Region

In the ν_4 region three modes are present; one A mode, one E mode, and one E_2 mode. All bands broaden and decrease in frequency. The E_1 and E_2 modes have frequencies of approximately 634 cm^{-1} and decrease in frequency to a value of 627 cm^{-1} at the phase transition. The A mode decreases from a value of 623 cm^{-1} at 25°C to 619 at 400°C. After the phase transition an x(zz)y experiment shows a band at 634 while an x(yz)y shows a band at 627 cm^{-1}. The frequency data are shown in Figure 5.13.

Sodium Potassium Sulfate: Temperature Dependence of Internal Modes

The solid solution $NaK_3(SO_4)_2$ is reported to have a phase transition at 471°C into a hexagonal $P6_3mc$ (C_{6v}^4) phase.[3] This temperature is somewhat dependent on the concentration of the potassium ion. The transition in this study is observed between 450-500°C.

The ν_1 Region

The ν_1 region in $NaK_3(SO_4)_2$ has one mode of A_{1g} symmetry with a frequency of 993 at 23°C. This mode broadens and decreases in frequency as the temperature is increased. The frequency just before the phase transition is 982 cm^{-1} at 450°C.

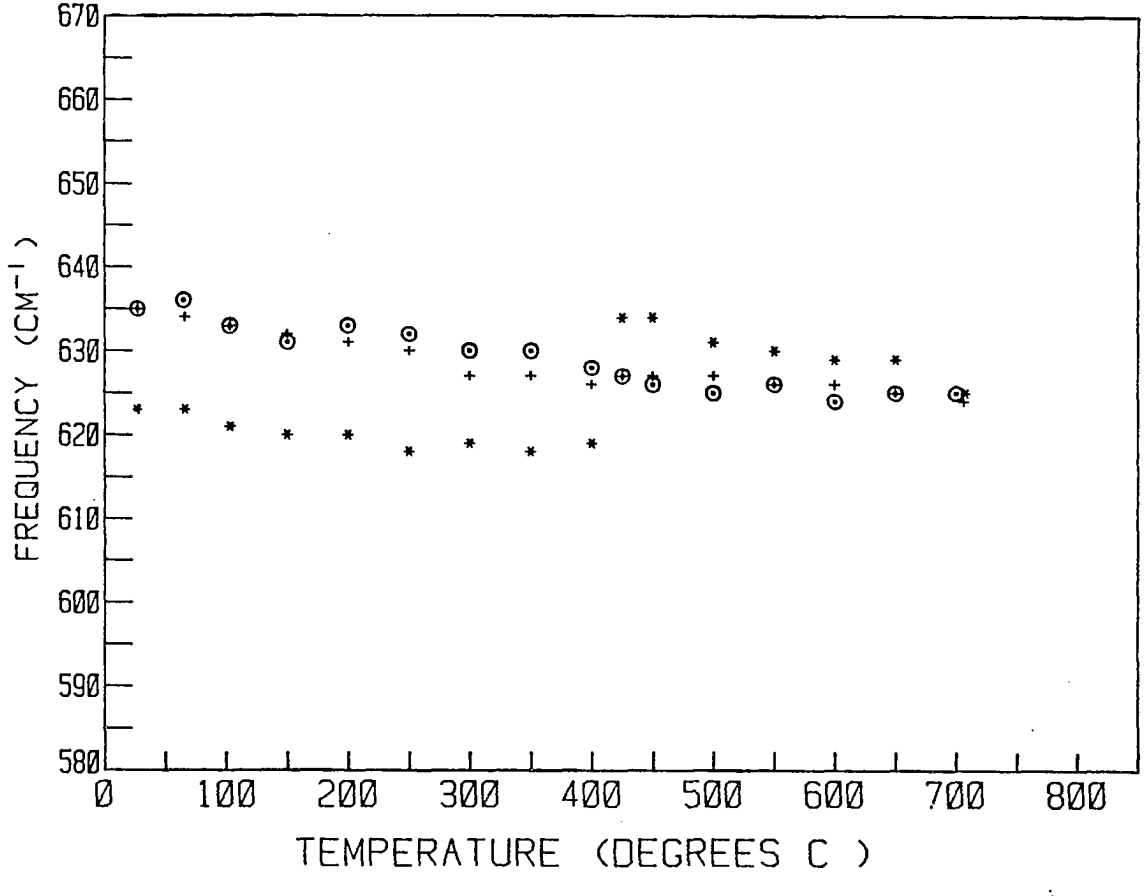


FIGURE 5.13. Temperature - dependent frequency for the modes in the ν_4 region in $LiKSO_4$. The circled points are E_1 band maximum data points as determined from an x(yz)y experiment. The + points are E_2 values from a x(yx)y experiment. The asterisks are A data from a x(zz)y experiment.

The phase transition causes only a slight broadening of the mode and slight decrease in frequency. The frequency continues to decrease to a value of 971 cm^{-1} at 775°C. The temperature-dependent spectra and frequency data are shown in Figures 5.14 and 5.15.

The ν_2 Region

The frequency of the one E_g mode at 452 cm^{-1} is very temperature insensitive. It broadens with temperature, but the frequency remains constant from 25°C to 775°C. Frequency vs. temperature data is shown in Figure 5.16.

The ν_3 Region

Two modes are found in the ν_3 region, an A_{1g} at 1203 cm^{-1} and an E_g at 1083 cm^{-1}. The A_{1g} broadens with temperature and decreases in frequency to a value of 1179 cm^{-1} at 450 cm^{-1}. After the phase transition occurs an x(zz)y experiment shows a very broad asymmetric peak at approximately 1155 cm^{-1} at 500°C. The E_g mode changes only slightly in temperature to 1081 cm^{-1} at 450°C. After the phase transition an x(yx)y experiment exhibits one broad peak at 1089 cm^{-1}, a broad shoulder at 1150 cm^{-1}, and another small broad peak at 1237 cm^{-1}. At approximately 350°C in the x(yx)y experiment and 400°C in the x(zz)y experiment a mode at approximately 1135 cm^{-1} appears and

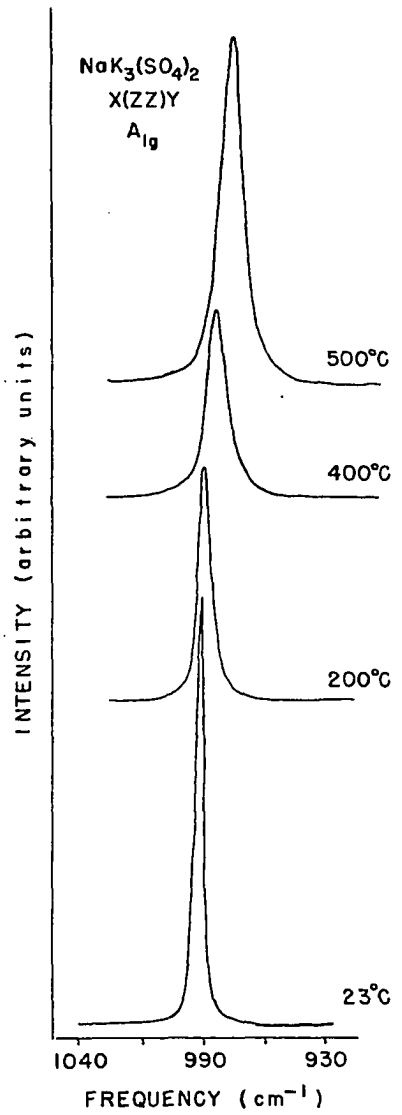


FIGURE 5.14. Raman spectra at various temperatures of the A_{1g} mode in the ν_1 region in $NaK_3(SO_4)_2$. Full scale intensities are: 25 and 200° C, 2 x 10^5 cps; 400°C 1 x 10^5 cps ; 500° C, 5 x 10^4 cps.

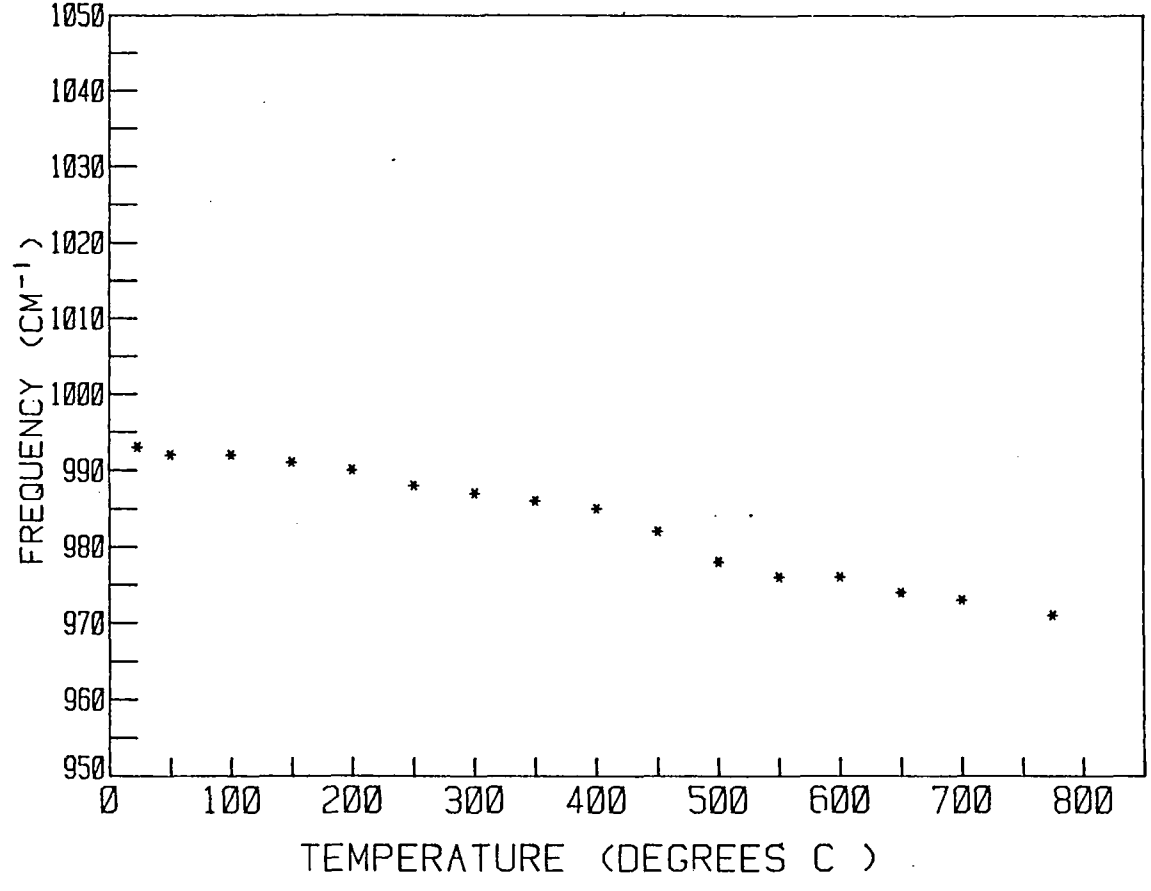


FIGURE 5.15. Temperature - dependent frequency data for the A_{1g} mode in the ν_1 region in $NaK_3(SO_4)_2$.

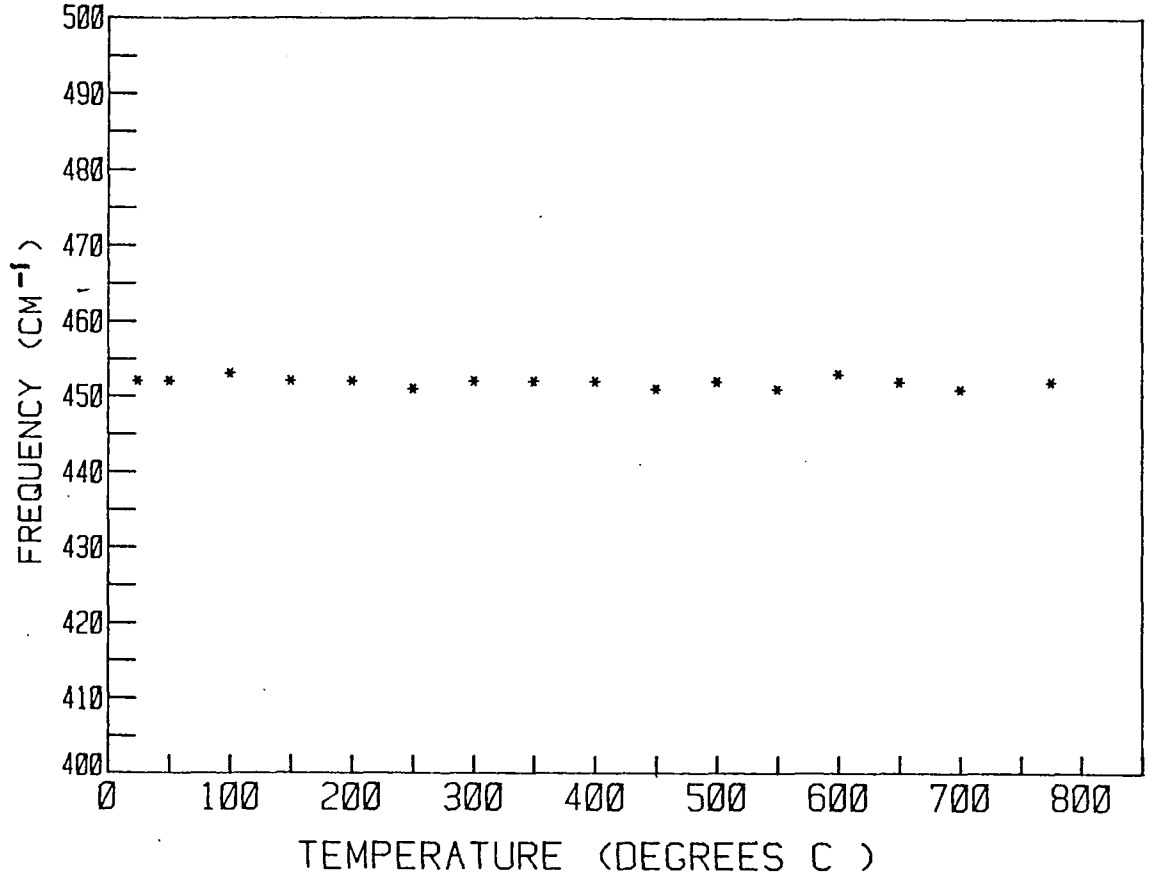


FIGURE 5.16. Temperature - dependent frequency data for the Eq. made in the ν_2 region in $NaK_3(SO_4)_2$.

increases in intensity as the temperature is increased. This mode is not observable above the phase transition. Temperature-dependent spectra are shown in Figures 5.17 and 5.18 with the corresponding frequencies shown in Figure 5.19.

The ν_4 Region

The ν_4 region has an A_{1g} mode and an E_g mode at 629 and 621 cm^{-1} respectively. The A_{1g} mode broadens and decreases in frequency to a value of 624 cm^{-1} at 450°C. The E_g mode broadens but changes only slightly in frequency. The temperature-dependent frequency data are shown in Figure 5.20.

Comparisons and Discussion

The potential energy environment of the sulfate ion in the three sulfate salts is affected by the phase transition as one would expect. The greatest effect seems to occur in $LiNaSO_4$ where frequencies change drastically after the phase transition occurs. As the temperature is increased modes in the ν_1 region merge as do the modes in the ν_2, ν_3 and ν_4 regions. At temperature above the phase transition only one broad mode which is unaffected by different types of polarized experiments is observed in each of the four sulfate internal mode regions.

A comparison of the three sulfates' temperature-dependent frequency data for a specific internal mode

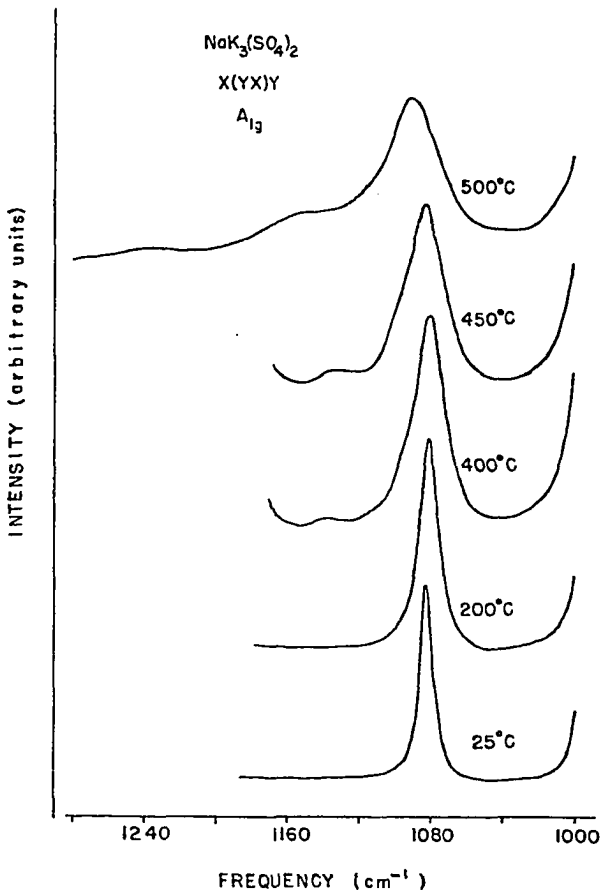


FIGURE 5.17. Raman spectra at various temperatures of the E_g modes in the ν_3 region in $NaK_3(SO_4)_2$. At 400 and 450°C a new mode appears at approximately 1137 cm^{-1}. Full scale intensities are 2×10^4 cps at 25°C and 1×10^4 cps at all other temperatures.

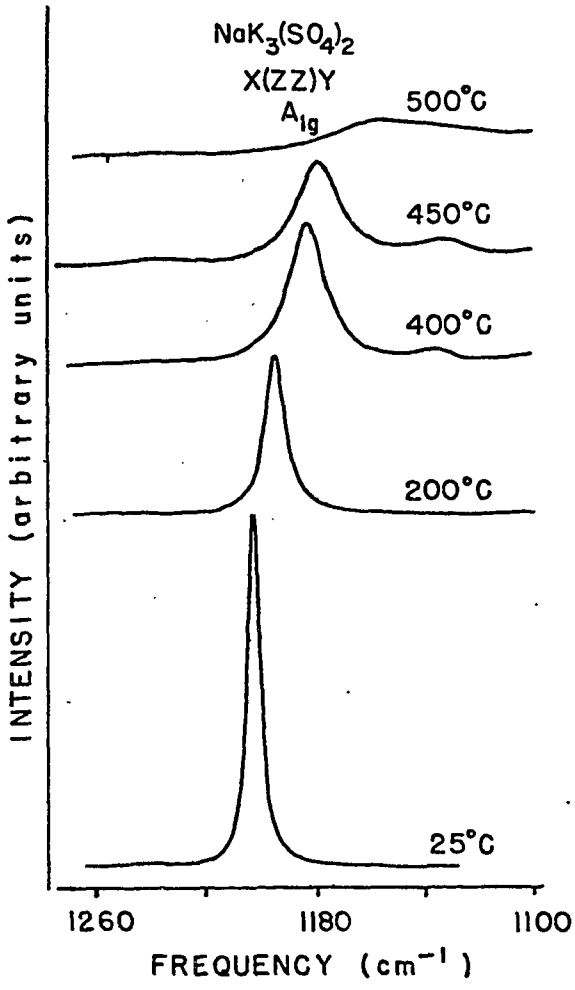


FIGURE 5.18. Raman spectra at various temperatures of the A_{1g} mode in the ν_3 region in in $NaK_3(SO_4)_2$. Full Scale intensities are 1 x 10^5 cps at 25 and 200° C and 5 x 10^4 cps at all other temperatures.

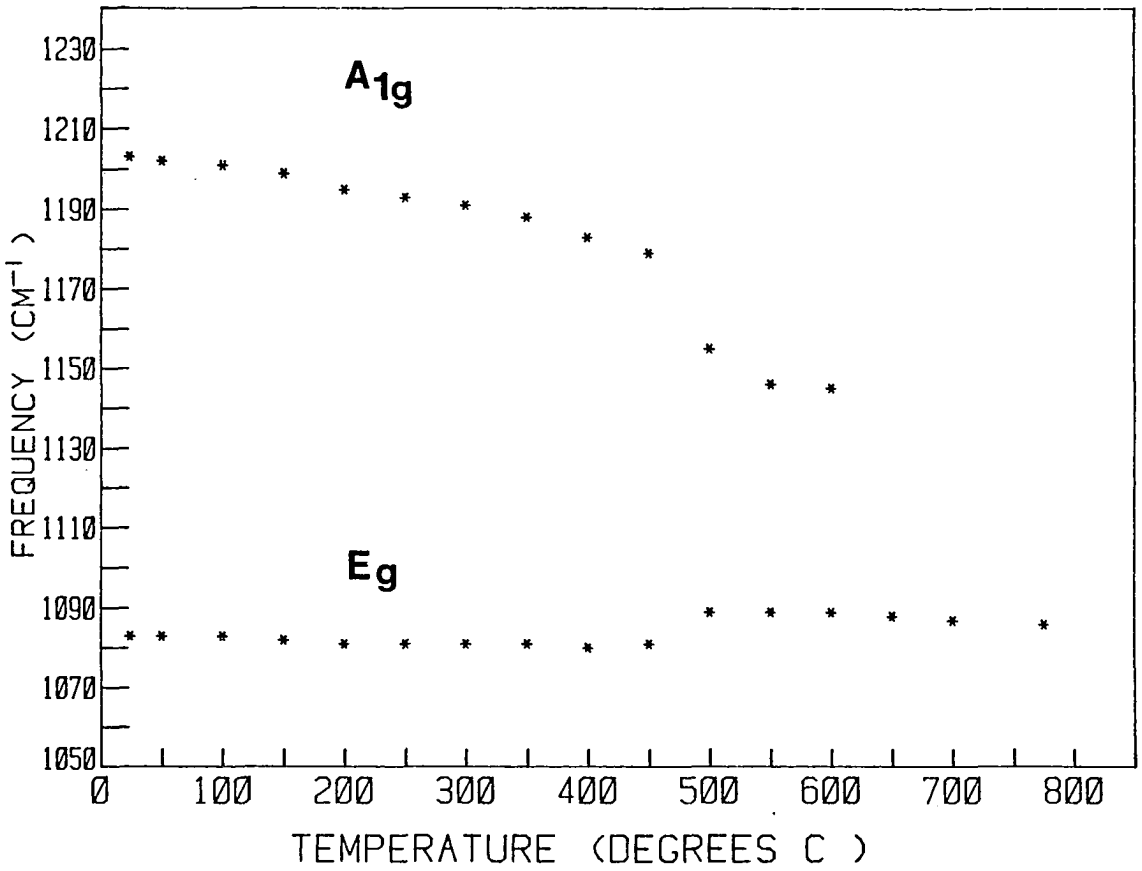


FIGURE 5.19. Temperature - dependent frequency data for the modes in the ν_3 region in $NaK_3(SO_4)_2$.

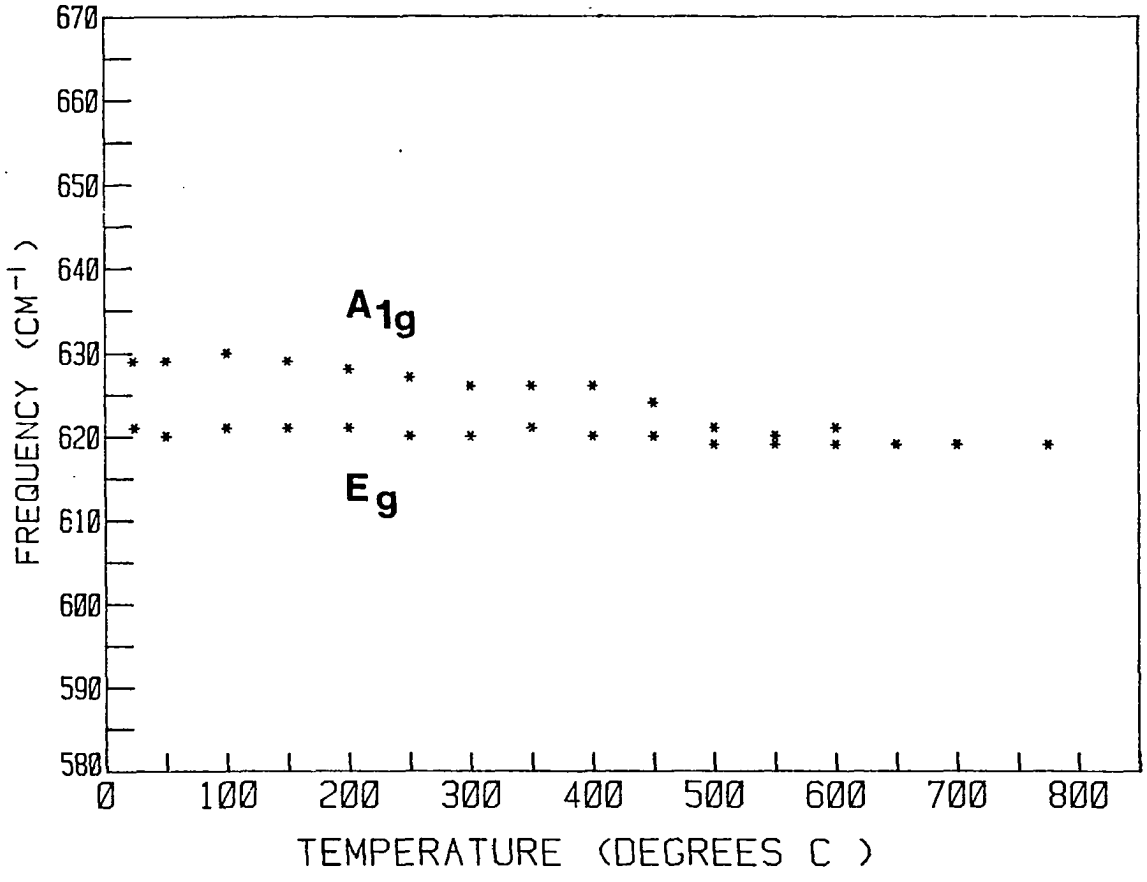


FIGURE 5.20. Temperature - dependent frequency data for the mode in the ν_4 region in $NaK_3(SO_4)_2$.

region demonstrates the sharp change in potential energy environment experienced in $LiNaSO_4$, In the ν_1 region modes whose frequencies are 977 and 995 cm^{-1} at 525°C merge into one broad mode at 970 cm^{-1} at temperature of 550°C (see Figure 5.2). The modes in the ν_1 region in $LiKSO_4$ (Figure 5.9) and $NaK_3(SO_4)_2$ (Figure 5.15) do not experience such a drastic change in frequency as they go through the phase transition. In the ν_4 region one also sees modes in $LiNaSO_4$ change from a frequency of 644 cm^{-1} (A_1 mode) and 635 cm^{-1} (E mode) at 525°C to a frequency of 628 cm^{-1} at 550°C (Figure 5.7). The temperature-dependent frequency data for $LiKSO_4$ (Figure 5.13) and $NaK_3(SO_4)_2$ (Figure 5.20) does not have such a drastic change in frequency for all modes involved.

Only the modes in the ν_3 region (Figure 5.12) and ν_4 region (Figure 5.13) experience abrupt changes in frequency as they go through the phase transition in $LiKSO_4$. The ν_3 region of $NaK_3(SO_4)_2$ (Figure 5.19) has modes that demonstrate a sharp change in frequency when passing through the phase transition.

One might expect the sulfate ion in $LiNaSO_4$ and $LiKSO_4$ to experience a greater change in potential energy environment than in the case of $NaK_3(SO_4)_2$. Lithium sodium sulfate undergoes a transition from a hexagonal P31c (C_{3v}^4)[7] to a body centered cubic phase[1] while $LiKSO_4$ goes from a hexagonal $P6_3$ (C_6^6) to an orthorhombic phase[2] and $NaK_3(SO_4)_2$

goes from a hexagonal $P\bar{3}ml$ (D_{3d}^3) to another hexagonal phase $P6_3mc$ (C_{6v}^4).[3] The phase transitions in $LiNaSO_4$ and $LiKSO_4$ might be expected to involve a change in potential energy environment of the sulfate ion of a greater magnitude than in $NaK_3(SO_4)$ which goes from one hexagonal phase to another. Another factor affecting the $LiNaSO_4$ modes at the phase transition could be the breaking of the strong lithium-oxygen interactions which must occur if the high temperature phase of $LiNaSO_4$ is to exhibit fast ion conduction. The fact that this interaction is broken in $LiNaSO_4$ while some type of interaction must remain in $LiKSO_4$, could partially explain the difference in temperature-dependent frequency data for the two crystals.

Consideration of the lithium-oxygen interaction might also be helpful in understanding the behavior of the ν_1 region in $LiNaSO_4$. Table 5.1 lists the frequencies of the ν_1 components for various sulfate salts.

The ν_1 region of $LiNaSO_4$ has three vibrational modes at the frequencies given in Table 5.1. Three modes are expected because there are three pairs of sulfate ions occupying three distinct crystallographic positions. Two pairs occupy Wyckoff b sites while one pair occupies an a site. The frequencies of the ν_1 modes for sulfates which contain Li ions are found to be higher than those which do not. Lithium-oxygen interaction could be responsible for "stiffening" the oxygen bond and hence increasing the

TABLE 5.1

FREQUENCIES OF THE ν_1 MODES FOR VARIOUS LITHIUM, POTASSIUM AND SODIUM SULFATE CRYSTALS

Sulfate (space group)	ν_1 frequencies (cm^{-1})	Reference
Li_2SO_4 (monoclinic)	1017	4
$LiKSO_4$ (hexagonal)	1012	5
$LiNaSO_4$ (hexagonal)	972, 998, 1026	This Work
$NaK_3(SO_4)_2$ (hexagonal)	996	6
K_2SO_4 (orthorhombic)	985	4
Na_2SO_4 (orthorhombic)	996	6

frequency of the ν_1 symmetric stretching mode. Even though these three modes caused by factor group splitting must contain contributions from all three pairs of sulfate ions, one could postulate that the mode at 1026 cm^{-1} contains the greatest contribution from sulfate ions interacting most strongly with the lithium ions. The tetrahedron formed by the oxygen atoms about the lithium ion is not regular.[7] It seems reasonable that the lithium ion could affect the sulfate ions to a differing degree. The ν_1 mode at 1026 cm^{-1} could be due in part to a strong lithium-oxygen interaction. It is this mode that is found to decrease in frequency to a greater rate with increasing temperature than any other internal mode in Li $NaSO_4$, $LiKSO_4$, or $NaK_3(SO_4)_2$. This could be indicative of weakening of the lithium-oxygen

interaction in $LiNaSO_4$ caused by increasing temperatures.

So far only differences in the three systems have been discussed; however, there is an apparent common trait observed in $LiNaSO_4$, $LiKSO_4$, and $NaK_3(SO_4)_2$ in the ν_3 region. In all three sulfates the modes of the ν_3 region broaden very fast and at temperatures above the phase transition scattering seems to occur from a density of states (Figures 5.4, 5.11, 5.17 and 5.18). This must involve the breakdown of the Raman selection rules due to disorder in the systems. The ν_3 modes for these sulfate systems seem to be the most sensitive to disorder caused by increasing temperature. The mode appearing at approximately $350^{o}C$ at 1135 cm^{-1} in $NaK_3(SO_4)_2$ is most likely due to the formation of a second phase of K_2SO_4 existing simultaneously with $NaK_3(SO_4)_2$. This simultaneous existence of two phases is indicated on the phase diagram for Na_2SO_4-K_2SO_4 given by Eysel.[3] The increasing intensity of the 1135 cm^{-1} mode with increasing temperature is due to the formation of more of the K_2SO_4 phase.

REFERENCES

1. T. Forland and J. Krogh-Moe, Act. Crystallogr. 11, 224 (1958).

2. K. Schroeder. Thesis, Goteborg (1975).

3. W. Eysel, Am. Mineral. 58, 736 (1973).

4. V. Ananthanorayanan, Indian J. Pure Appl. Phys. 1, 58 (1963).

5. J. Hiraishi, N. Taniguchi, and H. Takahashi, J. Chem. Phys. 65, 3821 (1976).

6. G. J. Wu and R. Frech, J. Chem. Phys. 66, 1352 (1977).

7. B. Morosin and D. L. Smith, Acta Crystallogr. 22, 906 (1966).

CHAPTER VI

SUMMARY OF CONCLUSIONS AND FUTURE STUDIES

Summary of Conclusions

Raman spectroscopic techniques have been used to investigate $LiNaSO_4$, $LiKSO_4$, and $NaK_3(SO_4)_2$ over a wide temperature range from 15 K to temperatures above their respective phase transitions. It has been postulated that transitions in sulfate systems can be interpreted in terms of the strength of the metal ion-oxygen interactions[1] and in the case of Li_2SO_4 in terms of rotation of the sulfate ion.[1,2] Both metal ion-oxygen interactions and librational (rotational) motion of the sulfate ions have been investigated here using vibrational spectroscopy.

Activation energies which are postulated to be associated with removal of the lithium ion from its tetrahedral coordination in $LiNaSO_4$ and $LiKSO_4$ were calculated in Chapter III. The values of .4 eV and .6 eV for $LiNaSO_4$ and $LiKSO_4$ respectively are very close in value suggesting that the tetrahedral coordination in both sulfates is very similar. Tetrahedral coordination of the lithium ion in $LiNaSO_4$ must be broken for

the fast ion conduction phase in this compound to occur. The activation energy for fast ion conduction in $LiNaSO_4$ given by Polishchuk and Shurzhal[3] is .37 eV which compares well with the value of .4 eV given above.

Another factor could also be involved in fast ion conduction in $LiNaSO_4$. Nilsson, Thomas, and Tofield[4] have postulated that the movement of lithium ions in the fast ion conducting phase of Li_2SO_4 is enhanced by rotational motion of the sulfate ions whose centers of mass remain localized about the lattice sites. This fast ion conducting phase is described as a plastic phase caused by rotational disorder of the sulfate groups.[4] As discussed in Chapter IV, a plastic phase is characterized by a large volume change at the phase transition and a larger heat of transition than heat of fusion. Polishchuk and Bogdanova[5] feel that the high temperature phase in $LiNaSO_4$ is a plastic phase; this speculation seems to be consistent with available data. Table 6.1 summarizes data for the solid — solid phase transition as well as the melt for Li_2SO_4 and $LiNaSO_4$, both of which have high temperature fast ion conducting phases. Data for $LiKSO_4$ and $NaK_3(SO_4)_2$ are also given so that comparisons can be made. In Table 6.1 T_{Tr} and T_m are the temperatures of the solid — solid phase transition and melt respectively, ΔH_{Tr} and ΔH_m are the enthalpy changes for the phase transition and melt, ΔS_{Tr} and ΔS_m are the entropy changes, and ΔV_{Tr} is the change in volume at the phase transition.

TABLE 6.1 Phase Transition and Melt Data for Li_2SO_4, $LiNaSO_4$, $LiKSO_4$, and $NaK_3(SO_4)_2$.[a]

Compound	T_{Tr} (°C)	T_m (°C)	ΔH_{Tr} (cal/mole)	ΔH_m (cal/mole)	ΔS_{Tr} (cal/mole K)	ΔS_m (cal/mole K)	ΔV_{Tr} (cm^3/equiv.)
Li_2SO_4	573(6)	860(6)	6500 (1)	1833 (7)	7.6 (7)	1.6 (7)	1.16 (8)
$LiNaSO_4$	520(6)	620(5)	5380 (5)	760 (5)	6.8 (5)	.8 (5)	2.70 (8)
$LiKSO_4$	436(6)	723(6)	2584 (9)	14161 (9)	3.7 (9)	13.1 (9)	.06 (8)
$NaK_3(SO_4)_2$	471(10)	884(11)	1750 (11)	4650 (11)	2.4 (11)	...	...

[a]References are given in parentheses following the value.

The data indicates that both Li_2SO_4 and $LiNaSO_4$ have a high temperature plastic phase while comparable data for $LiKSO_4$ and $NaK_3(SO_4)_2$ indicate that a plastic phase does not exist. For both $LiKSO_4$ and $NaK_3(SO_4)_2$ the heat of transition is smaller than the heat of melting. Changes in entropy for Li_2SO_4 and $LiNaSO_4$ at the solid phase transition are significantly larger than the corresponding values in $LiKSO_4$ and $NaK_3(SO_4)_2$. The change in volume is also relatively larger for Li_2SO_4 and $LiNaSO_4$ when compared with $LiKSO_4$. Large entropy changes and volume changes at the phase transition have been postulated to be associated with rotational disorder of the sulfate ion.[1,5] From this data one can assume that while Li_2SO_4 and $LiNaSO_4$ have a great deal of rotational disorder in the high temperature phase, $LiKSO_4$ and $NaK_3(SO_4)_2$ do not appear to have as much of this type of disordering. The disorder of the sulfate sublattice in $LiNaSO_4$ is spectroscopically demonstrated by the fact that no external modes are observable after the phase transition.

Nilsson et al.[4] estimated the frequency of reorientation for the sulfate ion in Li_2SO_4 in its fast ion conducting phase to be 27 cm^{-1}. In this study the lowest frequency external mode at 63 cm^{-1} in $LiNaSO_4$ was postulated to have a great deal of sulfate rotational contribution. This mode was found to soften in frequency and could be the analogous frequency of reorientation for the sulfate ion in $LiNaSO_4$.

In contrast the low frequency external modes in $LiKSO_4$ and $NaK_3(SO_4)_2$ are very temperature insensitive. An external mode at 202 cm^{-1} in $LiKSO_4$ was found to be the most temperature sensitive external mode both broadening and softening in frequency. This mode seems to have at least some ionic motion of translational character. Therefore, one might postulate that the transition in $LiKSO_4$ and $NaK_3(SO_4)_2$ could be predominently translational, with a sulfate sublattice involving significantly less rotational motion of the sulfate ion than occurs in $LiNaSO_4$.

The ionic radii for Li^+, Na^+, and K^+ are .68Å, .97Å, and 1.33Å respectively.[12] The larger size of the potassium ion may help to stiffen the sulfate sublattice in $LiKSO_4$, and $NaK_3(SO_4)_2$. Jansson and Sjoblom[8] found that even a small amount of potassium ion substituted into Li_2SO_4 results in a 50% reduction of the volume change with increasing temperature but the volume change is not further reduced by an increase of potassium ion. Potassium ion in even small amounts may hinder rotational motion of the sulfate ions in the sulfate sublattice preventing a large volume change at the phase transition.

Substitution of the smaller sodium ion into the crystal lattice of Li_2SO_4 does not have a large effect on volume change with increasing temperature.[8] Augustsson and Gustafsson[13] feel that the space available for the sodium ion in Li_2SO_4 is probably large enough so that the sodium ion has little affect on the sulfate sublattice. The sodium ion because of its

small size may have less affect on librational motion of the sulfate ions in the crystal lattice.

If rotational motion of the sulfate ions can enhance ionic motion in sulfate crystals as proposed by Nilsson et al.[4] it would seem that $LiNaSO_4$ would be an example. The rotational motion of the sulfate ions in $LiKSO_4$ and $NaK_3(SO_4)_2$ seem to be more hindered, possibly explaining the absence of fast ion conduction in these crystals.

Possible Future Studies

There are several studies that could complement or expand this study. One would involve a temperature-dependent infrared study of lithium modes in $LiNaSO_4$ and $LiKSO_4$. While the lithium vibrational modes are very weak Raman scatterers, they have very intense infrared bands. The lithium modes could possibly be observed after the phase transition in both crystals thus giving information about the differences in the lithium ion potential energy environment after the phase transition.

Another valuable study would be a temperature-dependent Raman study of Li_2SO_4. More studies have been done on this fast ion conducting sulfate than any other sulfate crystal. This sulfate was the original compound proposed to have a dynamically enhanced diffusion mechanism.[4] A temperature-dependent Raman study would complement the existing studies and the study of $LiNaSO_4$ given here.

REFERENCES

1. K. J. Rao and C. N. R. Rao, J. Mater. Sci. 1, 238 (1966).
2. A. F. Polishchuk, Russ. J. Phys. Chem. 47, 1088 (1973).
3. A. F. Polishchuk and T. M. Shurzhal, Elektrokhimiya 9, 838 (1973).
4. L. Nilsson, J. O. Thomas, and B. C. Tofield, J. Phys. C 13, 6441 (1980).
5. A. F. Polishchuk and A. K. Bogdanova, Russ. J. Phys. Chem. 51, 1195 (1977).
6. K. Schroeder, Thesis, Göteberg (1975).
7. N. K. Voskresenkaya and E. I. Banashek, Izvest. Sektora Fiz. -Khim. Anal., Inst. Obshchei i Neorg. Khim. Akad. Nauk S.S.S.R. 25, 150 (1954).
8. B. Jansson and C.-A. Sjoblom, Z. Naturforsch. A 25, 1115 (1970).
9. N. K. Voskresenkaya and E. I. Banashek, Izvest. Sektora Fiz. -Khim. Anal., Inst. Obshchei i Neorg. Khim., Akad. Nauk S.S.S.R. 26, 111 (1955).
10. W. Eysel, Am. Mineral. 58, 736 (1973).
11. T. Forland and J. Krogh-Moe, Acta Chem. Scan. 13, 1051 (1959).
12. Handbook of Chemistry and Physics (The Chemical Rubber Co., Cleveland, Ohio, 1971) 52nd ed., p. F-171.
13. B. Augustsson and J. Gustafsson, Z. Naturforsch. A 22, 1634 (1967).

ADDENDUM

The temperature dependent data for the lithium modes in $LiNaSO_4$ and $LiKSO_4$ were treated in Chapter III. This data had not been corrected for thermal population of vibrational levels as was done for the external mode study in Chapter IV. To check the affect that thermal population effects might have on the activation energies calculated by using Equations 3.1 and 3.3, the lithium mode data for $LiNaSO_4$ and $LiKSO_4$ were corrected by using the Bose-Einstein factor (Equation 4.6.). The corrected linewidths were fit to Equations 3.1 and 3.3 and activation energies calculated. The results are listed below.

Lithium Mode	Activation Energy (eV) Equation 3.1	Equation 3.3
$LiKSO_4$[a]		
A	.03	.06
E_2	.04 (12-475 K)	.07 (12-475 K)
	.09 (12-725 K)	.8 (12-725 K)
$LiNaSO_4$		
A_1 (314 cm^{-1} mode)	.2 $\pm$ .3	.2 $\pm$ .3
(404 cm^{-1} mode)	.4 $\pm$ 1	.5 $\pm$ 1
E	.4 $\pm$ .1	.4 $\pm$ .1

[a]The average error in these values is 40%.

The values given above differ only slightly from the activation energy values given in Tables 3.1 and 3.2.